

AN ABSTRACT OF THE THESIS OF

STANLEY BROWNING COLLINS for the Ph. D.
(Name) (Degree)

in Chemical Engineering presented on 4/10/67
(Major) (Date)

Title: DROP SIZE DISTRIBUTIONS PRODUCED BY TURBULENT
PIPE FLOW OF IMMISCIBLE LIQUIDS

Abstract approved:



(Signature)

Dr. James G. Knudsen

Drop size distributions produced by the turbulent pipe flow of dispersions of immiscible liquids were measured photographically. A mathematical model was developed which predicted both the shape of the experimentally observed distributions and the experimentally observed kinetics of the breakup process.

The mutually saturated water and organic phases were pumped separately and mixed by injecting the organic phase along the axis of the vertical, 0.745-inch ID, 40-foot pipe which formed the test section. Provision was made to allow the dispersion formed by the action of the turbulence to be photographed at 27, 209, 421, and 576 pipe diameters below the mixing jet. The position of the focal plane of the camera along the radius of the pipe could also be adjusted. Photographs were thus obtained at dimensionless distance of 0.05, 0.1, and 0.4 from the wall. Average flow rates were varied from

14 ft/sec to 20 ft/sec. Three organic phases were studied at concentrations ranging from 0.6% to 10% by volume. Dispersed phase viscosity and interfacial tension varied from 1 cp to 18 cp and 13 to 40 dyne/cm respectively.

The experimentally observed distributions were all skewed toward small drop sizes. No distribution law with any theoretical basis could be found in the literature by which experimental distributions could be correlated. Thus the distributions are presented in graphical form.

The stochastic model developed to describe the breakup process indicates that each breakup event leads to two daughter drops with uniformly distributed volume ratios and a very small satellite droplet. The model contains three parameters, the maximum stable drop size, the slope of the probability curve above the maximum stable drop size, and the size range of the satellite drops. An empirical correlation exists to predict the first parameter of the model, but none exists for the second and third parameters.

Drop Size Distributions Produced by
Turbulent Pipe Flow of Immiscible Liquids

by

Stanley Browning Collins

A THESIS

submitted to

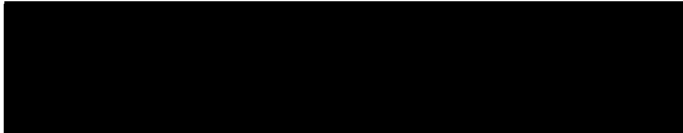
Oregon State University

in partial fulfillment of
the requirements for the
degree of

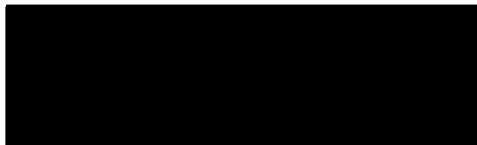
Doctor of Philosophy

June 1967

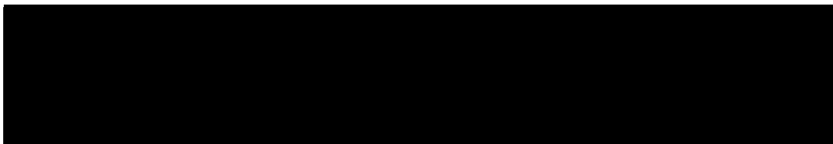
APPROVED:



Professor of Chemical Engineering
in charge of major



Head of Department of Chemical Engineering



Dean of Graduate School

Date thesis is presented

4/10/67

Typed by Donna Olson for Stanley Browning Collins

ACKNOWLEDGMENTS

The author wishes to express his sincere appreciation to Dr. James G. Knudsen for proposing the problem and providing encouragement and advice throughout the duration of this work.

Financial support for this project was provided by the National Science Foundation in the form of a Research Assistantship.

Finally the encouragement and assistance of my wife, Karla, without which this work could not have been completed, is gratefully acknowledged.

TABLE OF CONTENTS

| | <u>Page</u> |
|----------------------------------------|-------------|
| INTRODUCTION | 1 |
| PREVIOUS WORK | 3 |
| Droplet Breakup | 3 |
| Description of Drop Sizes | 24 |
| Measurement of Drop Size Distributions | 34 |
| EXPERIMENTAL PROGRAM | 41 |
| EXPERIMENTAL APPARATUS | 43 |
| Flow System | 43 |
| Photographic Equipment | 50 |
| EXPERIMENTAL PROCEDURE | 52 |
| EXPERIMENTAL RESULTS | 55 |
| DISCUSSION OF RESULTS | 85 |
| Mathematical Model | 85 |
| Comparison of the Model to Experiment | 101 |
| CONCLUSIONS | 114 |
| RECOMMENDATIONS FOR FURTHER WORK | 116 |
| BIBLIOGRAPHY | 118 |
| APPENDICES | 122 |
| NOMENCLATURE | 148 |

LIST OF FIGURES

| <u>Figure</u> | | <u>Page</u> |
|---------------|----------------------------------------------------------------------------------|-------------|
| 1. | Modes of deformation and breakup. | 5 |
| 2. | Representative drop size distributions measured by Clay (6). | 15 |
| 3. | Flow system schematic. | 44 |
| 4. | Mixing jets. | 46 |
| 5. | Self-aligning flanges. | 48 |
| 6. | Window arrangement for photographing the flowing dispersion. | 49 |
| 7. | Drop size distributions for 1.3% Shellsolv, $y/R_w = 0.1$. | 56 |
| 8. | The upper-limit distribution law applied to the distribution from Roll 89. | 58 |
| 9. | The Amsterdam distribution law applied to the distribution from Roll 89. | 59 |
| 10. | Reproducibility of distributions measured under similar experimental conditions. | 62 |
| 11. | Highly distorted drops. | 63 |
| 12. | Degree of drop deformation at various radial distances from the pipe wall. | 67 |
| 13. | Drop size distributions for 1.3% Shellsolv, $y/R_w = 0.05$, 16 ft/sec. | 70 |
| 14. | Drop size distributions for 1.3% Shellsolv, $y/R_w = 0.4$, 16 ft/sec. | 71 |
| 15. | Drop size distributions for 0.6% Shellsolv, $y/R_w = 0.1$, 16 ft/sec. | 72 |
| 16. | Drop size distributions for 5.0% Shellsolv, $y/R_w = 0.05$, 16 ft/sec. | 73 |

| <u>Figure</u> | <u>Page</u> |
|--------------------------------------------------------------------------------------------|-------------|
| 17. Drop size distributions for 5.0% Shellsolv, $y/R_w = 0.1$, 16 ft/sec. | 74 |
| 18. Drop size distributions for 10.0% Shellsolv, $y/R_w = 0.05$, 16 ft/sec. | 75 |
| 19. Drop size distributions for 1.3% Shellsolv, $y/R_w = 0.1$, 16 ft/sec, first floor. | 77 |
| 20. Drop size distributions for 1.3% Shellsolv, $y/R_w = 0.1$, 20 ft/sec. | 78 |
| 21. Drop size distributions for 5.0% light oil, $y/R_w = 0.05$, 16 ft/sec. | 79 |
| 22. Drop size distributions for 1.3% iso-octyl alcohol, $y/R_w = 0.05$, 16 ft/sec. | 81 |
| 23. Drop size distributions for 1.3% iso-octyl alcohol, $y/R_w = 0.1$, 16 ft/sec. | 82 |
| 24. Drop size distributions for 1.3% iso-octyl alcohol, $y/R_w = 0.4$, 16 ft/sec. | 83 |
| 25. Drop size distributions for 0.6% iso-octyl alcohol, $y/R_w = 0.05$, 16 ft/sec. | 84 |
| 26. Generalized subroutine MODEL. | 87 |
| 27. Drop size distribution for 1.3% Shellsolv, $y/R_w = 0.1$, 16 ft/sec. | 91 |
| 28. Frequency histogram for Roll 89. | 91 |
| 29. Model 1, log-probability plot. | 92 |
| 30. Model 1, frequency histogram, step 5. | 92 |
| 31. Model 3, log-probability plot. | 93 |
| 32. Model 3, frequency histogram, step 25. | 93 |
| 33. Model 4, log-probability plot. | 95 |

| <u>Figure</u> | <u>Page</u> |
|----------------------------------------------------------------------------------------------------------------------|-------------|
| 34. Model 4, frequency histogram, step 15. | 95 |
| 35. Model 5, log-probability plot. | 96 |
| 36. Model 5, frequency histogram, step 10. | 96 |
| 37. Model 6, log-probability plot. | 98 |
| 38. Model 7, log-probability plot. | 98 |
| 39. Model 8, log-probability plot. | 99 |
| 40. Model 8, frequency histogram, step 20. | 99 |
| 41. Model 9, log-probability plot. | 100 |
| 42. Model 9, frequency histogram, step 25. | 100 |
| 43. Model 10, log-probability plot. | 102 |
| 44. Model 10, frequency histogram, step 25. | 102 |
| 45. Model 11, log-probability plot, IMAXS = 200, KPROB = 700, SAT = 0.01. | 103 |
| 46. Model 11, frequency histogram, step 15. | 103 |
| 47. D32X vs. distance from the nozzle, 1.3% Shellsolv, IMAXS = 200, KPROB = 700, SAT = 0.01. | 105 |
| 48. D32X vs. distance from the nozzle, 5% light oil, IMAXS = 150, KPROB = 1250, SAT = 0.02. | 108 |
| 49. D32X vs. distance from the nozzle, 1.3% iso-octyl alcohol, IMAXS = 100, KPROB = 140, SAT = 0.05. | 109 |
| 50. Theoretical distributions for 5% light oil, IMAXS = 150, KPROB = 1250, SAT = 0.02. | 110 |
| 51. Theoretical and experimental frequency histograms for 5% light oil, IMAXS = 150, KPROB = 1250, SAT = 0.02. | 110 |

| <u>Figure</u> | <u>Page</u> |
|----------------------------------------------------------------------------------------------------------------------|-------------|
| 52. Theoretical distributions for 1.3% iso-octyl alcohol, IMAXS = 100, KPROB = 180, SAT = 0.05. | 111 |
| 53. Theoretical and experimental frequency histograms, 1.3% iso-octyl alcohol, IMAXS = 100, KPROB = 180, SAT = 0.05. | 111 |
| 54. Drop size distribution for 0.6% Shellsolv, $y/R_w = 0.05$, 16 ft/sec. | 123 |
| 55. Drop size distribution for 0.6% Shellsolv, $y/R_w = 0.4$, 16 ft/sec. | 124 |
| 56. Drop size distribution for 1.3% Shellsolv, $y/R_w = 0.4$, 20 ft/sec. | 125 |
| 57. Drop size distribution for 10% Shellsolv, $y/R_w = 0.1$, 16 ft/sec. | 126 |
| 58. Drop size distribution for 1.3% Shellsolv, $y/R_w = 0.1$, 16 ft/sec. | 127 |
| 59. Drop size distribution for 1.3% Shellsolv, $y/R_w = 0.4$, 16 ft/sec. | 128 |
| 60. Drop size distribution for 5% light oil, $y/R_w = 0.1$, 16 ft/sec. | 129 |
| 61. Drop size distribution for 0.6% light oil, $y/R_w = 0.4$, 16 ft/sec. | 130 |
| 62. Drop size distribution for 0.6% iso-octyl alcohol, $y/R_w = 0.1$, 16 ft/sec. | 131 |
| 63. Drop size distribution for 0.6% iso-octyl alcohol, $y/R_w = 0.4$, 16 ft/sec. | 132 |

LIST OF TABLES

| <u>Table</u> | | <u>Page</u> |
|--------------|------------------------------------------------------------------------|-------------|
| I | Mean diameters. | 26 |
| II | Summary of the experimental program. | 42 |
| III | Summary of D32X data. | 68 |
| IV | Mathematical models examined. | 89 |
| V | Empirical and theoretical average sizes. | 107 |
| VI | Complete picture quality, droplet distortion and average size data. | 134 |
| VII | Physical properties. | 137 |

DROP SIZE DISTRIBUTIONS PRODUCED BY TURBULENT PIPE FLOW OF IMMISCIBLE LIQUIDS

INTRODUCTION

Liquid-liquid dispersions are often encountered in industrial processes. The usual method of preparation of these dispersions is by subjecting the mixture to a laminar or turbulent flow field. Rational design of dispersed phase reactors and other dispersed phase contacting equipment requires a knowledge of the size distributions of the dispersed phase. When the major resistance to mass transfer is at the interface, mass transfer is affected by the character of the size distribution. Coalescence of the dispersion after processing is sensitive to the presence of very small drops in the dispersion. Momentum transfer in dispersed phase systems has also been shown to be size distribution dependent.

Previous studies of breakup in defineable fields of flow have been directed toward determining the factors influencing droplet breakup. An important result of these studies was the demonstration of the existence of a critical drop diameter below which drops are stable and the successful correlation of this maximum stable drop size to system parameters. Drop size distributions have been measured previously only in flow systems containing ill defined and variable regions of turbulence. Results of those studies indicated

that both breakup and coalescence played an important role in determining the observed size distributions.

The difficulties involved in measuring size distributions are probably responsible for the sparsity of experimental data. Recent work at Oregon State University resulted in the development of a photographic technique for the measurement of the drop size of distribution of liquid-liquid dispersions under turbulent flow conditions. One goal of the work described herein was to use this technique to measure the drop size distributions resulting from the action of the turbulent field produced by pipe flow of the liquids. Three different organic phases in water were studied. Distributions were measured as a function of distance from the inlet nozzle, radial distance from the wall, concentration, and flow rate. A second goal was to examine the distributions and draw conclusions from them regarding the nature of the mechanism of breakup in turbulent pipe flow. A mathematical model of the breakup process was developed for this purpose.

PREVIOUS WORK

Droplet Breakup

The splitting of liquid droplets while residing in various flow fields has been considered both theoretically and experimentally by several authors. Taylor (34) studied deformation and breakup in Couette and laminar hyperbolic fields. From the assumptions of small deformations and of no slip at the interface, he determined that the pressure drop across the interface of a nearly spherical drop was given by

$$\Delta P = -4G\mu_c \left[\frac{19 \mu_d/\mu_c + 16}{16 \mu_d/\mu_c + 16} \right] \cos 2\phi \quad (1)$$

where G is the velocity gradient in the flow field and ϕ is the polar angle measured from the y axis of either of the two flow fields described by the equations

$$\text{hyperbolic} \quad u = Gx/2 \quad v = Gy/2 \quad (2)$$

$$\text{Couette} \quad u = Gy \quad v = 0 \quad (3)$$

From a force balance between pressure forces given by Equation 1 and interfacial tension forces given by $4\sigma/D$, he showed that for small deformations ellipsoidal drops resulted. The deformation was given by

$$\text{Def.} = \frac{L-B}{L+B} = \frac{G\mu_c D}{2} \left[\frac{19 \mu_d/\mu_c + 16}{16 \mu_d/\mu_c + 16} \right] \quad (4)$$

where L and B were the lengths of the major and minor axes of the ellipsoid respectively. For small deformations Taylor obtained a rough experimental verification of Equation 4 by investigating the dependence of deformation on GD for three different systems.

Rumscheidt and Mason (26) extended Taylor's work in an extensive experimental program which verified Taylor's theory. Equation 4 may be rewritten in terms of the Weber number, the ratio of viscous forces to surface tension forces, to give

$$\text{Def.} = 1/2 N_{We} \quad (5)$$

Taylor (34) and Rumscheidt and Mason (26) also measured $(N_{We})_{crit}$, the value of N_{We} required for droplet bursting. For Couette flow Rumscheidt and Mason reported $(N_{We})_{crit} = 1.04 \pm 0.20$ for $00.0002 \leq \mu_d/\mu_c \leq 2.2$, but above $\mu_d/\mu_c = 3.8$ no breakup could be induced. These observations agreed with Taylor's except at low values of μ_d/μ_c where Taylor apparently failed to observe the release of small droplets from the main body of the drop. Rumscheidt and Mason observed the three classes of droplet distortion shown in Figure 1 for couette flow. Class A

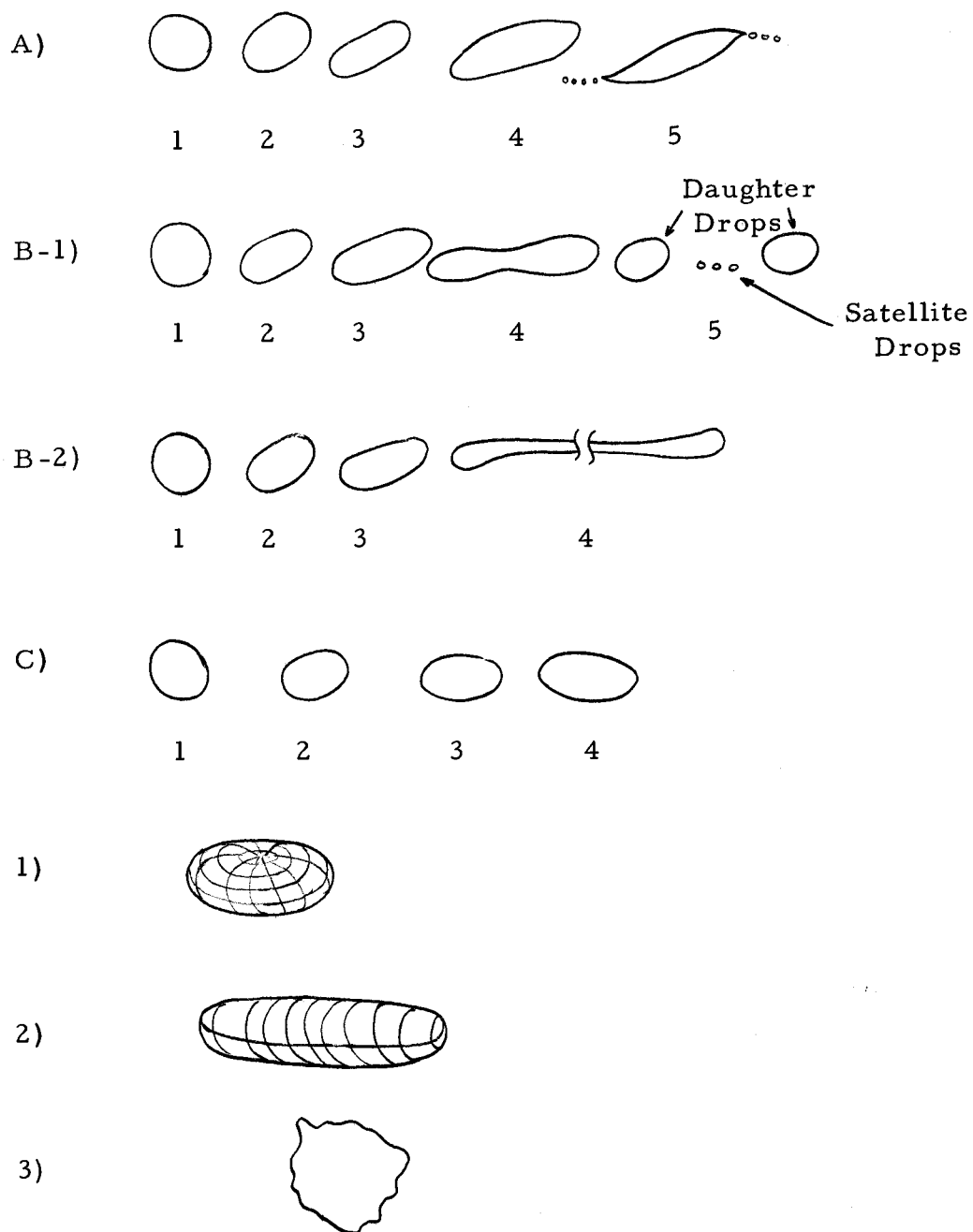


Figure 1. Modes of deformation and breakup.

deformation was observed for $\mu_d/\mu_c \leq 0.2$. Characteristically the droplet assumed a sigmoidal shape with pointed ends. Droplets with approximately 50 micron diameters were released from the pointed ends until $(N_{We})_{crit}$ was no longer exceeded after which the droplet assumed a spheroidal shape. Class B deformation was characterized by the formation of a dumbbell-shaped drop. Two subclasses were observed. Class B-1 resulted from the rapid thinning of the neck until two equal sized daughter drops and three satellite drops remained. If the neck extended until the initial drop became a long thread which then broke up into a large number of small droplets the deformation was class B-2. Class B deformation was observed for $0.03 \leq \mu_d/\mu_c \leq 2.2$. Class B-1 tended to the low end of the range and B-2 toward the high end of the range. It was also observed that systems which normally showed Class B-1 breakup would assume Class B-2 breakup if N_{We} were more than 10% higher than $(N_{We})_{crit}$. Above $\mu_d/\mu_c = 3.8$ Class C deformation occurred in which the droplet assumed a spheroidal shape that did not lead to fracture. Taylor (34) treated the limiting case of high viscosity ratio theoretically. He assumed interfacial tension forces resisting deformation were negligible compared to the viscous forces resisting deformation. For large N_{We} in Couette flow this lead to the prediction of a stable spheroid with a deformation given by

$$\text{Def.} = \frac{5}{4\mu_d/\mu_c + 6} \quad (6)$$

The existence of class C deformation is good qualitative proof of the theory. Quantitatively Rumscheidt and Mason (26) obtained deformation values 25-75% higher than those predicted by Equation 6.

For hyperbolic flow fields no such stability was predicted for systems with large μ_d/μ_c , and no stability was observed experimentally. The data of Taylor (34) and Rumscheidt and Mason (26) were limited in this case, but it indicated that $(N_{We})_{\text{crit}}$ was approximately 0.6 for $0.0002 \leq \mu_d/\mu_c \leq 20$. The deformation was class A for $\mu_d/\mu_c = 0.0002$ and class B-2 for $\mu_d/\mu_c \geq 1.0$. Insufficient observations were made to prove the existence of class B-1 deformation or to fix the position of the transition from class A to class B deformation.

Tomotika (35, 36) theoretically analyzed the instabilities of droplets distorted into long cylindrical threads similar to mode B-2. He was able to show that drops twice the diameter of the cylindrical thread were most likely. Rayleigh (23) showed that the same was true of a liquid jet. In an extension of Rayleigh's analysis, McDonald (as cited in 19, p. 7) showed that satellite drops 2.6 times smaller than the large drops were also predicted to result from the breakup of a liquid jet.

The breakup of droplets in turbulent fields has received theoretical treatment by several authors. Clay (6) was interested in both breakup and coalescence of droplets in turbulent fields. He proposed that drops could burst in a turbulent field by three possible mechanisms. The first mechanism was a laminar one such as Taylor had discussed earlier. The criterion for breakup in this case was written

$$C_a \approx \frac{2 \sigma}{D_{95} G} \quad (7)$$

where 95% of the total volume of the dispersed phase is found in drops with diameters less than D_{95} . C_a , a function of μ_d/μ_c , was measured by Taylor (34) to be from 7.0 at $\mu_d/\mu_c \gg 1$ to 0.8 for $\mu_d/\mu_c \ll 1$. The more recent results of Rumscheidt and Mason (26) indicate that C_a varies from 1.2 to 0.6 over the above range of viscosity ratios. Noting that Taylor had also expected turbulent shear to cause bursting, Clay proposed this as a second mechanism for droplet breakup and in this case stated that

$$C_a \approx \frac{2 \sigma \lambda}{D_{95} \mu_c \sqrt{u'^2}} \quad (8)$$

As a third possibility Clay proposed that breakup of droplets was due

to local turbulent pressure fluctuations. He reasoned that these pressure fluctuations would lead to local deformation of the droplet followed by the stripping of small fragments from the droplet and that this stripping should be most prevalent in the turbulent boundary layer where the intensity of the turbulent pressure fluctuations is the greatest. For this case

$$C_p \approx \frac{2\sigma}{D_{95}\sqrt{p'^2}} \quad (9)$$

where p' is the fluctuating component of the pressure.

Hinze (10) considered Taylor's experiment on breakup in laminar shear flow, the breakup of drops in an air stream and emulsification in a turbulent field and classified the deformation of drops into three types shown in Figure 1. Type one was lenticular or disc-shaped resulting from centrifugal forces on a rotating drop. Type two was an elongation of the drop corresponding to class B deformation observed earlier by Rumscheidt and Mason (26). Type three was bulgy deformation as proposed earlier by Clay (6). Hinze supposed all three types of deformation were present in turbulent field but that type two deformation was probably most prevalent.

Kolomogorov (14) and Hinze (10) independently developed the same expression for the critical Weber number of breakup in turbulent flow by dimensional arguments. Hinze from a consideration of

the forces acting on a drop, decided that the critical Weber number for a droplet splitting process should be a function of the viscosity group

$$N_{vi} = \mu_d / \sqrt{\rho_d \sigma} \quad (10)$$

He chose

$$(N_{We})_{crit} = C [1 + \psi(N_{vi})] \quad (11)$$

for the form of the function, where $\psi(N_{vi})$ decreases to zero as N_{vi} goes to zero and C is an experimentally determined constant.

He reasoned that viscous shear could not be responsible for breakup in turbulent fields as it had in laminar flow since not only the undeformed drop but also the deformed drop would have to be small compared to the local regions of viscous flow. This is not the case for droplet Reynolds numbers greater than one. Instead dynamic pressure forces due to velocity fluctuations over distances equal to the drop diameter were assumed responsible for deformation which gives

$$(N_{We})_{crit} = \frac{\rho_c U'^2 D_{max}}{\sigma} \quad (12)$$

U'^2 are the squared velocity differences between points D_{\max} distance apart averaged over the entire field. To find U'^2 isotropic homogeneous turbulence was assumed to exist. The main contribution to U'^2 will then be given by eddies whose wave numbers are distributed according to the Kolomogorov energy distribution law (Hinze (11), p. 189),

$$E(k, t) = C \epsilon^{2/3} k^{-5/3} \quad (13)$$

where E is the spectrum function for turbulent fluctuations, ϵ is the energy dissipation per unit mass and k is the wave number. From the definition of $E(k, t)$,

$$U'^2_k = \int_k^\infty E(k, t) dk \quad (14)$$

and Equation 13, it follows that

$$U'^2 = C_1 (\epsilon D_{\max})^{2/3} \quad (15)$$

If N_{vi} is assumed small compared to unity, Equation 11 after substitution of Equations 12 and 15 and rearrangement becomes

$$D_{\max} \left(\frac{\rho_c}{\sigma} \right)^{3/5} \epsilon^{2/5} = C \quad (16)$$

Levich (17, p. 457-464) reviewed Russian work. He treated the breakup of drops caused by the wall turbulence in a tube. As a starting point he used a logarithmic velocity profile for the wall region given by

$$U = \frac{u_*}{\sqrt{a}} \ln y/\delta_o \quad (17)$$

where u_* is the friction velocity, a is a constant, y is the distance from the wall and δ_o is the thickness of the laminar sublayer. With dynamic pressure forces given by ρU^2 and $D \ll y$ he showed that the difference in pressure on opposite sides of a drop of diameter D was given by

$$\Delta P = u_*^2 \rho \frac{D}{y} \ln y/\delta_o \quad (18)$$

A force balance on the drop lead to the result

$$D_{\max} \approx 1/u \left[\frac{\sigma y}{\rho \ln y/\delta_o} \right]^{1/2} \quad (19)$$

From the condition that the Reynolds number of a drop must be greater than ten for breakup to occur, Levich also predicted that the diameter of the smallest drop that could be produced by turbulent eddies was

$$D_{\min} = \frac{2\rho a^2 v}{\sigma} \quad (20)$$

where a is the same constant as found in Equation 17.

Clay (6) performed experiments on emulsion formation in turbulent flow fields in two different apparatuses. Most of his measurements were made in the turbulent field of flow in the space (width = 3/4", length = 1") between two coaxial cylinders, the inner one of which could be rotated. Measurements were also made in a flow loop constructed from four-inch pipe. The loop consisted of two parallel 22 foot straight sections of pipe connected by a 180° wide radius (2.8 feet) bend at one end and a centrifugal pump and two 90° wide radius (2.0 feet) bends at the other end. In the loop drop size measurements were obtained from photographs of the emulsion taken through an optical section mounted in the loop just prior to the 180° bend. Lens tubes with tapered caps projected through the pipe wall from opposite sides of the optical section and left a four mm gap about 3/4" in diameter along the center line of the pipe. Photographs were taken through the vertical depth (1") of the coaxial cylinder apparatus. The camera focal plane was located five mm below the top of the apparatus.

Clay's results consisted of tabulations of C (see Equations 7, 8, and 9), tabulations of the 95%, 50% and 10% points of the cumulative volume distribution curves and relative frequency

distribution curves for 100 to 300 drop sample sizes. The majority of his measurements were made in the coaxial cylinder apparatus which was not as cumbersome to operate as the loop. An additional difficulty with the loop was that the emulsion became polluted by rust particles as the liquids circulated. In the coaxial cylinder apparatus the range of investigation was μ_c from 0.6 to 10 cp, μ_d/μ_c from 0.3 to 30, σ from 1.0 to 49 dynes/cm, dispersed phase concentration from 0.9% to 4.8% and Reynolds number from 5000 to 10^5 . In the loop two systems were investigated. Water was the continuous phase in both cases. Liquid paraffin ($\mu = 60$ cp, $\sigma = 46$ dyne/cm, concentration 3.7% and 12%) and fusel oil ($\mu = 6.8$ cp, $\sigma = 4.9$ dyne/cm, concentration 2% and 5.5%) were the dispersed phases. Reynolds number was varied from 2.4×10^5 to 6.5×10^5 with liquid paraffin and from 0.5×10^5 to 1.1×10^5 for the fusel oil. Representative frequency distribution curves are shown in Figure 2. Curve one is for the coaxial cylinder apparatus, and curves two and three are for the loop apparatus. All of Clay's distributions exhibited a single mode skewed toward small drop diameters. Drop sizes ranged from 20 to 1200 microns in the coaxial cylinder apparatus and from 2 to 200 microns in the loop apparatus.

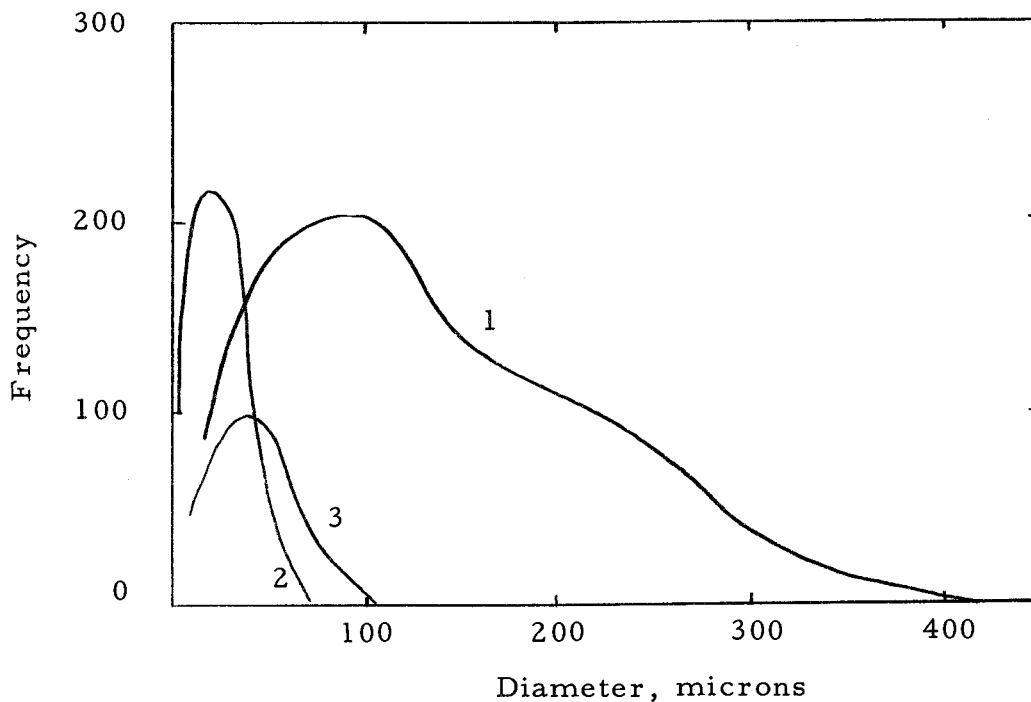


Figure 2. Representative drop size distributions measured by Clay (6).

Interpretation of Clay's results is difficult for several reasons. Characteristically emulsions were photographed after they had circulated for 20 to 60 minutes, and an equilibrium between breakup and coalescence had been established. Neither breakup nor coalescence are well understood, and the presence of both merely compounded the already difficult problem of interpretation. Clay attempted to separate the two phenomena by making a step change in the Reynolds number after equilibrium had been established and then observed the change in distribution after a short interval of time. He noted that breakup was a faster process than coalescence and reported qualitatively relative coalescence rates. Curves two and three in Figure 2

were typical of the change in the distribution curve in the pipe when the Reynolds number was decreased after equilibrium had been reached. The continuous phase was water and the dispersed phase liquid paraffin ($\rho = 0.88 \text{ g/cc}$, $\sigma = 46 \text{ dyne/cm}$). Curve two was observed after 22 minutes with a Reynolds number equal to 6.5×10^5 . Curve three was observed five minutes after the Reynolds number had been reduced to 4.2×10^5 . Clay attributed this change to what he termed cohesive coalescence in which the drops cling together for a period of time, while the liquid drains from between them, before coalescing. In the coaxial cylinder apparatus similar results were obtained.

The asymmetries of the flow systems lead to further problems in the interpretation of the results. Edge effects were important in the coaxial cylinder apparatus not only because the cylinders could not be assumed long but because the focal plane of the camera was only five mm from the lid of the apparatus. In addition the cylindrical geometry of the system generated vortices which added to the problem of describing the flow field. In the loop apparatus, the pump and the pipe bends created regions of high turbulence with vortices between the relatively low turbulence of the two straight pipe sections. Clay felt that the turbulence was most intense in the pipe bends and that they were more influential in the breakup process than the pump. Realizing these deviations from ideality and the

futility of trying to describe them, Clay ignored them and gave the following results for the coaxial cylinder apparatus:

$$C_a \approx \frac{2\sigma}{D_{95} \tau_w} \quad (21)$$

for the laminar mechanism,

$$C_a \approx \frac{2\sigma N_{Re}^{1/2}}{D_{95} \rho \omega^2 R_1^2} \quad (22)$$

for the turbulent shear mechanism and

$$C_p \approx \frac{2\sigma}{D_{95} \rho \omega^2 R_1^2} \quad (23)$$

for the pressure fluctuation mechanism where ω is the angular velocity in radians of the inner cylinder of radius R_1 .

The values of C_a calculated from the data were generally an order of magnitude higher than those measured by Rumscheidt and Mason (26) and appeared to show no dependence on N_{Re} although the data was quite scattered. This evidence together with the fact that Clay observed very few distorted drops lead him to favor the turbulent pressure fluctuation mechanism for droplet breakup.

Hinze (10) rearranged Equation 16 into the form

$$\frac{\rho_c \sigma D_{95}^2}{\mu_c} = 0.725 \left[\frac{\mu_c^5 \epsilon}{\rho_c \sigma^4} \right]^{2/5} \quad (24)$$

in order to test his theoretical result with Clay's data. A log-log plot of the data as $\rho_c \sigma D_{95}^2 / \mu_c^2$ vs $\mu_c^5 \epsilon / \rho_c \sigma^4$, though scattered, fit Equation 23 fairly well. (standard deviation = 0.315.)

From Equation 23 Hinze calculated $(N_{We})_{crit} = 1.2$. This value is close to that measured by Rumscheidt and Mason (26) for breakup by viscous shear in a couette flow field.

Experiments conducted by Baranayev, Teverovskiy and Tregubova (2) were designed to study the drop sizes formed when a jet of liquid (0.2 cm in diameter, $\mu = 1$ cp) was injected coaxially into a turbulent stream of water flowing in a glass tube 1.5 cm in diameter. Minimum drop sizes and Sauter mean diameters, D_{32} , (Equation 30) observed 113 tube diameters from the jet inlet were reported as a function of Reynolds number. The minimum diameter decreased from 2.4 microns to 1.2 microns while D_{32} decreased from 280 microns to 140 microns as the Reynolds number was increased from 1.7×10^4 to 4.5×10^4 . Levich (17) compared this data to theoretical formulas. He felt that the minimum drop diameter compared favorably with the theoretical result of four

microns given by Equation 20 for a Reynolds number of 4.6×10^4 .

The data also indicates that D_{32} decreases more slowly than as is inferred by Equation 19. Levich felt it "...very important to conduct more accurate measurements of the dependence of drop size distribution on the velocity of the liquid".

A paper by Sleicher (31) cleared up some of the questions posed by theoreticians. Sleicher measured the Reynolds number which caused only 20% of a group of equal diameter drops to break up in a turbulent field. He called this diameter the maximum stable drop diameter, D_{\max} , for the corresponding Reynolds number. Experiments were performed in a 1.5 inch ID pipe 48 feet long. A transient method of operation was employed in which drops were first injected into the pipe containing the continuous phase; and then by throwing a lever valve, the mixture was rapidly accelerated to the critical velocity and allowed to travel the length of the pipe. The effect of acceleration was observed to be negligible since no breakup was observed in the first five feet of pipe where acceleration took place. Percent breakup was determined by photographing the population as it passed a point 39 feet from the dispersed phase inlet. Tap water was used for the continuous phase in most of the experiments. The range of dispersed phase properties considered was $0.5 \text{ cp} \leq \mu_d \leq 32.1 \text{ cp}$ and $0.78/\text{cc} \leq \rho_d \leq 1.69/\text{cc}$. Interfacial tension varied from 1.8 to 45 dyne/cm. Dispersed phase

concentration was held below 0.5% to eliminate coalescence except in a few cases when a surface active agent was added to water, and concentrations were increased to 1.7%.

From dimensional analysis Sleicher determined that his results might be correlated by the relation

$$\frac{D_{\max} \rho_c U^2}{\sigma} = B \left(\frac{\sigma}{\mu_c U} \right)^b \quad (25)$$

A log-log plot of D_{\max} vs U revealed a good fit for a straight line of slope -2.5 indicating that the exponent b equals 1/2. This value for b was further confirmed by a log-log plot of D_{\max} vs $\frac{\sigma}{\mu_c U}$ which gave a slope of 1.5.

To compare his data with the Hinze-Kolomogorov Equation (Equation 16), Sleicher rearranged it into the form

$$D_{\max} \left[\frac{\rho_c}{\sigma} \right]^{3/5} \left[\frac{U^3}{D} \right]^{2/5} \left[\frac{DU\rho_c}{\mu_c} \right]^{-4/25} = 1.9 \quad (26)$$

The proportionality of D_{\max} to $V^{-1.12}$ and $\sigma^{0.6}$ as indicated by Equation 25 was in sharp disagreement with his data.

In order to reconcile this result with Hinze's (10) earlier fairly good fit of the Hinze-Kolomogorov equation by Clay's data, Sleicher concluded that Hinze's choice of coordinates was misleading with respect

to the relation between D_{95} and ϵ since almost all of the change in the coordinates was caused by variation of the physical properties not D_{95} and ϵ . A log-log plot of D_{95} vs U for Clay's data revealed lines of best fit with slopes of -2.5 which agree with Equation 24 but not with Equation 25. Sleicher regarded the fit of Clay's data to Equation 24 as accidental due to coalescence and the complicated nature of the turbulence in the field between the two cylinders.

To explain why the Hinze-Kolomogorov equation did not fit the data, Sleicher noted that homogeneous isotropic turbulence was one of the underlying assumptions in its derivation, but that in every case he had observed breakup only very close to the wall where the turbulence was least homogeneous and least isotropic. In high speed motion pictures of drops moving 15% faster than required to make them unstable, two types of breakup were seen. The most prevalent was breakup into two approximately equal drops after having been deformed to a shape similar to that shown in Figure 1 for class B-1 deformation in laminar shear flow. A second breakup mechanism resulted in the stripping of a small drop from a larger one. This type of breakup was less frequent than the first and Sleicher thought it improbable for a marginally unstable drop.

To account for dispersed phase viscosity effects, Sleicher used Equation 11 with $N_{vi} = \mu_d U / \sigma$ which gave

$$\frac{D_{\max} \rho_c U^2}{\sigma} \sqrt{\frac{\mu_c U}{\sigma}} = 38 \left[1 + 0.7 \left(\frac{\mu_d U}{\sigma} \right)^{0.7} \right] \quad (27)$$

This equation correlated all the data within 35%. A subsequent study by Paul and Sleicher (21) revealed that C in Equation 26 was proportional to the 0.1 power of the pipe diameter. In a review of the work of Baranayev et al. (2), Paul and Sleicher pointed out that for flow conditions in which Baranayev observed continuing breakup, they found no breakup for drops five times as large in a pipe six times as long. High coalescence rates coupled with breakup of the resulting drops were given as the probable causes for this discrepancy.

Bromfield and Sleicher (3) supplemented Clay's data on breakup in a coaxial cylinder apparatus by measuring maximum stable drop sizes in an apparatus which confined the flow between an inner rotating cylinder (diameter 21 cm and length 60 cm) and a fixed outer cylinder (diameter 28 cm). The D_{\max} for a given flow condition was determined by photographing the drops resulting from exposure of a 0.33% mixture of two phases to the flow condition for a predetermined time (0.5 to 20 minutes). The variables, interfacial tension (15.0 to 42 dynes/cm) and velocity of the inner cylinder ($1.85 \leq N_{Ta} \leq 580$), were studied. N_{Ta} is the Taylor number defined by

$$N_{Ta} = \frac{\rho_c U t}{\mu_c} \left[\frac{t}{R_1} \right]^{1/2} \quad (28)$$

where R is the radius of the inner cylinder and t is the width of the annular space between the cylinders. Results were correlated quite well for Taylor numbers less than 580 by

$$(N_{We})_{crit} = \frac{D_{max} U^{3/2}}{\sigma} N_{Ta}^{1/2} = 14. \quad (29)$$

Clay's data (6) showed D_{95} to be approximately five times as large as that predicted by Equation 29. The difference is unexplained.

Ward (38, p. 144-159) in a study of the momentum transfer characteristics of liquid-liquid dispersions presented observations on the effect of dispersed phase viscosity and concentration on drop size distributions. Because his flow system contained a turbine pump, a stirred tank and numerous bends in the piping, he made no attempt to study quantitatively the genesis of the distributions he observed. Organic phases with viscosities of 1, 15, and 200 centipoise were studied when mixed with water at concentrations from 1 to 50 volume percent. Interfacial tensions ranged from 48 to 52 dynes/cm. Drop size distributions with dispersed phase viscosity equal to one centipoise were bimodal with peaks of equal height at

approximately 25 and 50-70 microns except for low concentrations which gave a single lower peak. Thus it was postulated that the lower peak characterized the breakup process and the other peak characterized the coalescence process. As dispersed phase viscosity increased the distribution spread both in position of the peaks and in width of the peaks. With dispersed phase viscosity equal to 15 centipoise and a concentration of 20%, this shift resulted in a broad low peak at 110 microns and a peak five times as high at about 15 microns. The distribution had a single peak at about ten microns when the dispersed phase viscosity was increased to 200 centipoise. Ward explained this behavior by proposing that breakup was predominately by splitting into two approximately equal sized drops when the dispersed phase viscosity was low, but that as dispersed phase viscosity increased breakup by the stripping of a small drop from a large one was favored.

Description of Drop Sizes

It is a well-known fact that populations of small particles contain a range of sizes. In a specific problem, knowledge of one or more of the various types of average sizes is sometimes sufficient, but often the complete size information offered by the size-distribution itself is required. Empirically such size-distributions can be found by dividing the size range of the population into a number of

increments and then counting the number of particles which fall into each interval. If the fraction of the total count which is found in an interval is plotted against the average size of the particles in the interval, a frequency diagram or histogram results. In the limit, as the number of particles becomes very large and the size of the increments very small, the histogram becomes a continuous curve, $f(x)$, called the size-distribution of x .

Mugele and Evans (20) gave a general equation

$$D_{qP}^{q-p} = \frac{\int_0^{\infty} D^q f(D) dD}{\int_0^{\infty} D^p f(D) dD} \quad (30)$$

for computing the common average sizes from a knowledge of the distribution function. The significance of the various mean diameters is shown in Table 1 due to Mugele and Evans.

Table 1. Mean Diameters

| | Name of mean diameter | Field of application |
|----------|-----------------------|--------------------------------------|
| D_{10} | Linear | Comparisons, evaporation |
| D_{20} | Surface | Surface area controlling, absorption |
| D_{30} | Volume | Volume controlling, hydrology |
| D_{21} | Surface diameter | Adsorption |
| D_{31} | Volume diameter | Evaporation, molecular diffusion |
| D_{32} | Sauter | Efficiency studies, mass transfer |

Size-distribution may also be generalized to include those where $f(D)$ is weighted by length, surface or volume. When $f(D)$ is known only in the form of a histogram, the conversion can be handled by a method due to Wise (39). He pointed out that the grouping of particles into intervals made it impossible to perform an accurate conversion directly because the size of the particle which should be used to represent the group of particles in the interval was ambiguous. However, he showed that the conversion could be made with no difficulty if it were formulated as

$$W_p(r_1) = \frac{r_1^p F(r_1) + p \int_{r_1}^{\infty} r^{p-1} F(r) dr}{r_0^p + p \int_{r_0}^{\infty} r^{p-1} F(r) dr} \quad (31)$$

where $W_p(r_1)$ is the cumulative fraction of the total number of particles weighted to an order p found above the size r_1 , r_0 is a size less than the smallest size observed, and

$$F(r_1) = \int_{r_1}^{\infty} f(r) dr. \quad (32)$$

The advantage results from the fact that $F(r_1)$ need only be known at the boundaries of intervals.

Early attempt to find size-distribution functions were directed toward the discovery of empirical distribution laws often having little or no theoretical basis. A few representative examples are cited below.

Green (9) used the normal distribution described by

$$f(x) = \frac{1}{\sqrt{2\pi}\sigma} e^{-\frac{(x - \bar{x})^2}{2\sigma^2}} \quad (33)$$

to represent the size distributions of $Z_n O$ particles where \bar{x} is the mean, σ is the standard deviation of the population and $f(x)$ is the probability that a size x occurs in a population.

Kottler (15) pointed out that Galton had warned as early as 1887 of

the contradiction involved in the use of the normal distribution to represent size-distributions. He observed that Equation 33 implied the existence of sizes less than zero. To correct this absurdity Galton proposed the use of the log-normal distribution given by

$$f(x) = \frac{1}{xs\sqrt{2\pi}} e^{-\frac{(\ln x - \ln \bar{x})^2}{2s^2}} \quad (34)$$

where s is the geometric standard deviation of the population.

Rossi and Rammler (25) correlated size distribution of powders with a strictly empirical function that bears their names. It is usually written in the form

$$v(x) = 1 - e^{-(x/a)^\delta} \quad (35)$$

where $v(x)$ is the cumulative volume fraction undersize, δ is a dispersion parameter and a is a size parameter.

The Nukiyama and Tanasana equation (as cited in 19)

$$f(x) = bx^m e^{-cx^\delta} \quad (36)$$

represents a generalization of Equation 35. m is usually taken as two, and b is a normalization constant. c and δ are determined empirically.

Tate and Marshall (33) found empirically that the square roots of the diameters of drops emerging from a pressure nozzle were distributed normally. Thus the distribution function had the form

$$f(x) = \frac{1}{2\sqrt{2s\pi x}} e^{-\frac{(\sqrt{x} - \sqrt{\bar{x}})^2}{25}} \quad (37)$$

Intuitively Mugele and Evans (20) proposed that experimental data on sprays be fit with an upper-limit function in which the parameter y defined by

$$y = \ln \frac{aD}{D_{\max} - D} \quad (38)$$

is distributed normally where D_{\max} is a maximum drop size and a is a constant. They compared the upper-limit distribution with those given by Equations 5, 6 and 7 for several sets of data taken from the literature. They found that the upper limit equation gave the proper trend in all cases as well as a good quantitative fit. Mixed results were found for the other equations so it was concluded that the upper limit equation should be accepted as the most accurate.

Epstein (7) described a statistical model of a breakage mechanism which leads to a log-normal distribution. He pointed out that Kolomogorov and Halmos had earlier treated similar

problems but that their treatments were sketchy and difficult to interpret as physical models. As a first hypothesis Epstein proposed that it is meaningful to talk about a breakage event--that any breakage process may be considered to be made up of discrete steps. Second he hypothesized that the probability of breakage was independent of the size of the piece, the presence of other pieces and the number of previous breakage steps. The third was that the distribution of daughter pieces was independent of the size of the parent. Epstein then proved with the help of the central limit theorem that the distribution after a large number of breakage events approached a log-normal distribution. Epstein also noted that his hypotheses may not be unique in their ability to produce a log-normal distribution but did not explore the problem further. In a later paper (8), Epstein reiterated the arguments mentioned above and made calculations which showed that for the case of equal-binary breakup, a log-normal distribution was indeed obtained when his hypotheses were satisfied.

Both Kottler (15) and Rajagopal (22) have considered the problem further. By drawing parallels between the exponential law of decay and the breakup process and assuming that time, not a size dimension, was normally distributed, Kottler showed that a log-normal size distribution resulted. Similarly he independently arrived at the upper-limit equation of Mugele and Evans. Rajagopal

postulated a collision mechanism for breakup of droplets in a turbulent field. He showed under the hypotheses that only a finite number of daughter droplets can be produced in any finite interval of time, that the probability of very big or very small daughter droplets is very small and that when distribution of daughter droplets is independent of time and size of the parent drop, a log-normal distribution resulted.

Kottler (15) and Rajagopal (22) both pointed out the pitfalls involved in the use of log probability paper in the fitting of data to the log-normal distribution. They warned that although the distribution should appear as a straight line, the errors, both statistical and experimental, are magnified at both ends of the non-linear probability scale. Rajagopal recommended that all points above 99% and below 1% be ignored completely and that those above 85% and below 15% be given reduced weight.

Swartz and Bezemer (27) theoretically derived what they called the Amsterdam distribution equation. They derived a general expression for the probability that a given size interval contains n particles. Then they hypothesized that intervals of equal surface to volume ratio be used and that the total surface generated by a given emulsification process was a constant. The most probable distribution was

$$v = Ve^{-(a/D_{\max} - a/D)} \quad (39)$$

where v is the cumulative volume below size D , V is the total volume, D_{\max} is the maximum drop size and a is a constant. Swartz and Bezemer compared the Amsterdam distribution to the Rossi and Rammler distribution and the log-normal distribution for several sets of data taken from the literature. They concluded on the bases of goodness of fit and of the ability of the distribution function to predict average diameters, that the Amsterdam distribution was in general slightly superior to the log-normal distribution, but they were both far superior to the Rosin-Rammler distribution.

Valentas, Bilous, and Amundson (37) undertook the development of a mathematical model which related the steady state size distribution of a dispersion to the breakup process in a perfectly mixed tank. With the assumption of no coalescence, they showed that simultaneous mass and number balances on the vessel lead to an integral equation of Volterra type

$$NA(m) = \frac{n_A A(m)}{f(m) + g(m)} + \frac{1}{f(m) + g(m)} \int_m^L v(\mu) g(\mu) \beta(\mu: m) NA(\mu) d\mu \quad (40)$$

where the variables are defined as follows:

1. N = the total number of drops in the vessel.
2. $A(m)$ = the fraction of drops in the vessel with a size between m and $m+dm$.
3. n_A = the number rate of drops in the feed.
4. $f(m)$ = the fraction of the droplets in the vessel with a size between m and $m+dm$ flowing out per unit time.
5. $g(m)$ = the fraction of drops with size between m and $m+dm$ which breakup per unit time.
6. $\nu(m)$ = the average number of daughter droplets.
7. $\beta(m:\mu)d$ = the fraction of droplets with mass between μ and $\mu+d\mu$ formed by breakup of a droplet of mass m .
8. L = the upper size limit in the effluent and the vessel.

The size distribution was shown to be very sensitive to the breakage kernel, $\nu(\mu)g(\mu)\beta(\mu:m)$. An increase in the number of daughter droplets produced by each breakage decreased the spread of the distribution and moved the mode to a lower value. The incorporation of a maximum stable drop size shifted the mode of the distribution markedly toward the maximum stable drop size at least in the case of binary breakup.

Measurement of Drop Size Distributions

Drop size distribution is one of the most difficult properties of a dispersion to predict theoretically or to measure experimentally. A variety of experimental techniques have been devised by previous investigators, but no one method has been found which allows the rapid accurate determination of drop size distributions containing a wide range of diameters.

Langloise, Gullberg and Vermeulen (16) proposed that a light transmittance technique involving the use of a photocell be employed to measure the Sauter mean diameter, D_{32} of a coarse emulsion generated in a stirred tank. They noted that the ratio of incident to transmitted light was given by

$$I_o/I = BD_{32} + 1 \quad (41)$$

where B is a constant depending on refractive indices and geometry but relatively independent of drop size distribution and volume fraction of the dispersed phase. Rodger and Trice (24) later designed a light transmittance probe which was less sensitive to changes in geometry than the probe used by Langloise et al. (16). They claimed to be able to measure D_{32} within ten percent of the value obtained from photographs of a dispersion in a stirred tank containing drops with diameters ranging from 50-2000 microns. Roy

and Rushton (as cited in 24) and Kessie and Ruston (as cited in 31) later used similar probes to measure D_{32} in a pipe. Scott, Hayes and Holland (20) measured D_{32} downstream of an orifice mixer by the same method. Cengle et al. (5) studied the effects of flow rate, mixing time and dispersed phase concentration on light transmittance. Their measurements were made in a flow system similar to Ward's with a commercial solvent (Shellsolv 360) dispersed in water. Light transmittance was shown to be independent of the flow rate and independent of mixing time after ten minutes of circulation. Their results indicated that in the range zero to five percent solvent, light transmittance might be used to measure concentration of dispersed phase but above five percent the method becomes insensitive to concentration changes. Subsequent photographic measurements of the drop sizes by Ward (38, p. 155) indicated that a large percentage of the drops were below 50 microns in diameter. He pointed out that the apparent insensitivity to changes in drop size and distribution was probably due to the fact that the drop sizes were approaching the lower limit of the light transmittance method as set by the condition that the drops must be much larger than the wavelength of the incident light (0.6 microns).

Lloyd (18) determined average diameters of colored emulsions by reflectance. He found that reflectance of incident light was related to D_{32} by

$$R = CD_{32}^{-k} \quad (42)$$

where C and k must be determined experimentally. His measurements were made with concentrations of 50 percent by volume with a range of D_{32} from 2.5 to 60 microns.

A light scatter technique developed by Sloan, which locates the mode of a distribution and also gives a semi-quantitative measure of size range, was used by Sullivan and Lindsey (32) to study dispersion in a stirred tank. The method depends on the fact that the scattering angle for incident light is dependent on the diameter of the drop that scatters it. In practice a sample of the emulsion was pumped through a cell external to the tank where a thin layer of emulsion scattered the incident light beam. For valid results, light transmittance must be between 40 to 80 percent, and the drops must range in size from 1 to 50 microns.

Baranayev, Teverovskiy and Tregubova (2) used direct microscopic examination of unstable emulsions to determine drop size distributions, a method normally reserved for stable emulsions and solid particles. Coalescence was minimized by equalizing the densities of the two phases and by careful collection of samples. Freezing of a low-melting wax dispersed phase to prevent coalescence during and after sampling was employed by Shinnar (29). Actual size distributions were measured from photomicrographs of the

solidified drops. By the same method Shinnar also achieved a measure of coalescence by injecting a small amount of colored wax into the system and noting the relative number of drops which had been lightened in color due to dilution with the uncolored wax.

Direct photography of a flowing liquid-liquid dispersion has been employed by several investigators. Large drops (diameter > 200 microns) at low concentration present no inherent photographic difficulties. Kinter et al. (13) presented a review of many techniques which had been adapted to bubble and drop research. Brown and Govier (4) used a Fastax high-speed motion picture camera to study the motion of large (diameter 6000 to 12000 microns) oil drops in water flowing upward in a tube at low flow rates. Sleicher took both still pictures and high-speed motion pictures of drops (diameter 2000 to 8000 microns) at very low concentrations.

Ward (38, p. 51) pointed out that the following difficulties arose when concentration increased and drop size decreased:

1. Light transmittance of the dispersion decreases with increasing concentration and decreasing drop size.
2. Magnification by the camera magnifies the speed of the droplet image relative to the negative necessitating very short exposure times.
3. Droplet images may be distorted by the layer of droplets between the plane of focus and the lens.

4. Any distortion of the flow field necessary to meet conditions one and three must be accomplished without changing the shape or size of the dispersed drops.

Clay (6) was able to obtain satisfactory photographs of his dispersions by keeping concentrations below five percent. In his coaxial cylinder apparatus, the focal plane of his camera was located five millimeters into the dispersion, and the light was transmitted through approximately one inch of liquid. Drops with diameters from 20 to 1200 microns were observed. In his pipe loop dispersions were photographed as they passed through a four millimeter gap formed by two lens tubes which projected from the walls of the pipe. Drops from 2 to 200 microns in diameter were observed in the pipe. Scott et al. (28) photographed a water in kerosene dispersion (diameter 20 to 250 microns) as it flowed between windows placed in a flattened section of pipe designed to maintain a constant cross-sectional area for flow as the gradual transition from round to flat to round was accomplished. Ward (38, p. 61-68) developed a photographic section which allowed him to photograph drops (diameter 1 to 800 microns) in dispersed phase concentrations up to 50% by volume while they were flowing at velocities up to 16 feet per second. Because of the low transmittance of concentrated dispersions, he found it necessary to provide a better light path through the dispersion than the dispersion itself. A 1/8 inch glass rod projecting through

the tube wall into the flow stream provided such a path for the light which was produced by a strobe with a 1.2 microsecond duration and an intensity of 2.2 million candlepower. Photographs were taken through a flat glass window in the pipe wall with a 35 millimeter camera mounted on a microscope. The focal plane of the microscope was located two to five millimeters from the inside surface of the window. Ward used an image-to-print magnification of 120 in most cases but found that it was necessary to double the magnification to 260 at high concentrations thus reducing the depth of field and the number of drops that were in focus. He found that prints on Kodabromide F-5 paper made from Tri-X negatives gave good results. He also determined that the presence of the glass rod in the flow stream did not change the distributions significantly.

Elimination of the long, tedious effort needed to obtain drop size distributions from photographs has also received some attention. Adler et al. (1) used the sweep of a narrow light beam and a photocell to measure drop size distributions from photographic negatives. As the negative was successively swept with the light beam, the photocell generated random pulses. Statistical analysis of the resulting pulses was shown to result in drop size distribution close to those measured directly from photographs. The principle difficulty with the method is that it cannot discriminate between images which are in focus and those which are out of focus. Until

this obstacle is overcome, laborious measurement of large numbers of individual droplets from photographs appears to be the best method available for the determination of drop size distribution of unstable liquid-liquid dispersions.

EXPERIMENTAL PROGRAM

The primary goal of the experiments to be described was to characterize the drop size distributions formed when a liquid-liquid dispersion was exposed to turbulent pipe flow. Previous investigators (6, 38) have determined distributions in turbulent flow systems, but the test apparatus has included pumps, tanks, and pipe bends all of which have unknown effects on the distribution and thus create very difficult problems of interpretation.

A summary of the experimental conditions under which distributions were measured is given in Table II. Three organic phases with a viscosity ranging from 1 to 17 centipoise and an interfacial tension ranging from 13 to 40 dynes/centimeters were used. The majority of the measurements were made with Shellsolv which had a viscosity of 1 centipoise and an interfacial tension of 40 dynes/centimeter. In addition to studying the effect of physical properties, dispersed phase concentration ($0.6 \pm 10\%$), nozzle size ($3/16''$, $1/4''$ diameter), flow rate (14 to 20 ft/sec), distance from the nozzle (27 to 576 pipe diameters) and radial distance from the wall ($y/r = 0.05, 0.1, 0.4$) were investigated. Of these variables, the last two were studied most extensively.

Table II. Summary of the experimental program.

| Dispersed phase (Run CODE) | Conc. (Vol%) | Nozzle size (in) | Flow rate (ft/sec) | Linear position (floor)* | | | | Radial position (y/R_w) | | |
|----------------------------------|-----------------|------------------------|--------------------------|--------------------------------|---|---|---|-----------------------------------|----|----|
| | | | | 3 | 2 | 1 | B | .05 | .1 | .4 |
| Shellsolv | | | | | | | | | | |
| 1SS | 0.6 | 3/16 | 14 | | | x | | | | x |
| 2SS | " | " | 16 | x | | x | | x | x | x |
| 3SS | " | " | 20 | | | x | | | x | |
| 4SS | 1.3 | " | 14 | | | x | | | x | x |
| 5SS | " | " | 16 | x | x | x | x | x | x | x |
| 6SS | " | " | 18 | | | x | | | x | x |
| 7SS | " | " | 20 | x | | | | x | x | x |
| 7SS | " | " | 20 | | | x | | | x | x |
| 8SS | 5 | " | 16 | x | | | | x | x | x |
| 8SS | " | " | " | | x | | | | | x |
| 8SS | " | " | " | | | | x | | x | |
| 9SS | 1.3 | 1/4 | " | x | x | x | | | x | x |
| 10SS | 5 | " | " | x | | | | x | | |
| 10SS | " | " | " | | x | | | x | x | |
| 10SS | " | " | " | | | x | | | x | x |
| 10SS | " | " | " | | | | x | | x | |
| 11SS | 10 | " | " | x | x | | | x | x | |
| 11SS | " | " | " | | | x | | x | x | x |
| 11SS | " | " | " | | | | x | x | | x |
| Light Oil | | | | | | x | | | | x |
| 1LO | 0.6 | 3/16 | " | x | | | | x | | |
| 1LO | 0.6 | " | " | | x | | | x | | x |
| 2LO | 5 | " | " | x | | | x | x | x | |
| 2LO | 5 | " | " | | x | | | x | | x |
| Iso-Octanol | | | | | | | | | | |
| 1OA | 0.6 | " | " | x | | | x | x | x | x |
| 2OA | 1.3 | " | " | x | | | x | x | x | x |
| 2OA | 1.3 | " | " | | x | | | x | | x |
| 3OA | 5.0 | " | " | | x | | | x | | |

*Distances from the nozzle to the window were as follows:

3 - 27.1 pipe diameters

2 - 209 pipe diameters

1 - 421 pipe diameters

B - 576 pipe diameters

EXPERIMENTAL APPARATUS

The experimental apparatus used in this study is shown schematically in Figure 3. The apparatus was designed to produce through turbulent pipe flow an unstable dispersion of immiscible liquids and to allow the dispersion to be photographed at intervals along the length of the pipe as well as at varying distances from the pipe wall. Separate pumping of the water and organic phases was provided to eliminate dispersion caused by the high shear in a pump. Flanges in the test section allowed the photographic window to be mounted at various locations along the length of the test section. The narrow focal plane of the camera-lens system located a sufficient distance from the lens surface permitted photographs to be taken at varying distances from the tube wall.

Tap water was used as the continuous phase in all experiments. Three organic liquids were used for the dispersed phases. They were Shellsolv 360, Standard of California White Oil Number One and a commercial grade iso-octyl alcohol (Chipman Chemical Co., Portland, Oregon). The physical properties of these liquids and the methods used to determine them are included in the appendix.

Flow System

The large combination storage and settling tank, A, was constructed from a galvanized iron culvert pipe two and one-half feet in

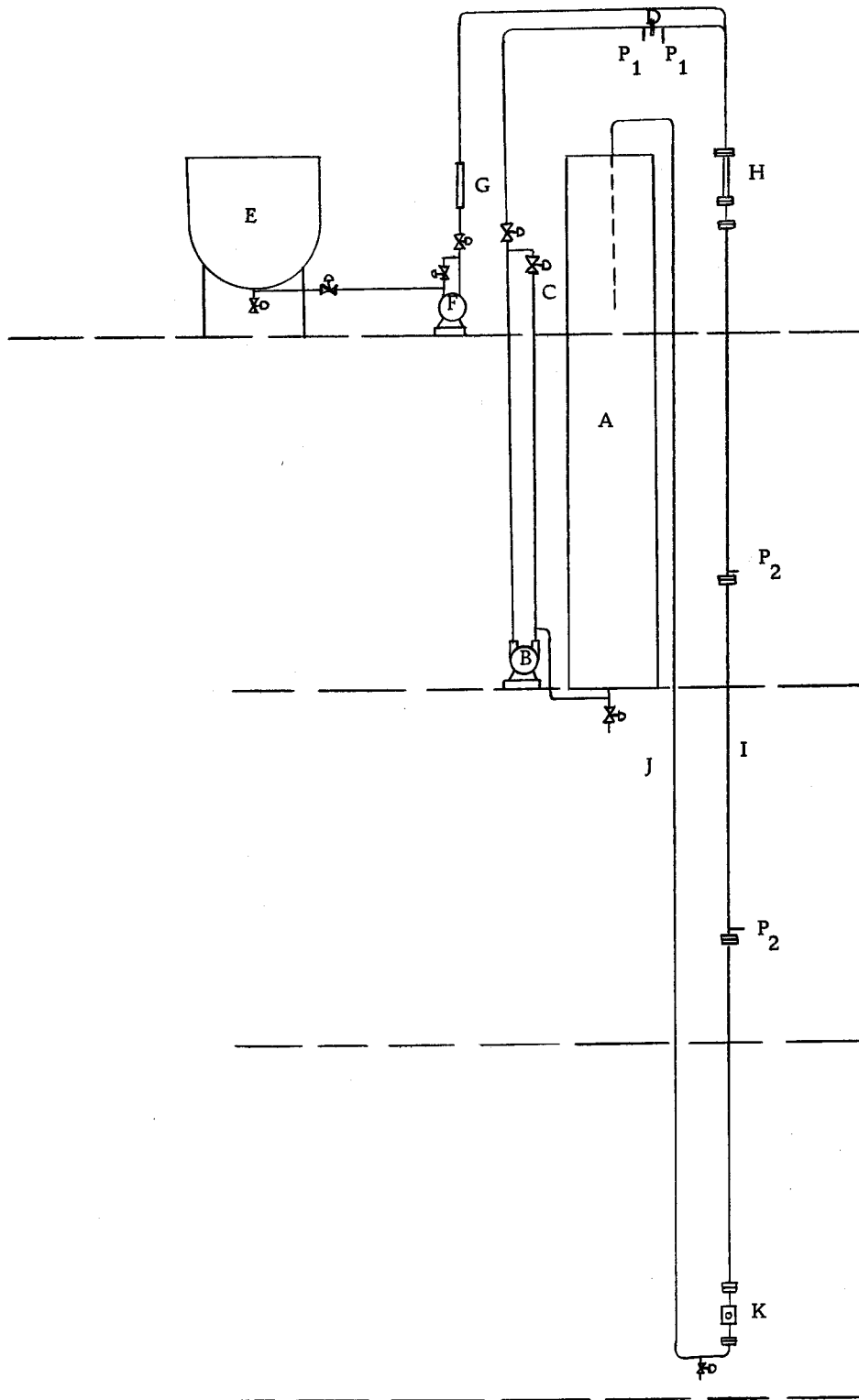


Figure 3. Flow system schematic

diameter and sixteen feet long. The inside of the tank was coated with tygon paint, type TP-81, purchased from Central Scientific Company. The resulting tank had a working capacity of 300 gallons of liquid.

Mounted at the base of the storage tank was a Worthington type TC brass turbine pump, B, equipped with a mechanical seal and powered by a 7-1/2 hp 1750 rpm electric motor. The water flow rate to the test section was controlled by a motor operated valve, C, on the by-pass line and was measured with a calibrated orifice meter, D,

The organic phase was stored in a 100 gallon stainless steel tank, E. A small gear pump, F, with a by-pass line provided a stable, easily controllable flow of organic phase to the mixing jet. A Stabl-Vis Rotameter, G, manufactured by the Fischer & Porter Company was used to measure organic phase flow rates. Two interchangeable rotameters were used, one for high flow rates and another for low flow rates.

Two mixing jets of 1/4 and 3/16 inch OD were constructed from thin wall stainless steel tubing as shown in Figure 4. All connections were made with silver solder, and all joints and edges were carefully machined to eliminate any lips or protrubances which might have disturbed flow past the jet. A 9-1/2 inch section of 0.745 inch ID transparent plastic pipe, H, was installed in place of the red brass

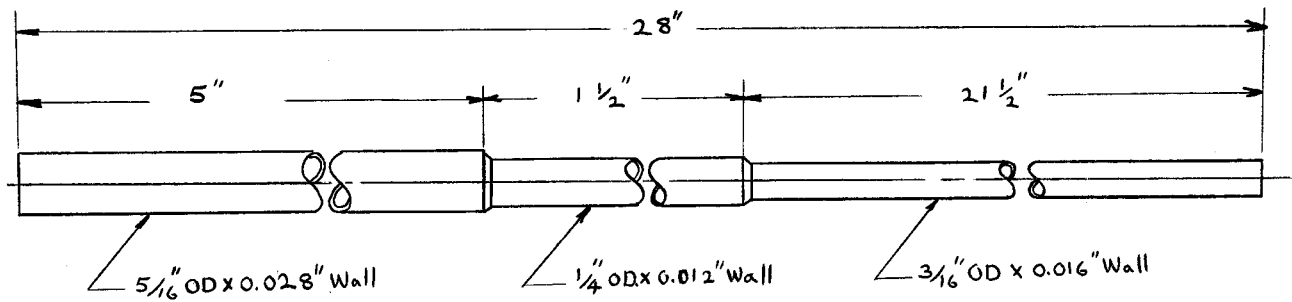
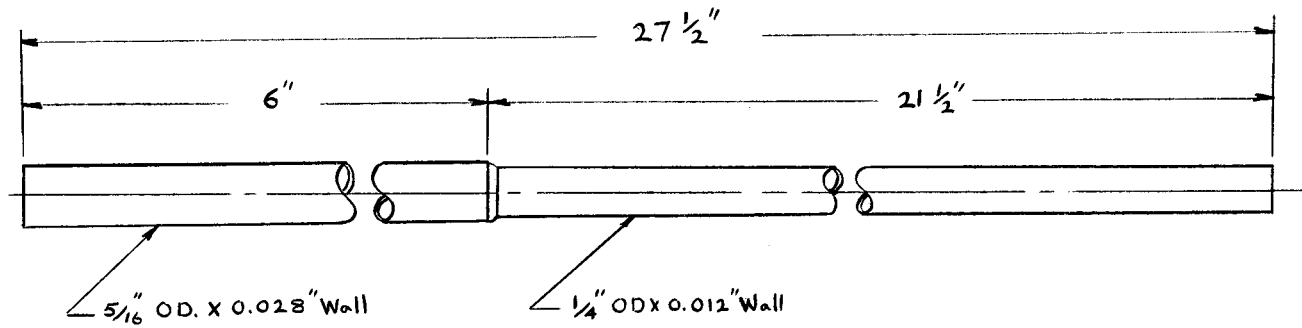


Figure 4. Mixing jets.

pipe in the area of the jet outlet to facilitate centering the jet in the test section. The jet outlet was located two inches below three tapered centering screws mounted radially in the top flange of this plastic section which allowed the jet to be maintained concentric with the test section.

The vertical test section, I, consisted of lengths of 0.875 inch OD 0.745 inch ID red brass tubing connected by self-aligning flanges which are detailed in Figure 5. These flanges permitted the discontinuity of the tube wall to be held below 0.001 inch at the joint. The flange system permitted photographs to be taken at 27.3, 209, 421, and 576 diameters below the mixing jet. Pressure taps, p_2 , were provided one inch above the flanges located on the first and second floors to measure friction losses in the test section.

The return leg of the test section, J, was constructed of 1-1/4 inch copper tubing. The discharge of the return leg was located under the surface of the liquid in storage tank A. Thus a constant net head was maintained on the turbine pump B as the liquid level raised in storage tank A, and a very stable overall flow rate resulted.

The photographic window, K, is shown in detail in Figure 6. The design minimized flow disturbance and eliminated leakage at high operating pressure. The test section was constructed by casting a block of polyester resin (Taylor & Art, Inc., Oakland 6, California) around the middle of a ten inch piece of test section tubing. After the

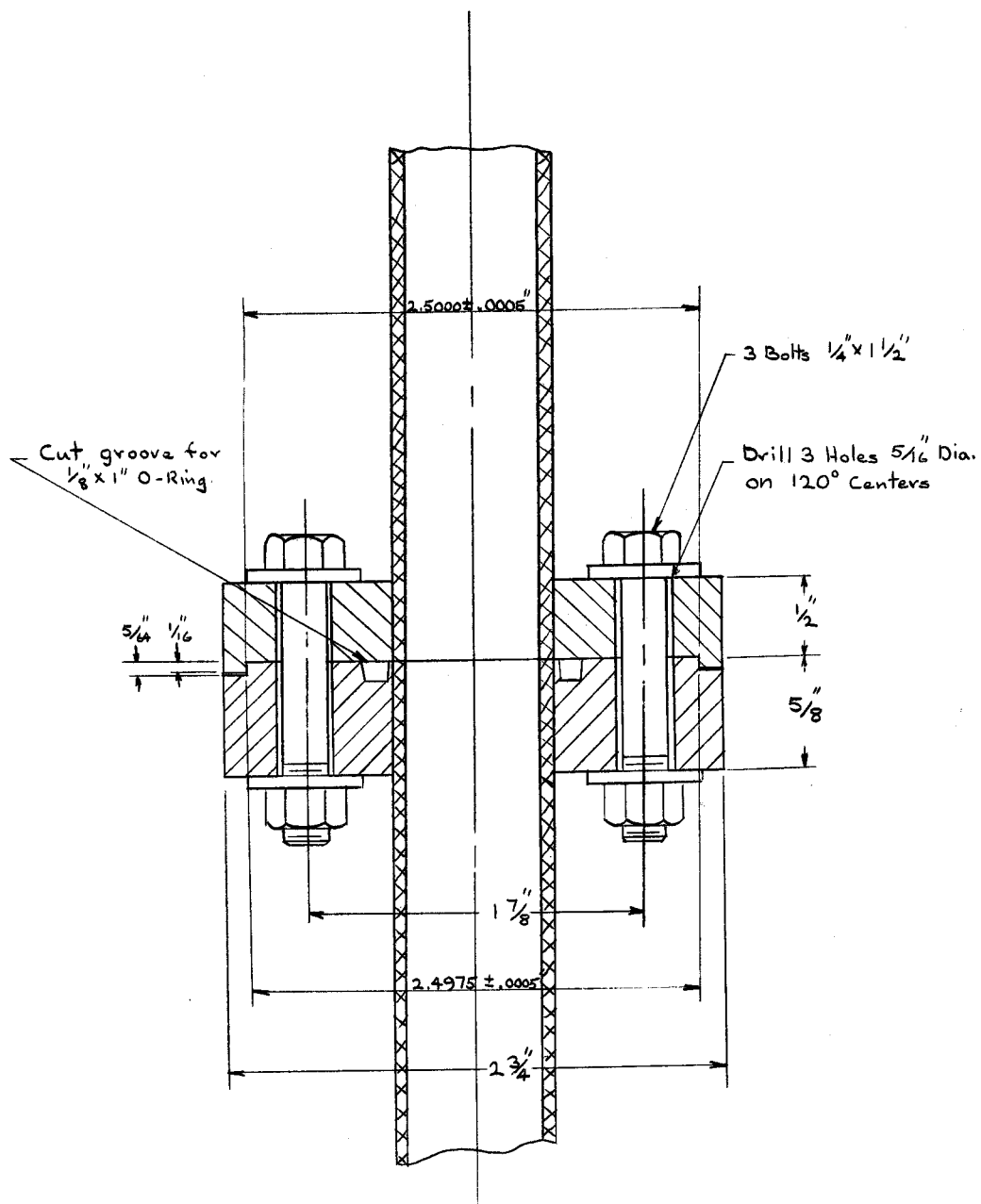


Figure 5. Self-aligning flanges.

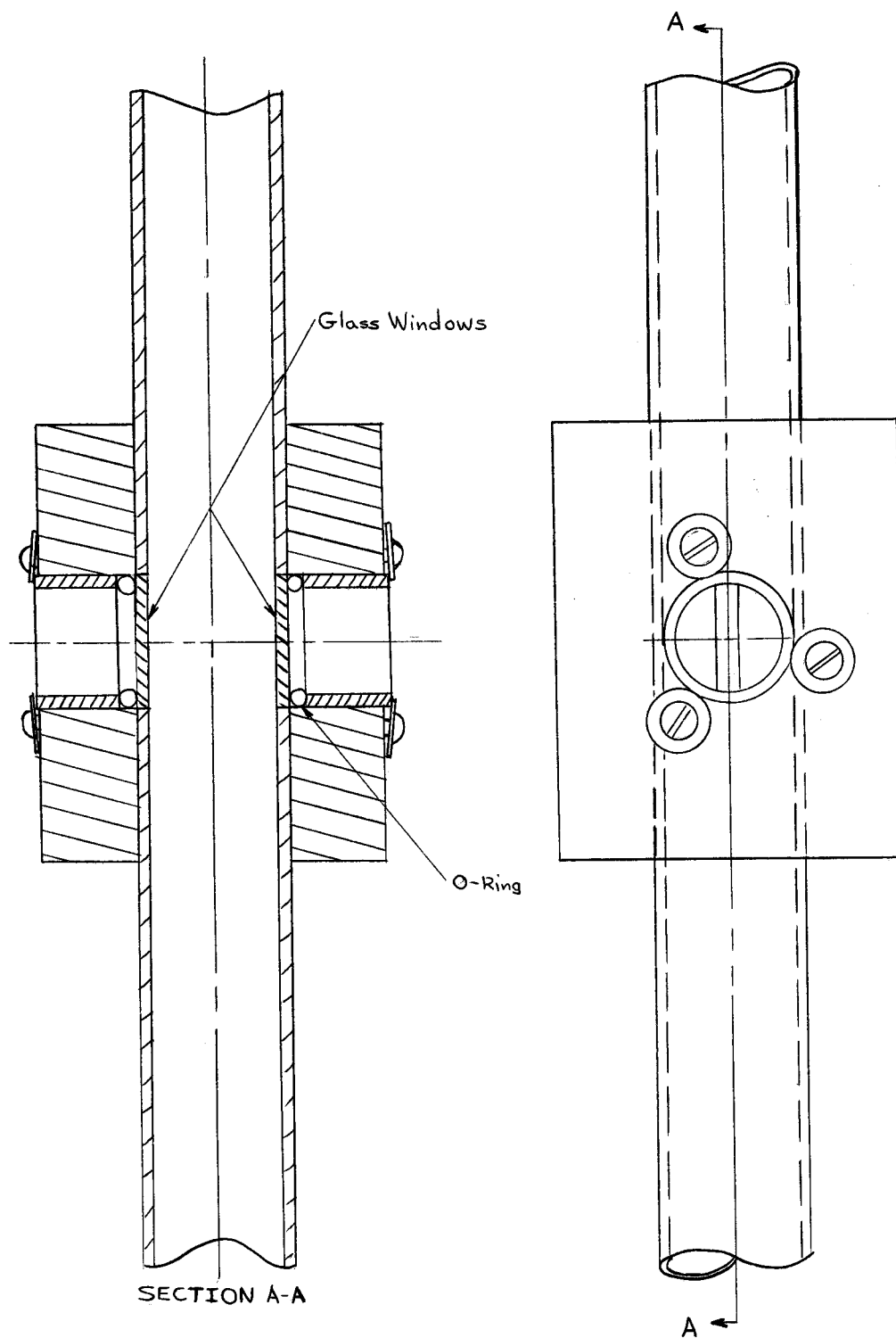


Figure 6. Window arrangement for photographing the flowing dispersion.

plastic hardened, an endmill was used to machine $3/4$ inch diameter flat bottom holes in opposite sides of the block to a depth sufficient to create slots $3/16$ inch wide on opposite sides of the tube. Glass discs $3/4$ inch in diameter and $1/16$ inch in thickness cut from microscope slides were inserted in these holes. Rubber o-rings and plastic retaining rings secured by screws completed the photographic section. The maximum discontinuity at the wall was 0.010 inch. The resulting assembly was leak free with an internal pressure of 75 psi.

Photographic Equipment

Photographs of the dispersion were taken with a Hasselblad Model 1000F single lens reflex camera equipped with an 80 mm lens and a 100.2 cm extension tube. The resulting optical system produced an image approximately twelve times actual size on the film and had a depth of focus of approximately 1500 microns.

The camera and extension tube were rigidly mounted on the sliding table of a heavy cast iron base. The position of the table with respect to the base was measured with a dial indicator graduated in 0.0005 inch divisions. A lead screw incorporated in the cast iron base could be used to position the sliding table. The whole assembly rested on a table which was clamped to the test section nine inches below the photographic window. Thus the position of the focal plane of the camera with respect to the pipe wall could be easily adjusted

as desired by means of the lead screw and the dial indicator.

Backlighting of the dispersion was accomplished by means of a General Radio Strobotac Model 1531A strobe light. The strobe produced 2.2 million candle power with a 1.2 microsecond duration on the medium intensity setting. With the strobe set on medium intensity and located one foot away from the photographic window, sufficient light was available for photographing dispersions with a concentration below five percent. For concentrations above five percent a Bell and Howell three inch f2 projection lens was used between the strobe and the photographic window to concentrate the light on the dispersion.

Kodak Tri-x panchromatic 120 film with an ASA rating of 400 was used for all photographs. The negatives were developed with Acufine developer and printed on high contrast, F-5, kodabromide paper with Dectol developer. Droplet images on the prints were 34.2 ± 0.1 times actual size in all cases.

EXPERIMENTAL PROCEDURE

A typical experiment was begun by pouring a small amount of the organic phase into the bottom of the large storage tank and then filling the tank with approximately 300 gallons of city water. The contents of the tank were then allowed to stand over night to insure that the water phase was saturated.

The camera was positioned before the test section was filled with water. The inside wall of the window was located by noting the mean of the dial indicator readings at which small water droplets adhering to the inside of the window appeared slightly out of focus because they were too far from or too close to the lens. In practice the average of three successive pairs of such information was taken as the position of the inside wall and used to locate the camera with respect to the wall. This value was reproducible to within ± 0.001 inch.

Final adjustment of the water temperature was accomplished by starting the water pump and allowing frictional heating to bring the temperature of the water of $68 \pm 1^{\circ}\text{F}$. The water rate was then adjusted, the organic-liquid pump was started and the flow rate adjusted. There followed a period approximately 10 minutes in length during which pictures could be taken before the entrained organic phase began to pass through the water pump. The end of this period

was evidenced by a marked decrease in the light transmittance due to a sharp increase in the number of very small drops due to break-up in the pump. Observations showed that frictional heating increased the temperature less than one degree Fahrenheit during this ten minute period.

Two operators were required to operate the equipment due to the short time during which pictures could be taken. One operator operated the photographic equipment as rapidly as possible. Typically three rolls of film could be exposed before entrainment occurred. The second operator watched the rotameter on third floor and made any adjustments necessary to keep the organic flow rate constant to within $\pm 1\%$ of the desired flow rate. The water flow rate remained constant within $\pm 0.5\%$ with no further adjustments. After the pumps were shut off, a sample of the organic phase was taken for subsequent interfacial tension measurements. The majority of the organic phase was recovered and reused after filtering through Whatman number one filter paper. The interface and the water phase were discarded. When the organic phase was changed, the entire apparatus was flushed out with water, then water and Shellsolv and finally twice with water and the new organic phase.

One complete roll of 13 pictures was taken at each set of experimental conditions. This was usually sufficient to yield samples of 250 drops in focus which were measured with the aid of a

transparent plastic ruler which was graduated to read directly in 25 micron increments. Since the decision as to which drops were in focus and which were not was some what subjective, all of the measurements were made by one person. In the case of distorted drops, all diameters were measured parallel to one another such that the diameter appeared to bisect the area of the drop. The random orientation of the drops thus eliminated biasing of the measurements. A CDC3300 computer was used to convert the size frequency data to cumulative frequencies weighted with respect to volume, surface, or diameter and to the various weighted average values.

EXPERIMENTAL RESULTS

When the drop size distributions had been obtained experimentally, considerable effort was expended to find a distribution law which would describe them. If an adequate distribution law could be found, comparison of the distributions could be accomplished by noting the changes in the parameters of the distribution instead of the more cumbersome visual comparison of the distribution curves themselves. A search of the literature had revealed three promising distribution laws: the log-normal distribution, the upper-limit law of Mugele and Evans, and the Amsterdam distribution law.

The inadequacy of the log-normal distribution law (Equation 34) is best illustrated by a log-probability plot of a representative set of data shown in Figure 7. Two nonlinear scales are employed in such a plot. Distance along the ordinate is proportional to the logarithm of the particle size. Distance along the abscissa is proportional to the normal deviate expressed as the cumulative percent undersized. If a distribution is log-normal, it will appear as a straight line on such a plot. Clearly this is not the case for the data shown in Figure 7, although the data below the 80% point for Roll 65, observed closest to the nozzle (27 diameters below the nozzle) fall on what appears to be a straight line. As the mixture flows through the pipe, the distribution is increasingly divergent from the log-normal type. Extrapolation to the nozzle would indicate nearly

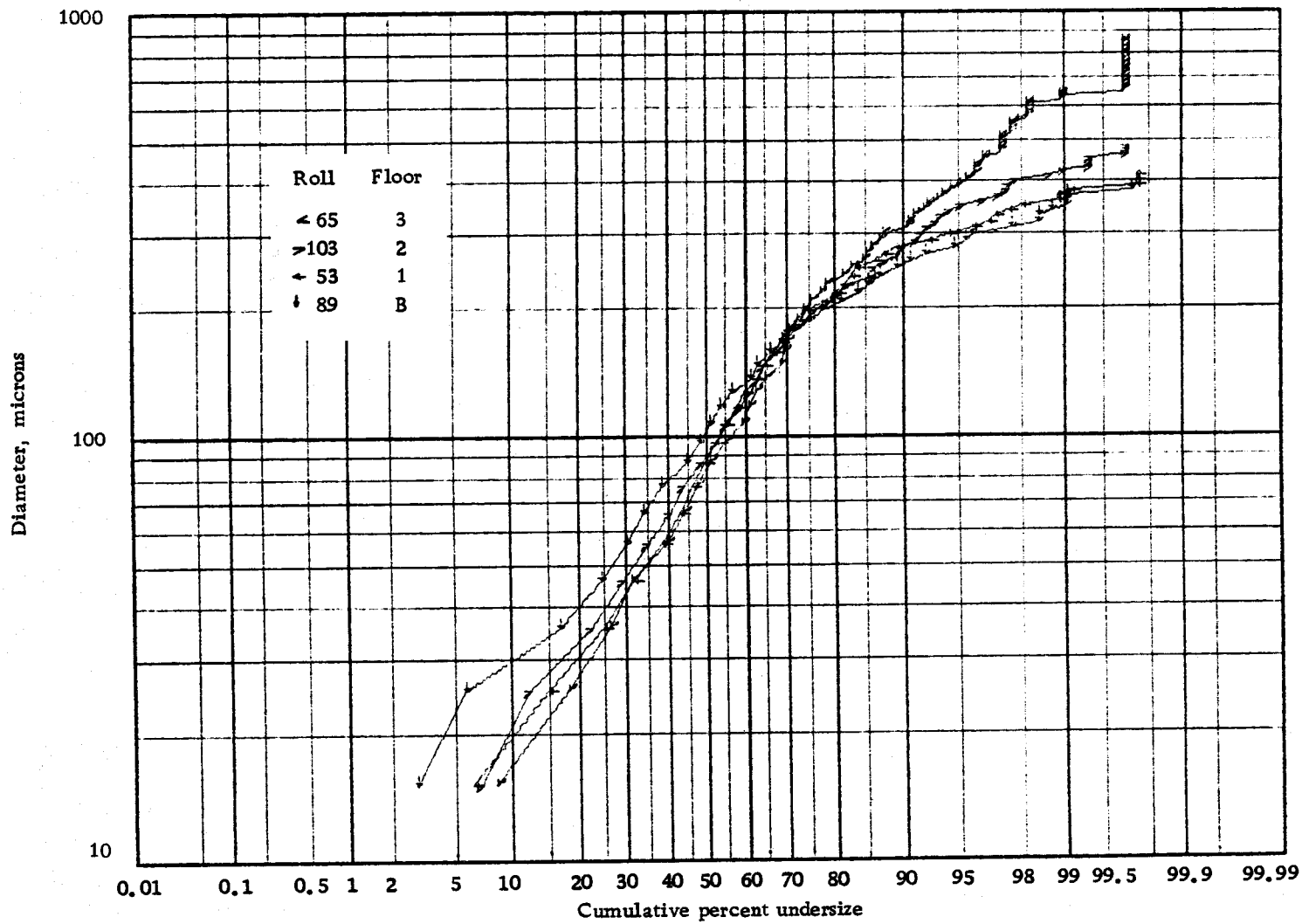


Figure 7. Drop size distributions for 1.3% Shellsolv, $y/R_w = 0.1$.

log-normal distribution at that point, but the action of turbulence was not to generate a log-normal distribution.

The upper-limit law of Mugele and Evans (Equation 38) gives a better fit of the data than the log-normal distribution as seen in Figure 8. However, a chi square test of the data for several systems indicated that in all cases the hypothesis that distribution obeyed the upper limit law could be rejected with only a 0.5% chance of error. The primary contribution to the chi square seemed to occur in the regions of largest and smallest drops. It was also noted that the maximum stable drop size predicted by Sleicher's correlation (Equation 27) was lower than the maximum stable drop size which gave the lowest value of the chi square for a specific set of data. For Roll 89 a D_{\max} of 230 microns was predicted by Equation 27 but 350 microns gave the best fit of the experimental data. In the case of a light oil system, Roll 115, the values of D_{\max} were 170 microns and 530 microns respectively. In view of these difficulties, the upper-limit equation does not appear to be an adequate representation of the data.

The results of applying the Amsterdam Distribution law (Equation 39) to the data of Roll 89 are shown in Figure 9. If the data followed this law, it would fall on a straight line when plotted in this manner. A portion of the data does fall on a straight line, but below a drop size of 150 microns there is a marked deviation from linearity.

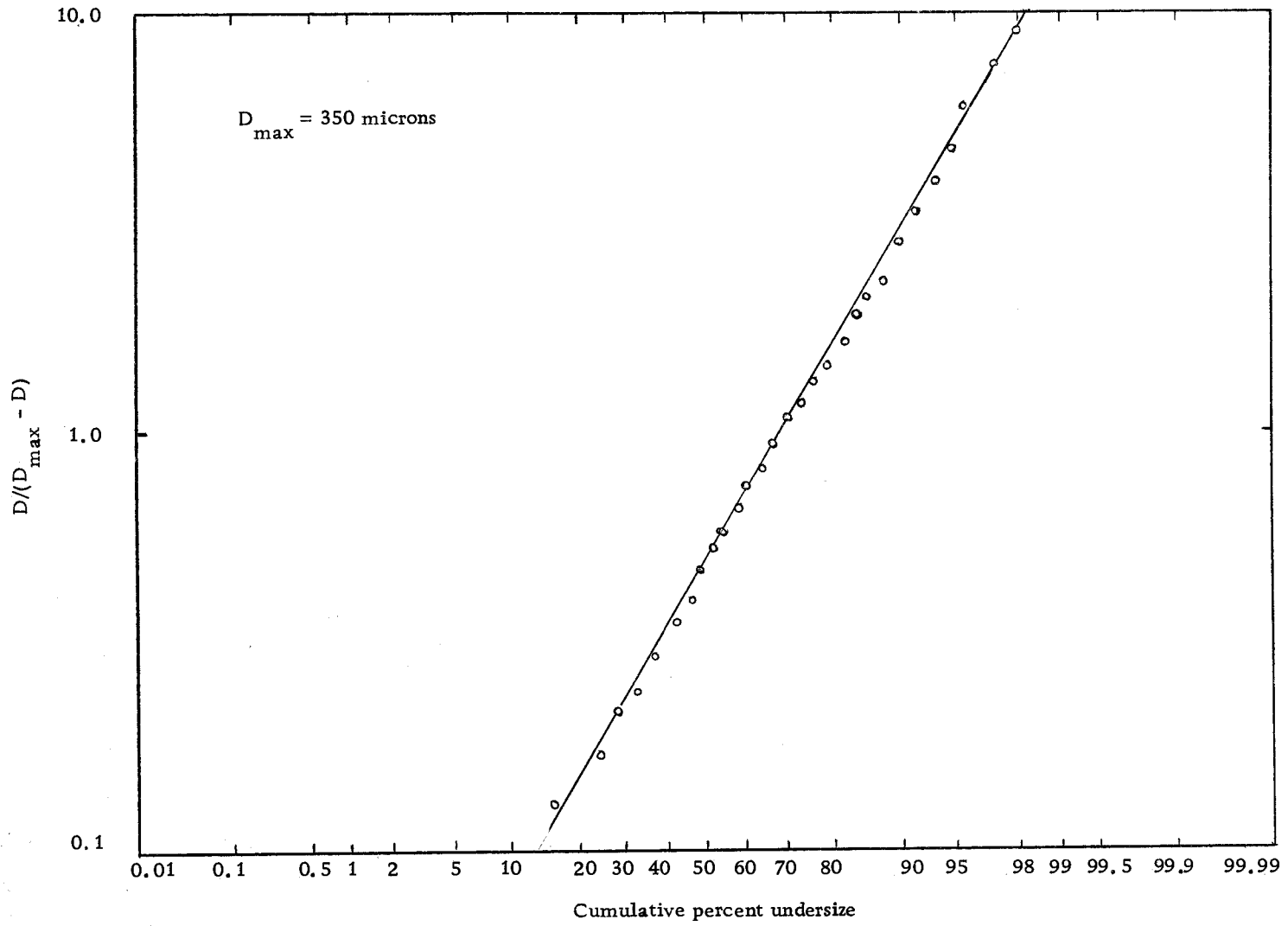


Figure 8. The upper-limit distribution law applied to the distribution from Roll 89.

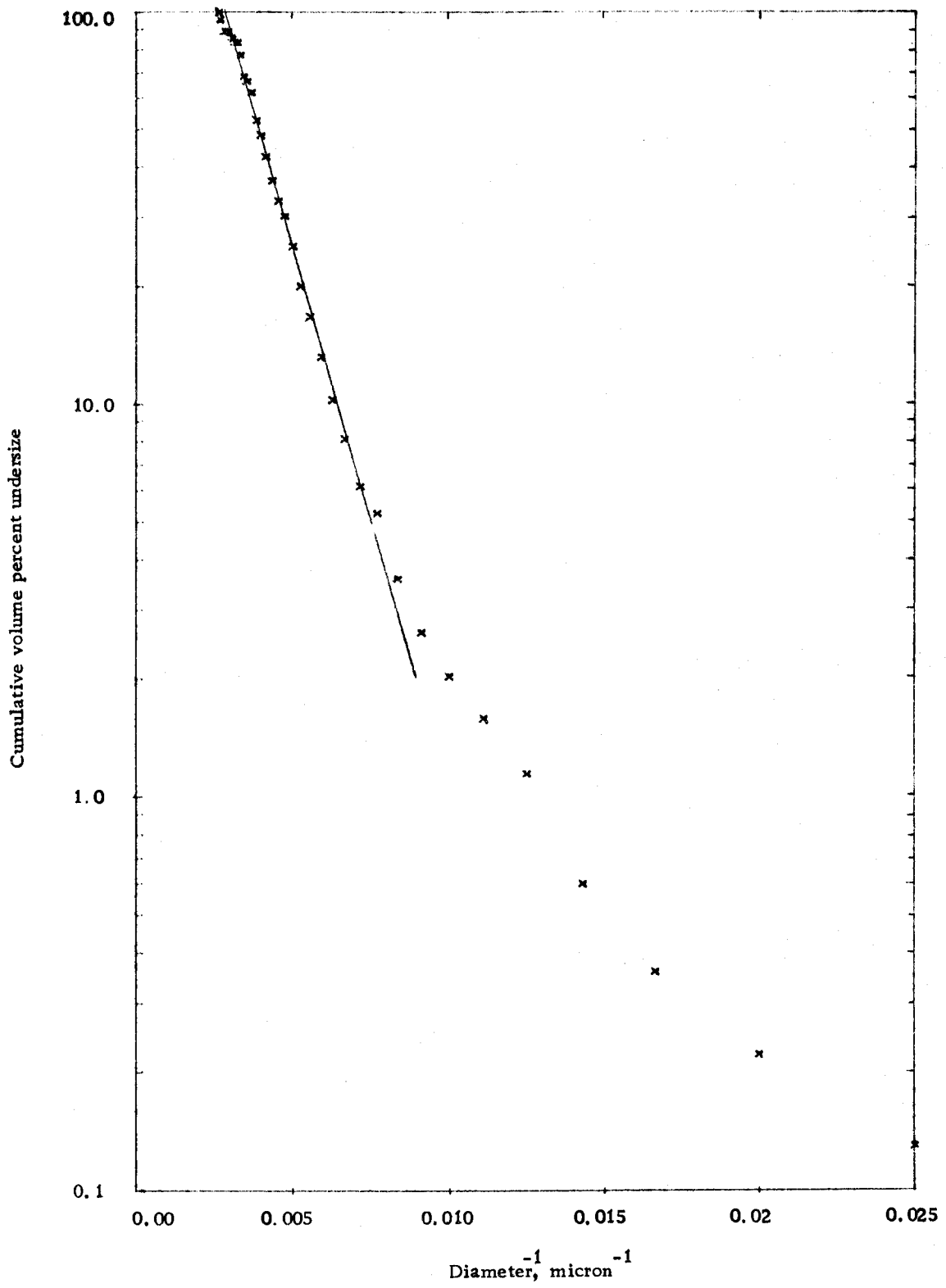


Figure 9. The Amsterdam distribution law applied to the distribution from Roll 89.

On a number basis, 70% of the total drops counted had a diameter less than 150 microns. Thus the Amsterdam equation does not appear to be a desired distribution law.

Because no adequate distribution law could be found, the data are presented and compared in graphical form. Also, the various average sizes as calculated by Equation 30 are presented. Although the distributions were not log-normal, log-probability plots of the distributions were found to be very useful for comparative purposes. Representative distributions are presented below. The remainder of the distributions are found in the appendix. Complete average size data are also listed in the appendix.

Before examining the experimental evidence, some investigation of the error in the data is necessary. Errors fall into two broad classes: empirical and statistical. Empirical errors arise from variations in the experimental conditions but in this work probably mostly from variations in picture quality. Theoretically experimental conditions enter into the distribution via the maximum stable drop size as given by Sleicher's correlation (Equation 27) which gives

$$D_{\max} = K \sigma^{1.5} \rho_c U^{-2.5} \quad (41)$$

Velocity, density, and interfacial tension were known to be constant

within $\pm 0.5\%$, $\pm 1\%$, and $\pm 4\%$ respectively. Thus the relative error of D_{\max} due to variations of experimental conditions was $\pm 3\%$ within one standard deviation of the mean.

Deterioration in picture quality was caused in most cases by the increase in concentration of the dispersion and somewhat less by the increase in distance between the camera focal plane and the wall of the pipe. The quality of the pictures was subjectively graded into four classes as shown in the appendix. Class A photographs were judged very sharp and easy to process. Class D photographs were difficult to evaluate and the distributions obtained from them are of questionable value. Although some picture quality was lost in reproduction, the picture quality can be illustrated with the pictures shown in Figure 11. No pictures which would be judged A quality photographs are shown, but pictures A and N are very close. Pictures O, R, and G would be judged B, C and D quality photographs, respectively. The primary effect of poor picture quality was to bias the distribution toward large drops. An idea of the reproducibility of the data can be obtained from Figure 10 which shows distributions measured at the same experimental conditions. Roll 89 and Roll 140 were A and B quality photographs respectively and were exposed on dates separated by a period of three months. Figure 10 also indicates that a sample size of 250 drops was adequate to give good results. A sample of 278 drops was used to obtain the distribution for

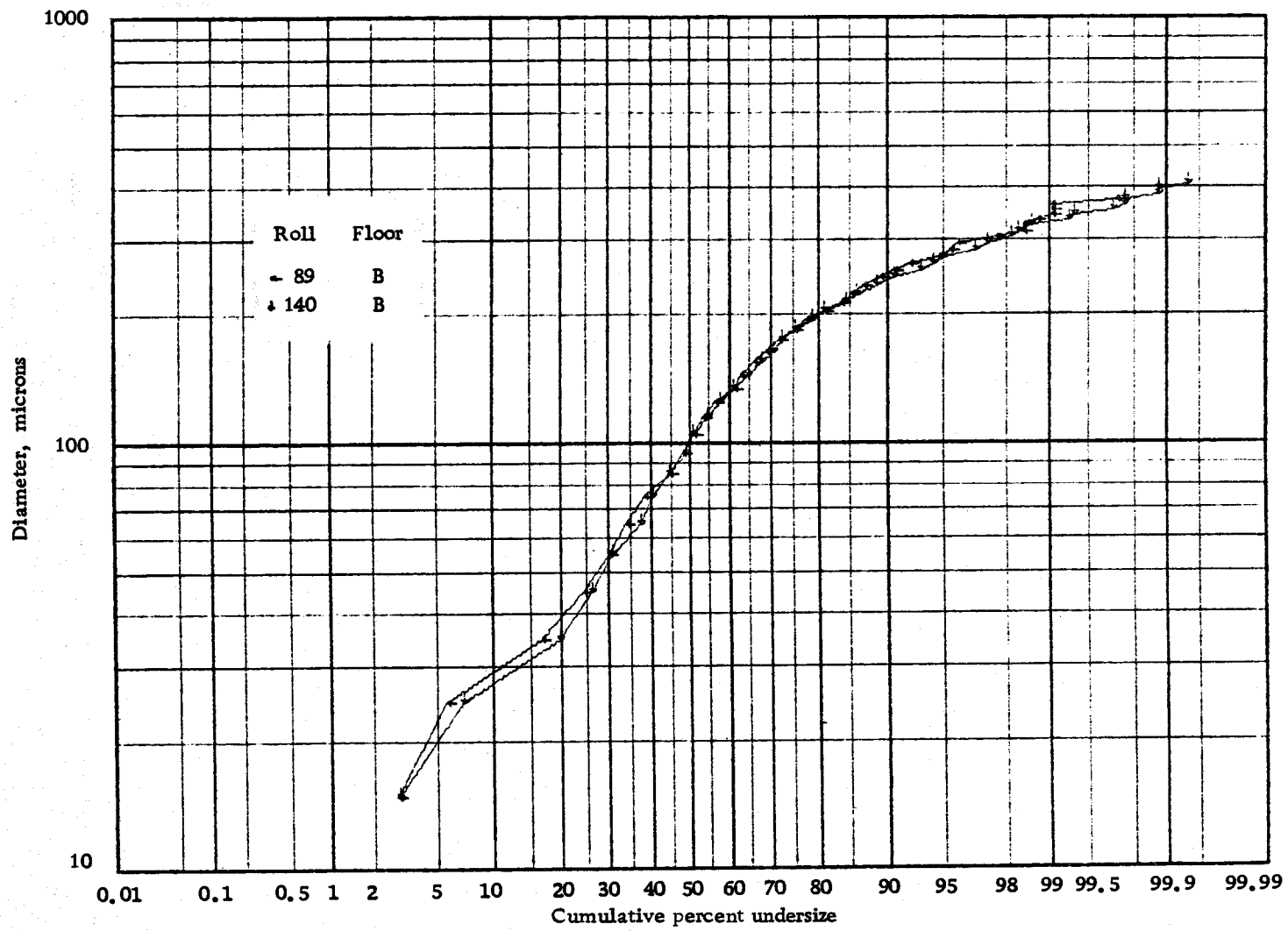


Figure 10. Reproducibility of distributions measured under similar experimental conditions.

Shellsolv



A. 0.05, 10%, 27D



B. 0.1, 1.3%, 27D



C. 0.1, 5%, 421D



D. 0.05, 1.3%, 209D



E. 0.1, 1.3%, 209D



F. 0.1, 1.3%, 576D

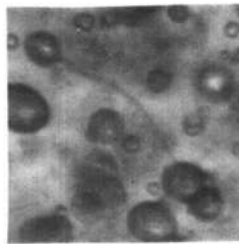


G. 0.1, 5%, 576D

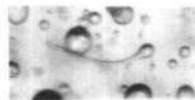


H. 0.1, 5%, 576D

Iso-octyl Alcohol



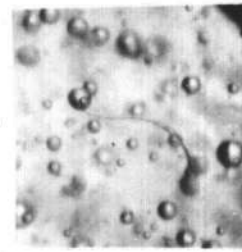
I. 0.1, 1.3%, 27D



J. 0.05, 1.3%, 27D



K. 0.05, 1.3%, 27D



N. 0.4, 1.3%, 576D



L. 0.05, 1.3%, 27D



M. 0.05, 1.3%, 27D

Light Oil



O. 0.05, 5%, 27D



P. 0.05, 5%, 576D



Q. 0.05, 5%, 576D



R. 0.05, 5%, 576D



S. 0.05, 5%, 576D

Figure 11. Highly deformed drops, 34,2X.

Roll 89; 1309 drops were used to obtain the distribution for Roll 140. Examination of the average drop size data for Rolls 89, 136, 137 and 138 indicates that the relative error of the average sizes varies from $\pm 3.0\%$ for D10X of 118 microns to $\pm 1.5\%$ for a D32X of 218 microns within one standard deviation. Similarly three 250 drop samples from Roll 130 gave D10X equal to 43.6 microns $\pm 3.0\%$ and D32X equal to 73.3 microns $\pm 2.2\%$. The data considered so far was for systems with 1.3% dispersed phase by volume. With 5.0% dispersed phase the data for Rolls 18 and 98 indicate that the errors in D10X and D32X are in the neighborhood of $\pm 10\%$ and $\pm 5\%$ respectively.

A composite photograph of highly deformed drops observed under a variety of experimental conditions is shown in Figure 11. The drops shown were chosen so as to illustrate the modes of deformation observed and the variety of conditions under which deformation occurs. The experimental conditions for each picture are specified as to dimensionless radius, distance from the wall, dispersed phase concentration, and distance from the nozzle in pipe diameters, respectively. The flow rate was 16 ft/sec in all cases. The most highly deformed drops appear dumbbell shaped with two relatively large globules of liquid connected by a thin filament of liquid (drops A, I, J, K, N, O, P, Q, R, and S). What appear to be fragments of drops photographed shortly after the rupture of the thin filament were also observed (drops C, D, G, and L) which is strong

evidence that the dumbbell shaped deformation does lead to breakup. Highly deformed drops were much more prevalent when iso-octyl alcohol or light oil was the dispersed phase than when Shellsolv was the dispersed phase. This was probably a result of the higher dispersed phase viscosity of the former pair as compared to the latter, which logically would increase the time scale of the breakup process. The probability of photographing the breakup process would then increase.

In none of the nearly 1300 prints examined during this study were any events indentifiable as coalescence observed. Two possible explanations for this apparent absence of coalescence event are that the coalescence event happens extremely fast or that it occurs very infrequently. Two mechanisms for coalescence have been proposed by Clay (6). The first was a rapid direct coalescence in which a small impinging drop merges almost instantaneously with a larger drop. A rough calculation shows that with a flash duration of approximately one microsecond a 50 micron drop would have to be traveling about ten times faster than the average velocity of the liquid in the tube if it were not to be seen entering the profile of the larger drop. Such velocities do not seem very likely. The second proposed mechanism was a slower process in which two drops cling together, the continuous phase between them drains away and the drops merge. Clay states that one or more small drops were seen

clinging to a larger drop very often in his photographs, whereas highly deformed drops were never seen. The fact that Clay observed coalescence events and they were not observed during the present study using comparable flash deviations rules out the second process fairly decisively. Thus it was concluded that coalescence phenomena could be legitimately neglected in the present study and that the drop size distributions observed were characteristic of the breakup process alone.

In the appendix, the relative distortion of the drops found on each roll of film was subjectively graded into four classes. Class 1 indicates that all the drops for that roll had circular profiles. Class 2 photographs exhibited a few mildly distorted drops. Photographs with frequently occurring deformed drops with moderate deformations (Figure 11, drop R) were termed class 3. Class 4 was reserved for photographs exhibiting highly deformed drops. The relative frequencies of each class of deformation at each of the three radial positions used are shown in Figure 12. Clearly high deformation and therefore breakup is much more probable close to the wall in the buffer layer of the turbulent velocity profile than in the turbulent core. This result is in agreement with Sleicher's (31) observation that drops tended to breakup in the wall region of the pipe.

Table III presents collected Sauter mean diameters (D_{32X}) observed for each of set of experimental conditions. The general

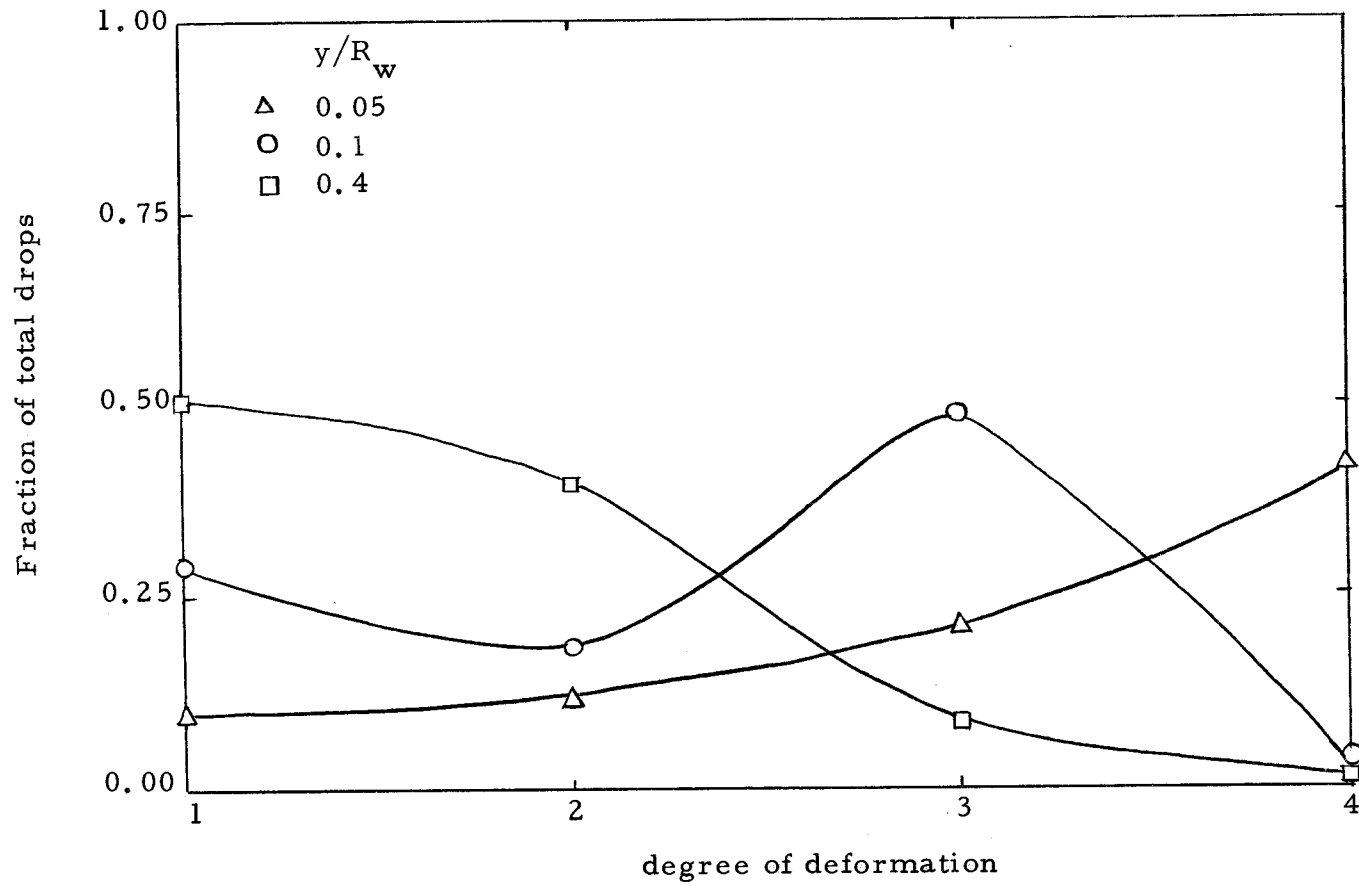


Figure 12. Degree of drop deformation at various radial distances from the pipe wall.

Table III. Summary of D32X data

| Experimental Conditions (Run Code) | Floor | Radial Position | | |
|------------------------------------------|-------|-----------------|------------------------|-------|
| | | 0.05 | 0.1 (D32X, Microns) | 0.4 |
| 2SS | 3 | 183.3 | 195.7 | 239.8 |
| | 1 | 148.6 | 189.2 | 241.6 |
| 5SS | 3 | 346.6 | 401.7 | 370.3 |
| | 2 | 246.6 | 273.2 | 279.7 |
| | 1 | 241.6 | 248.5 | 269.9 |
| | B | 219.8 | 223.5 | 249.0 |
| 9SS | 3 | | 216.2 | 234.0 |
| | 2 | | 195.4 | 219.4 |
| | 1 | | 179.1 | 215.3 |
| 8SS | 3 | 347.7 | 1096.3 | 597.5 |
| | 2 | | | 384.4 |
| | B | | 206.6 | |
| 10SS | 3 | 311.2 | | |
| | 2 | 270.2 | 394.1 | |
| | 1 | | 336.1 | 373.9 |
| | B | | 213.3 | |
| 11SS | 3 | 555.2 | 592.5 | |
| | 2 | 303.9 | 331.5 | |
| | 1 | 217.3 | 331.3 | 339.8 |
| | B | 199.2 | | |
| 2LO | 3 | 448.9 | 794.7 | |
| | 2 | 330.3 | | 338.1 |
| | B | 245.8 | 262.5 | |
| 10A | 3 | 130.6 | 101.1 | 108.4 |
| | B | 64.5 | 70.5 | 64.5 |
| 20A | 3 | 113.3 | 132.4 | 175.2 |
| | 2 | 82.7 | | 97.0 |
| | B | 70.9 | 72.5 | 83.7 |

trend is for larger D_{32X} values in the turbulent core region of the velocity profile than in the buffer layer. The differences were often small and masked in experimental error so no quantitative conclusions can be drawn. If all of the breakup occurred near the wall as indicated by the photographs, the small change in D_{32X} with radial position indicates that the dispersions were well mixed by the turbulent field in the pipe.

Distributions for 1.3% by volume Shellsolv with an average linear velocity in the tube of 16 ft/sec are shown in Figure 7, 13, and 14. Similarities are immediately apparent. The distributions observed at the same radial position in the pipe seem to intersect at a common point. This intersection is caused by a decrease in the relative number of small drops as breakup proceeds, coupled with an increase in the curvature of the distribution curve. This behavior was observed in almost all cases although the point of intersection varied widely with the system under consideration.

The effects of concentration and nozzle size were strongly coupled and difficult to separate. Figures 6, 15, 16, 17, and 18 illustrate typical results obtained as dispersed phase concentration was increased from 0.6% by volume to 10% by volume. Concentration and nozzle size primarily affected the initial distribution observed 27 diameters below the inlet. At 0.6% by volume dispersed phase, only 5% of the drops measured had diameters above 230

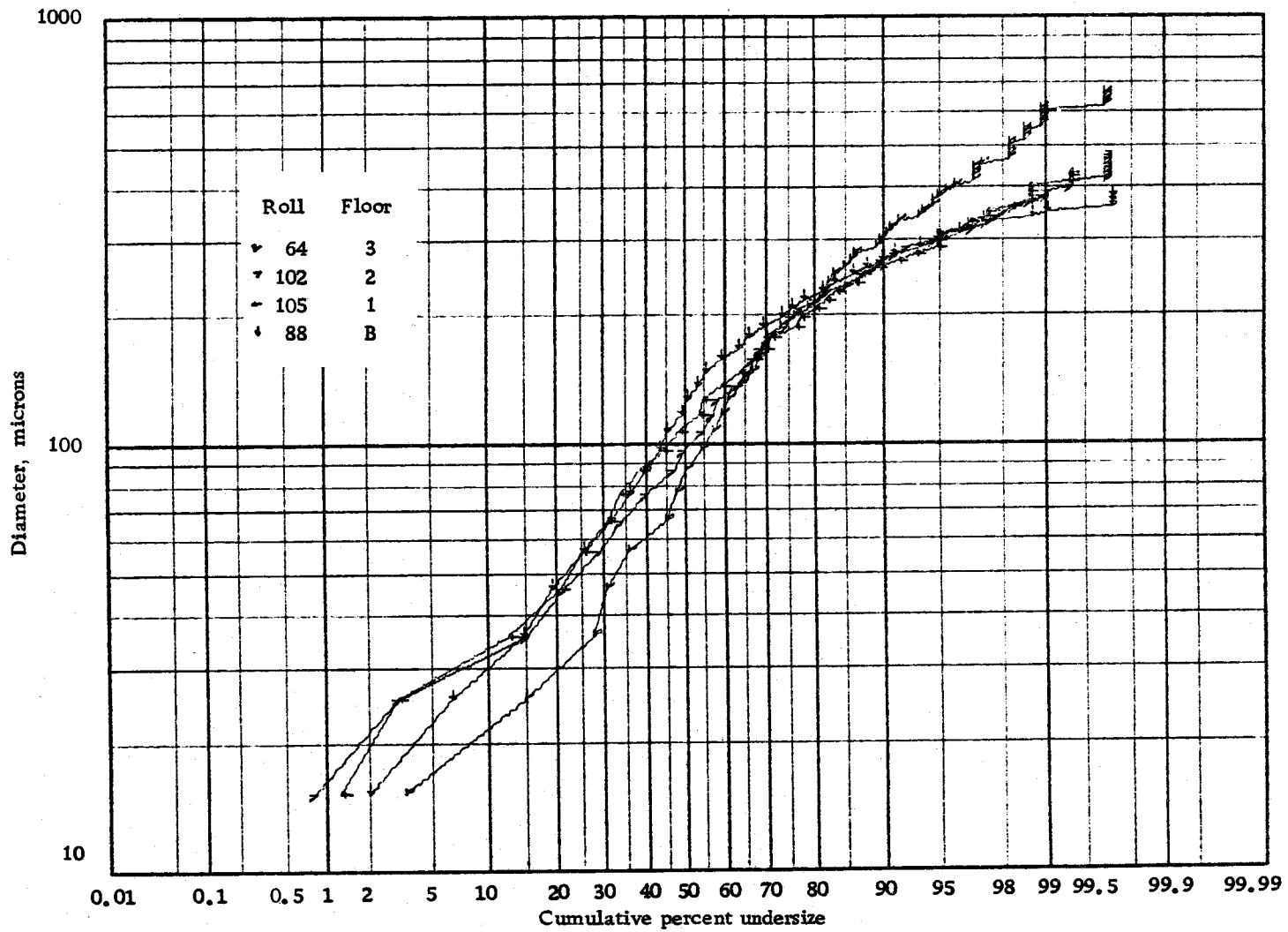


Figure 13. Drop size distributions for 1.3% Shellsolv, $\gamma/R_w = 0.05$, 16 ft/sec.

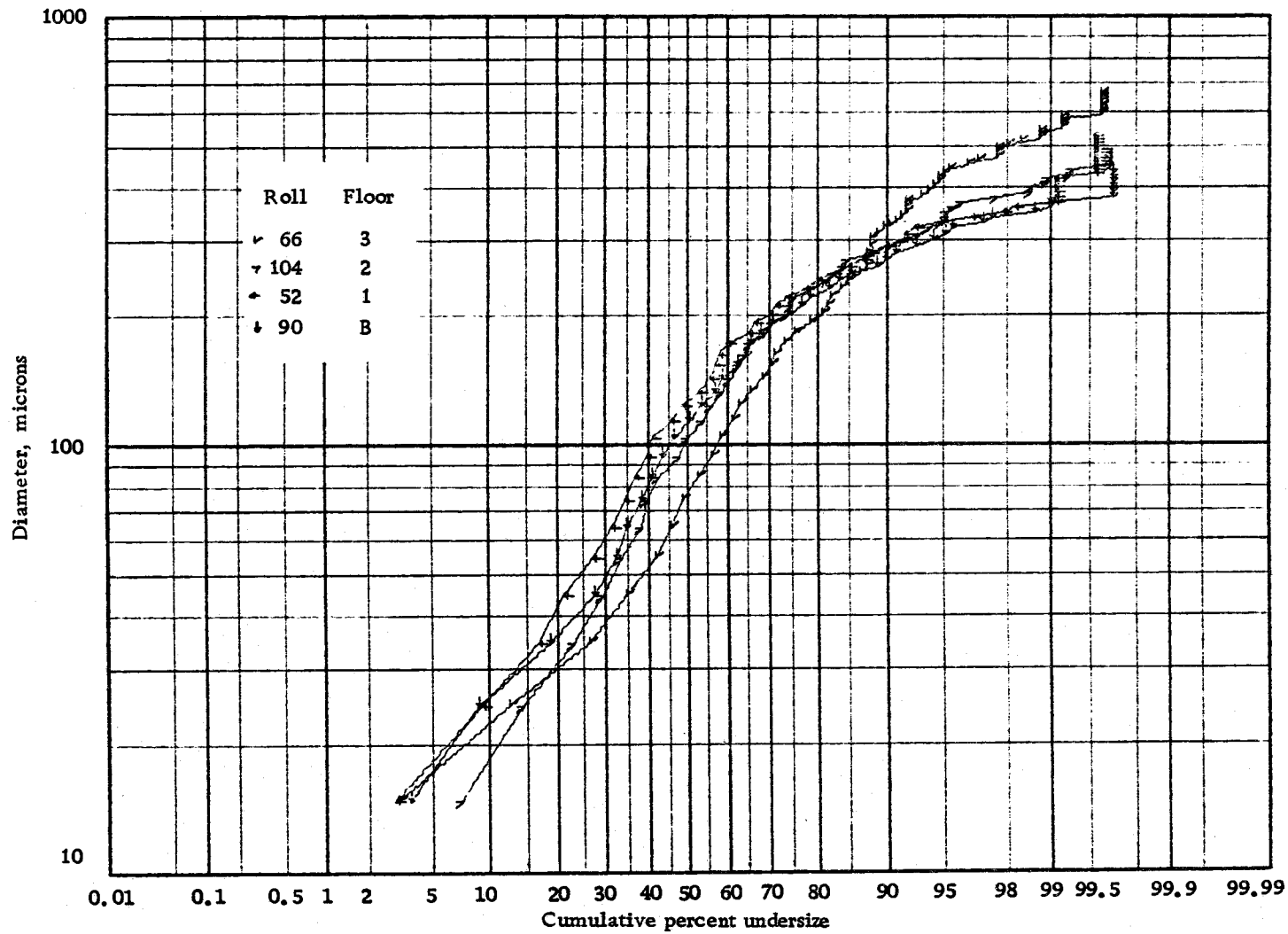


Figure 14. Drop size distributions for 1.3% Shellsolv, $\gamma/R_w = 0.4$, 16 ft/sec.

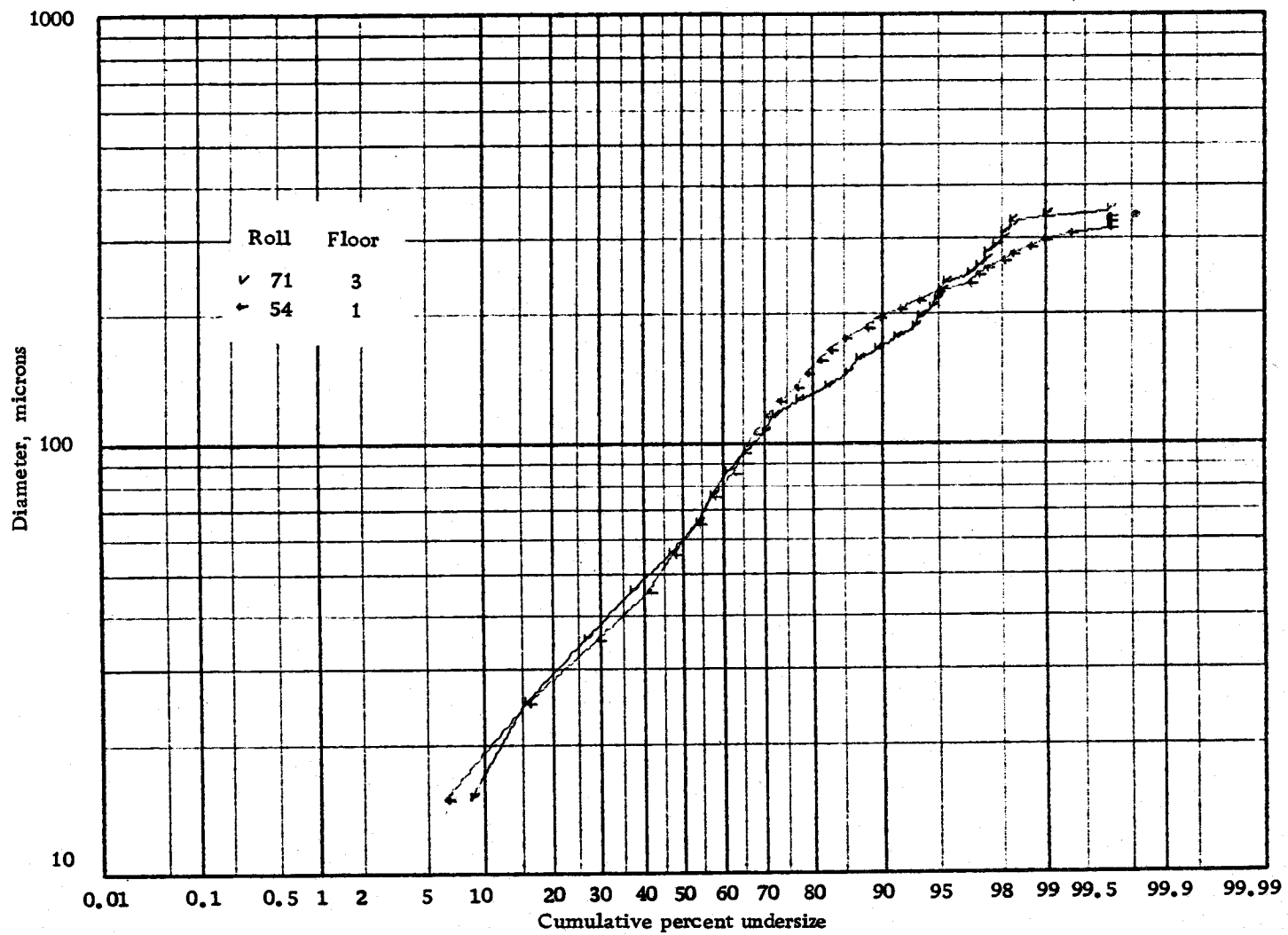


Figure 15. Drop size distributions for 0.6% Shellsovl, $\gamma/R_w = 0.1$, 16 ft/sec.

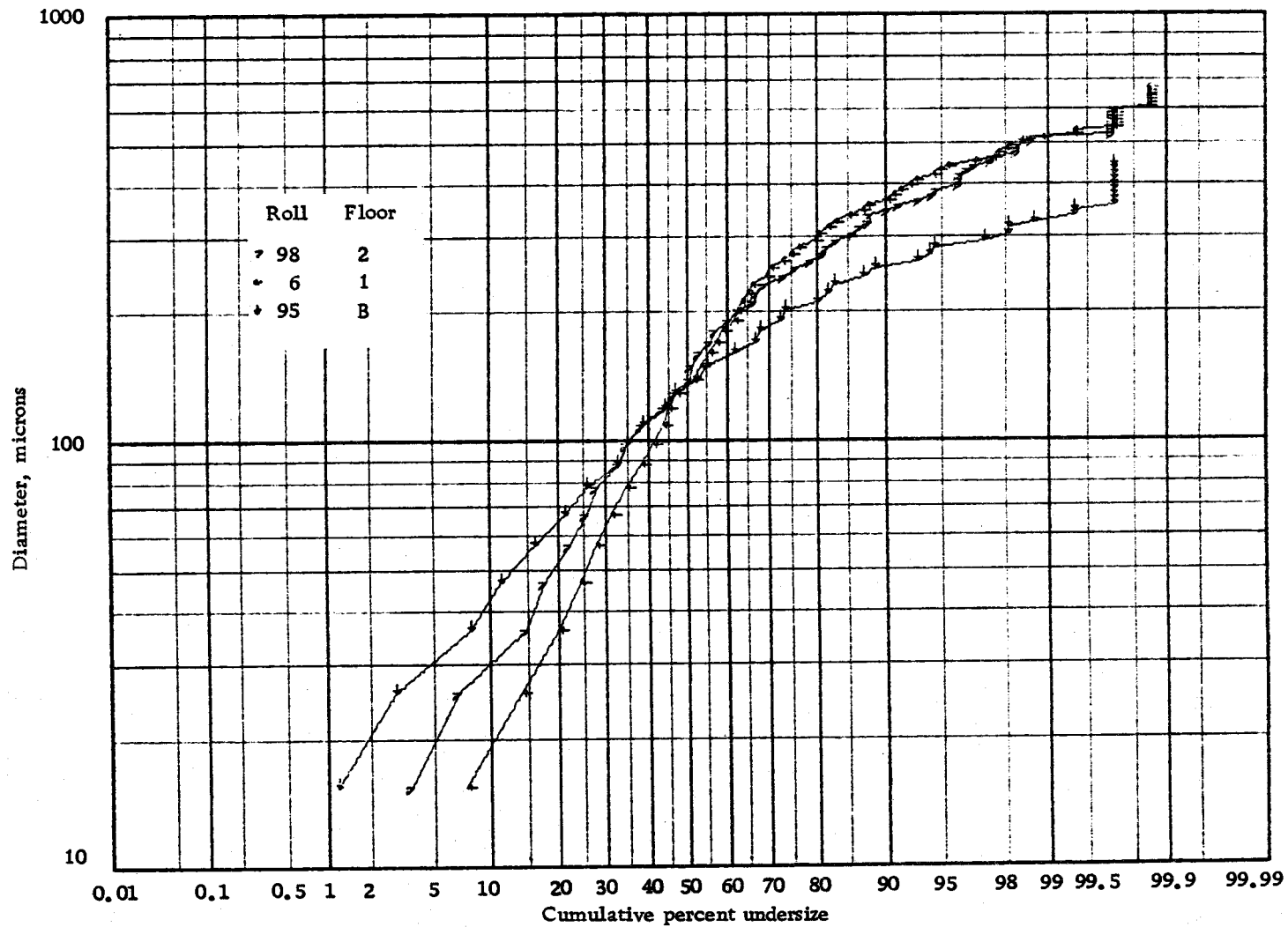


Figure 16. Drop size distributions for 5.0% Shellsolv, $\gamma/R_w = 0.05$, 16 ft/sec.

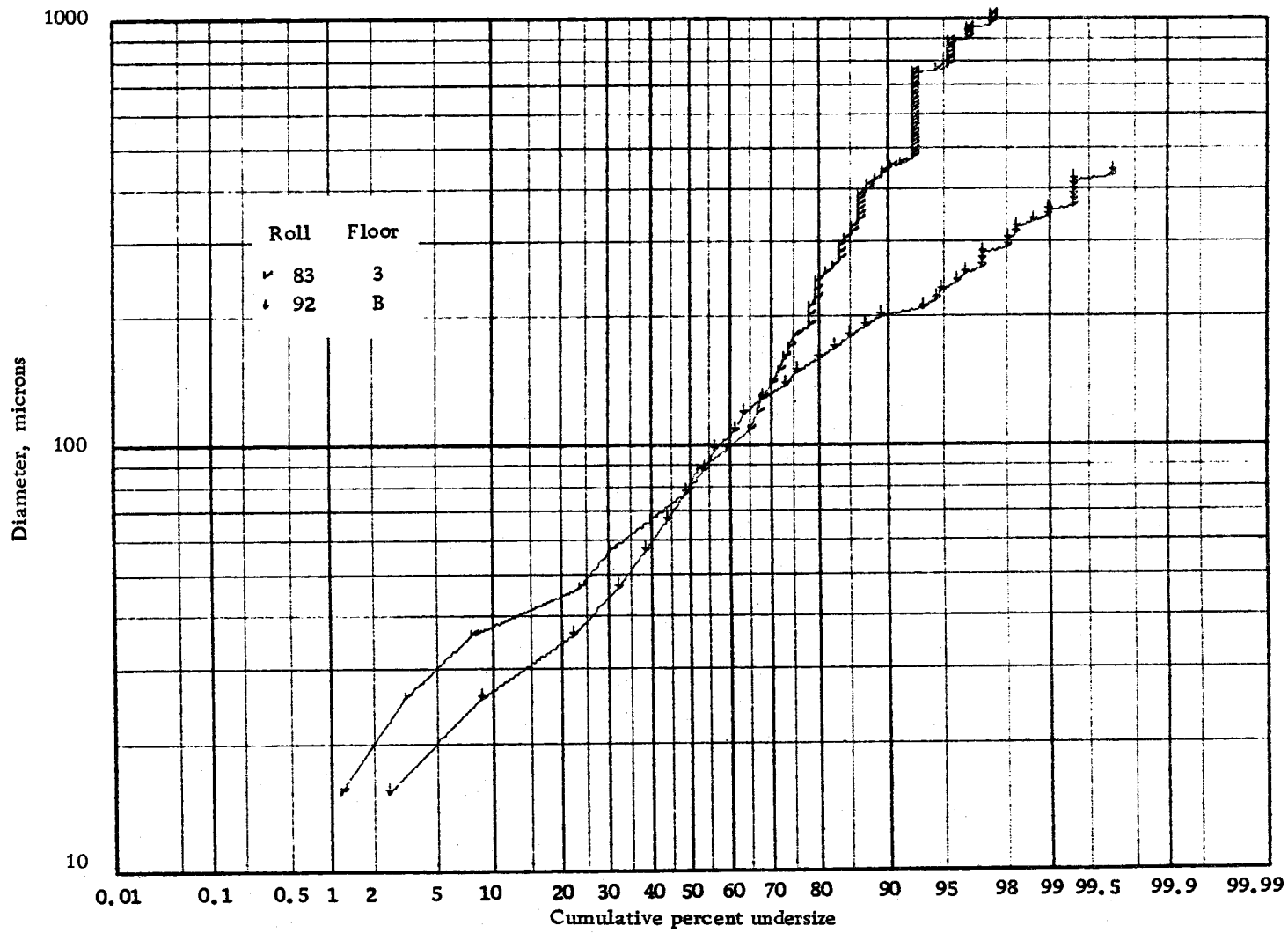


Figure 17. Drop size distributions for 5.0% Shellsolv, $y/R_w = 0.1$, 16 ft/sec.

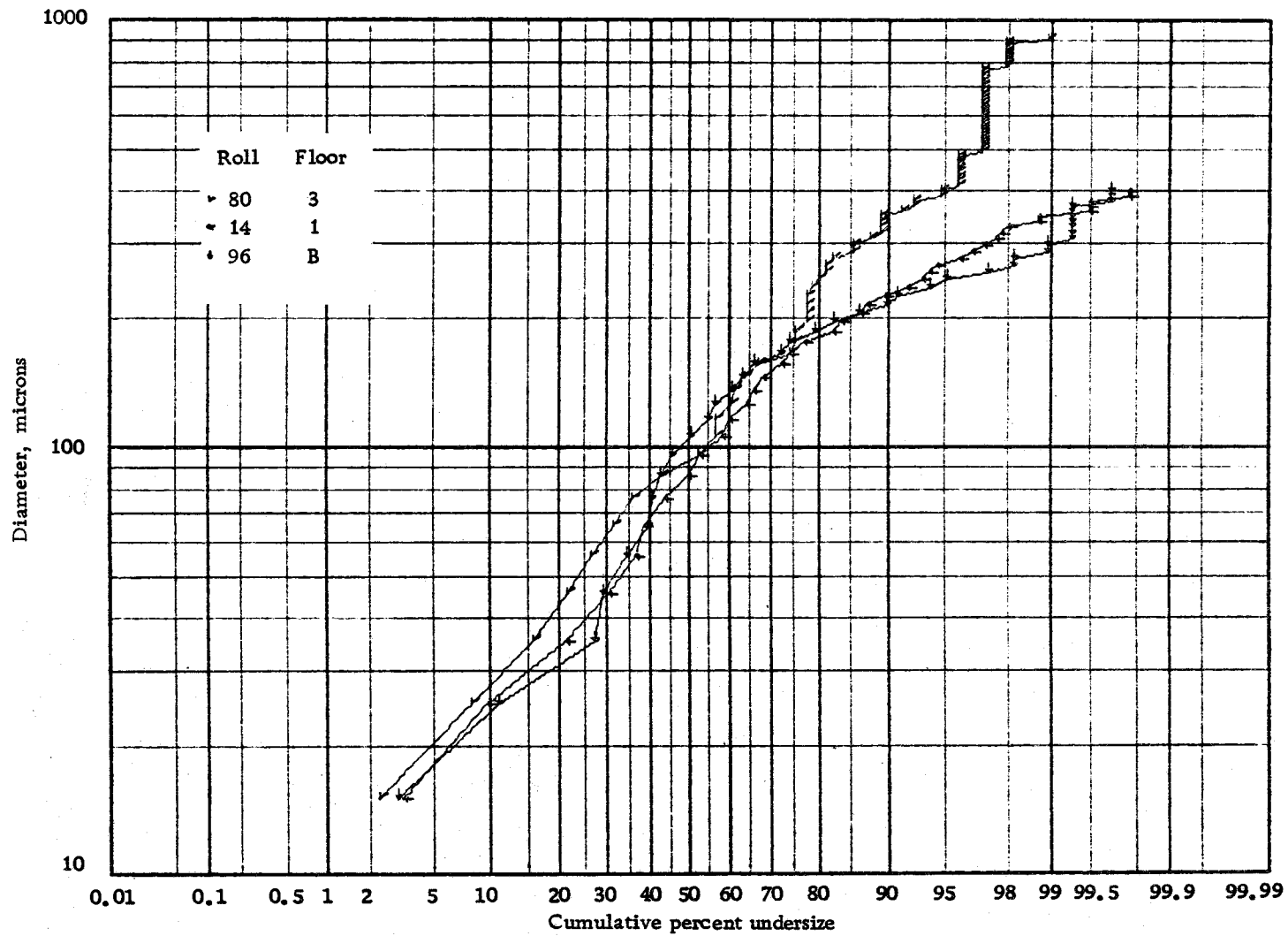


Figure 18. Drop size distributions for 10.0% Shellsolv, $\gamma/R_w = 0.05$, 16 ft/sec.

microns, the maximum stable drop size as predicted by Sleicher's correlation (Equation 27). Figure 15 indicates that little breakup occurred at this concentration which is not surprising in view of the small number of unstable drops present. For concentrations of 1.3%, 5% and 10%, the percentages of drops with diameters greater than 230 microns were 19%, 23%, and 22% respectively. Considerable breakup is evident in Figures 7, 16, 17, and 18. The same general trends in the distributions are noted in all of these figures.

Figure 19 shows distributions observed 421 diameters below the inlet nozzle when the average linear velocity was varied. The distributions all have the same form indicating that the mechanism of breakup remained the same over the range of average velocities between 14 and 20 ft/sec ($7 \times 10^4 \leq N_{Re} \leq 10^5$). Roll 46 exhibited a smaller percentage of very small drops. The distributions pictured in Figure 20 indicate that this change is a result of a change in the distribution produced by the nozzle and not a change in the breakup mechanism.

Figure 21 shows distributions obtained for a light oil system. The distribution from Roll 118 is shifted about 15% to the left of the position which would be expected from earlier results. Roll 118 gave Class C prints, so one plausible explanation for this shift would be that the distribution was biased toward large drops by poor print quality and the distribution shown is not representative of the

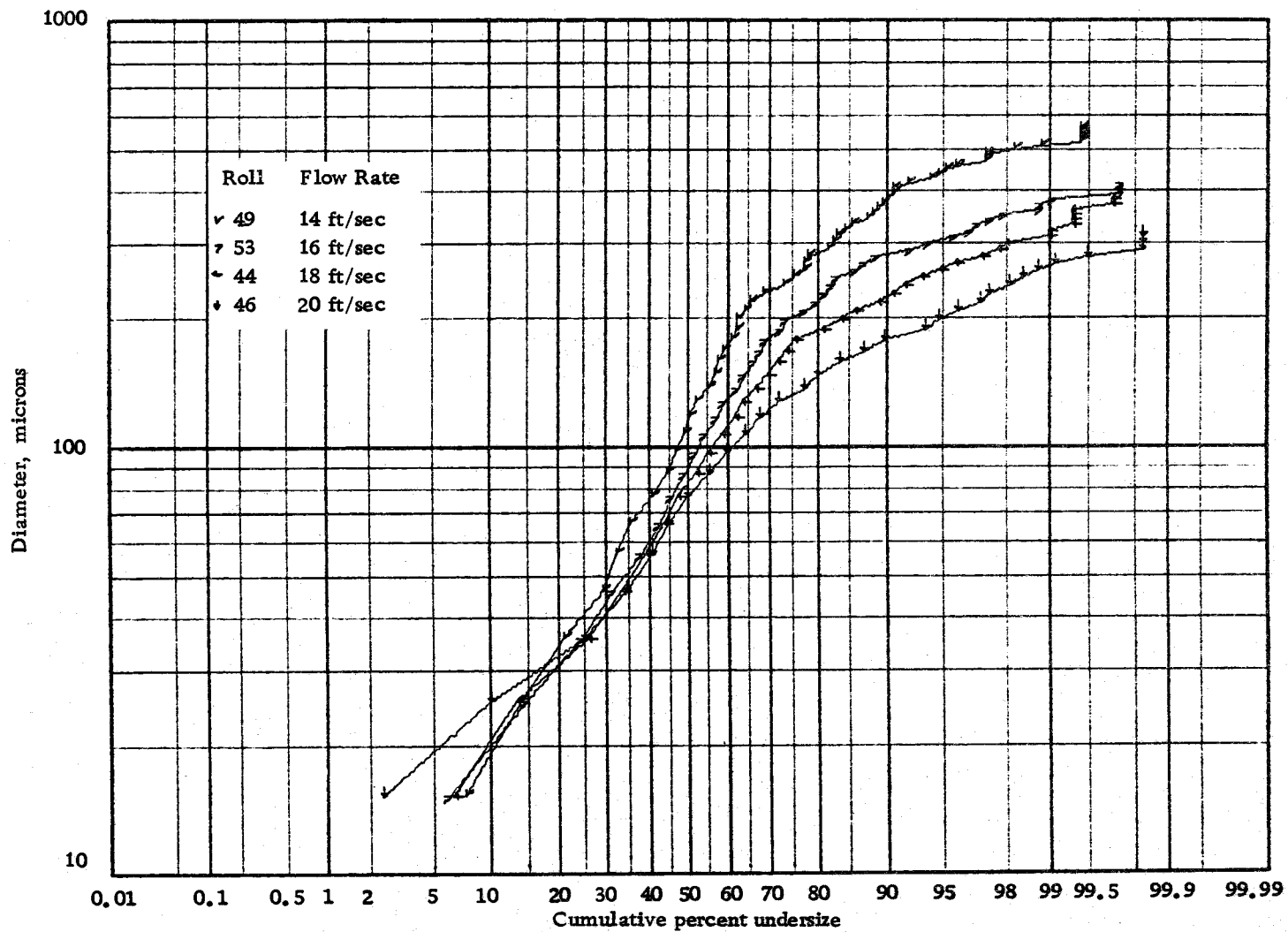


Figure 19. Drop size distributions for 1,3% Shellsolv, $\gamma/R_w = 0.1$, 16 ft/sec, first floor.

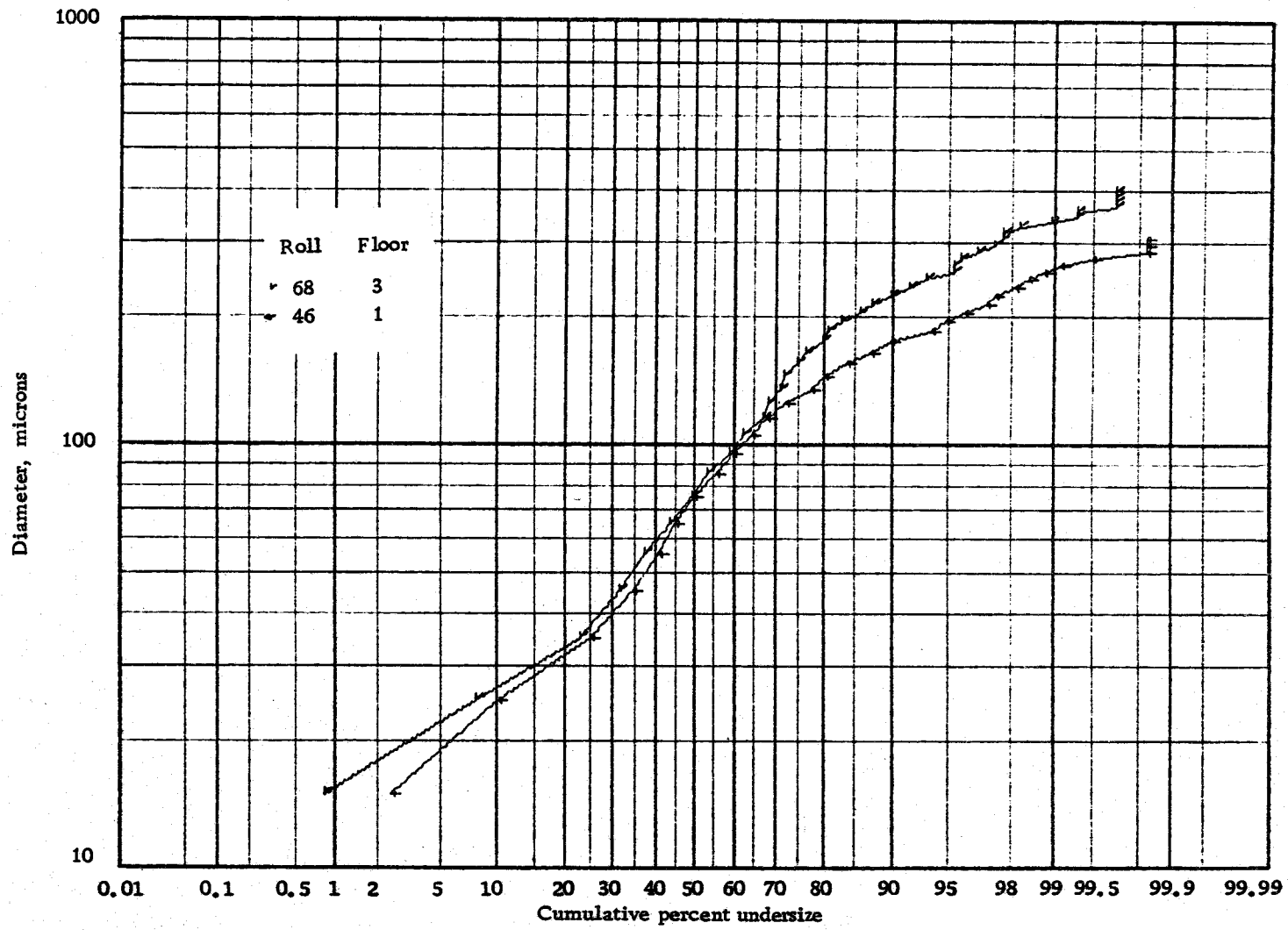


Figure 20. Drop size distributions for 1.3% Shellsolv, $\gamma/R_w = 0.1$, 20 ft/sec.

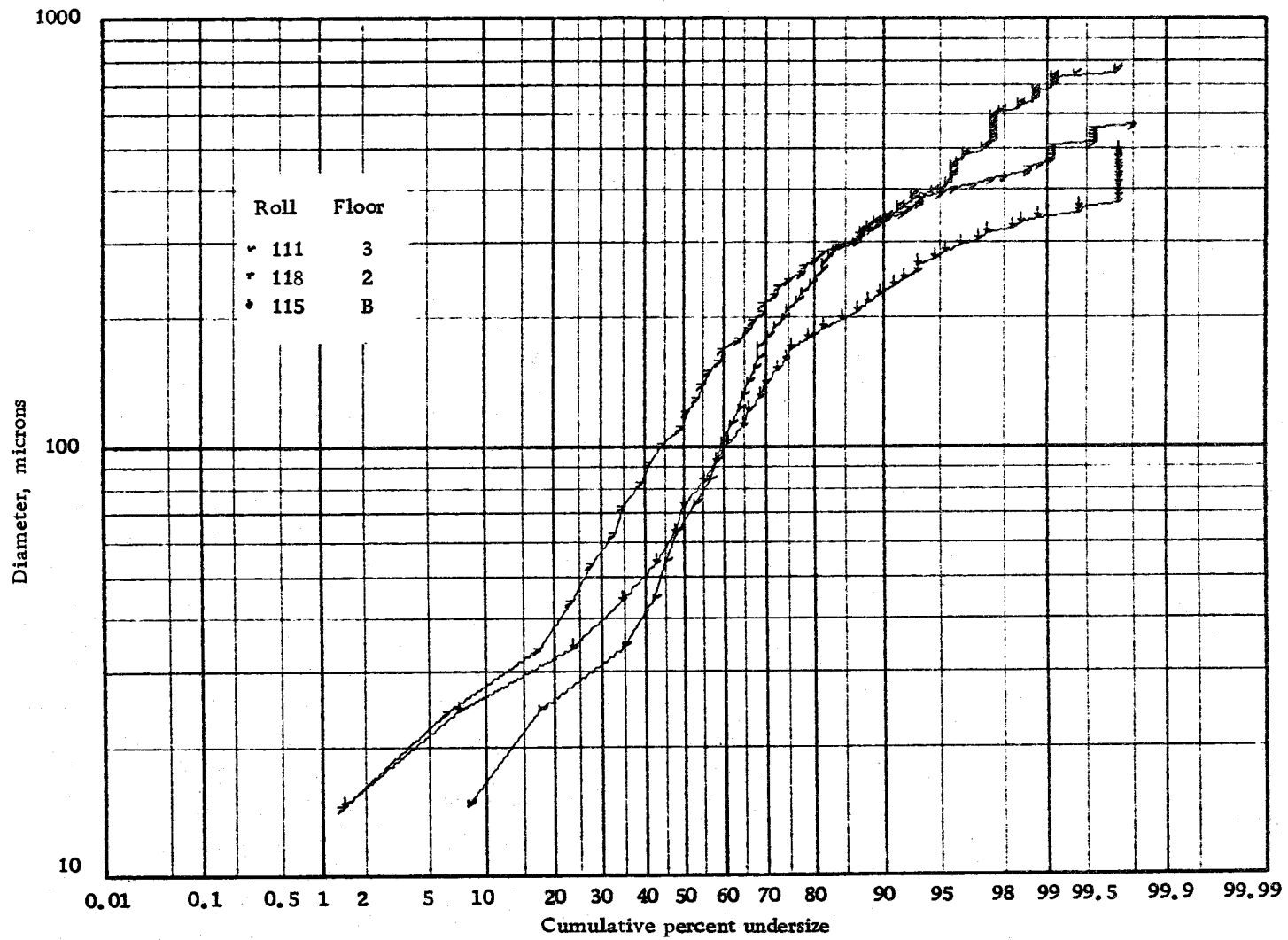


Figure 21. Drop size distributions for 5.0% light oil, $\gamma/R_w = 0.05$, 16 ft/sec.

actual distribution. The form and position of distributions from Rolls 111 and 115 were reproduced quite well by distributions from Rolls 112 and 116 as shown in the appendix and were therefore judged to be representative of the system.

Figures 22, 23, 24, and 25 are representative of the results obtained for the iso-octyl alcohol system. The most noticeable change in the distributions was the shift in the point of intersection of the distribution toward the range of small drops. This shift and the other properties of the distributions are treated in the discussion section.

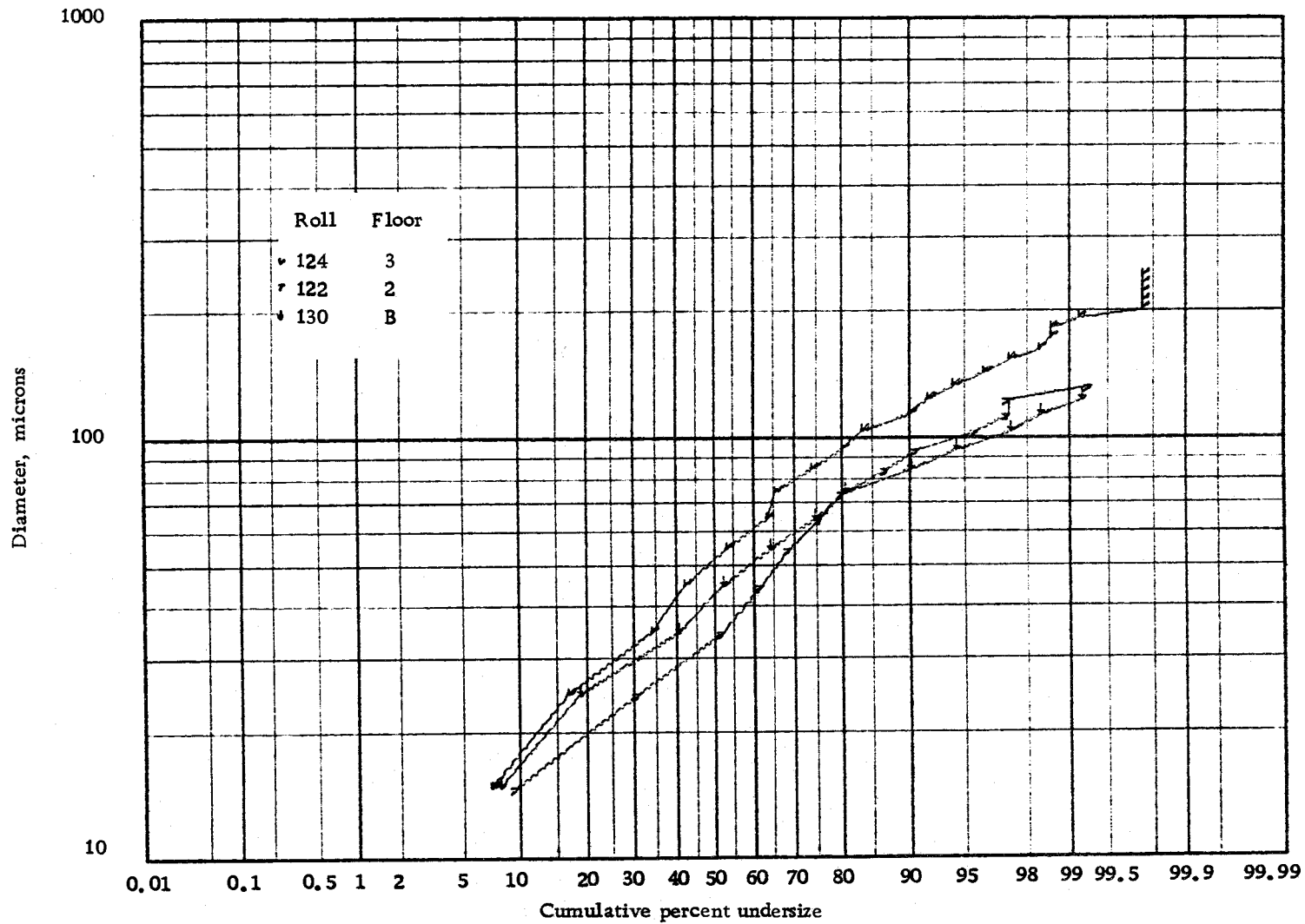


Figure 22. Drop size distributions for 1.3% iso-octyl alcohol, $\gamma/R_w = 0.05$, 16 ft/sec.

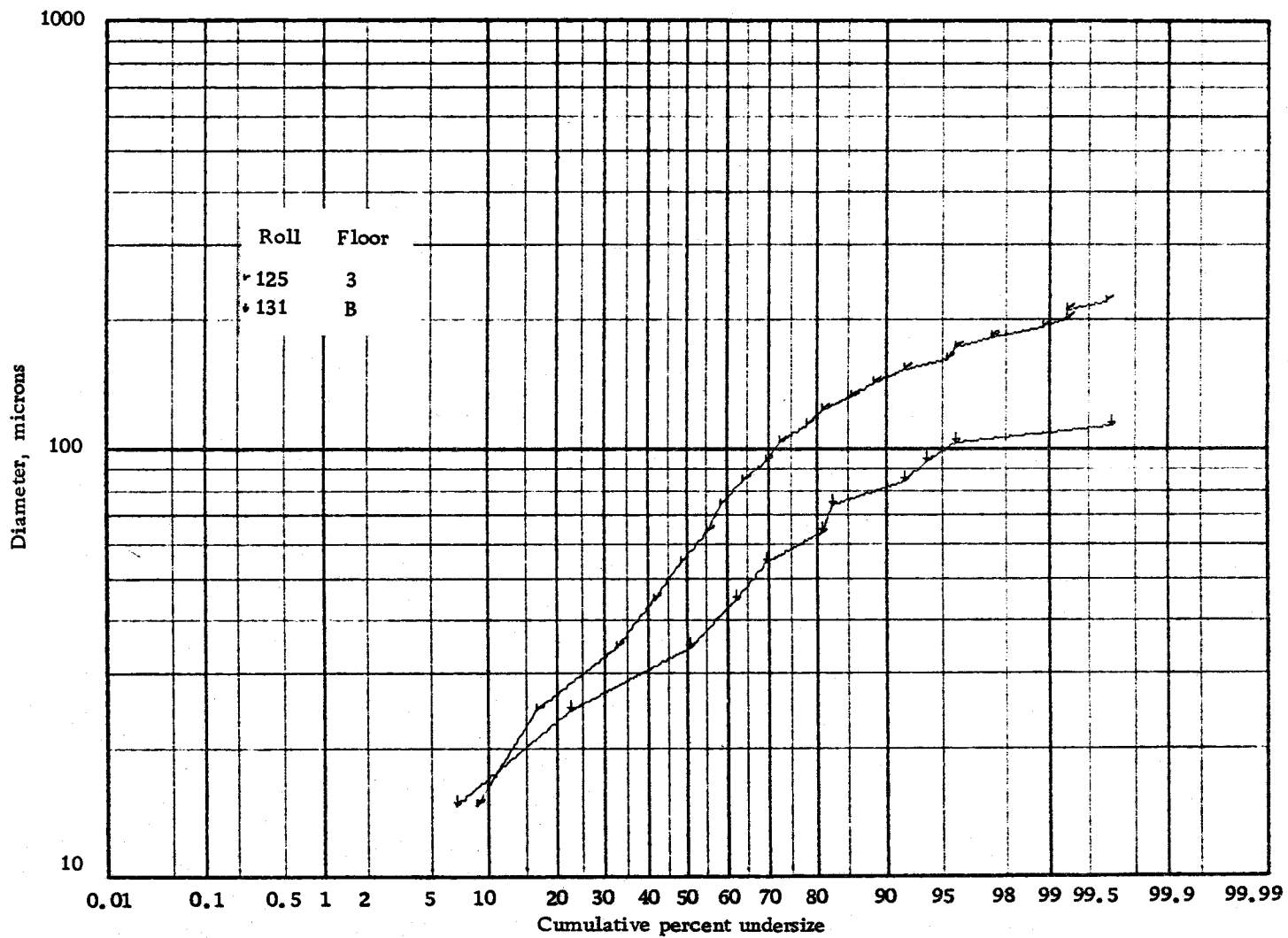


Figure 23. Drop size distributions for 1.3% iso-octyl alcohol, $\gamma/R_w = 0.1$, 16 ft/sec.

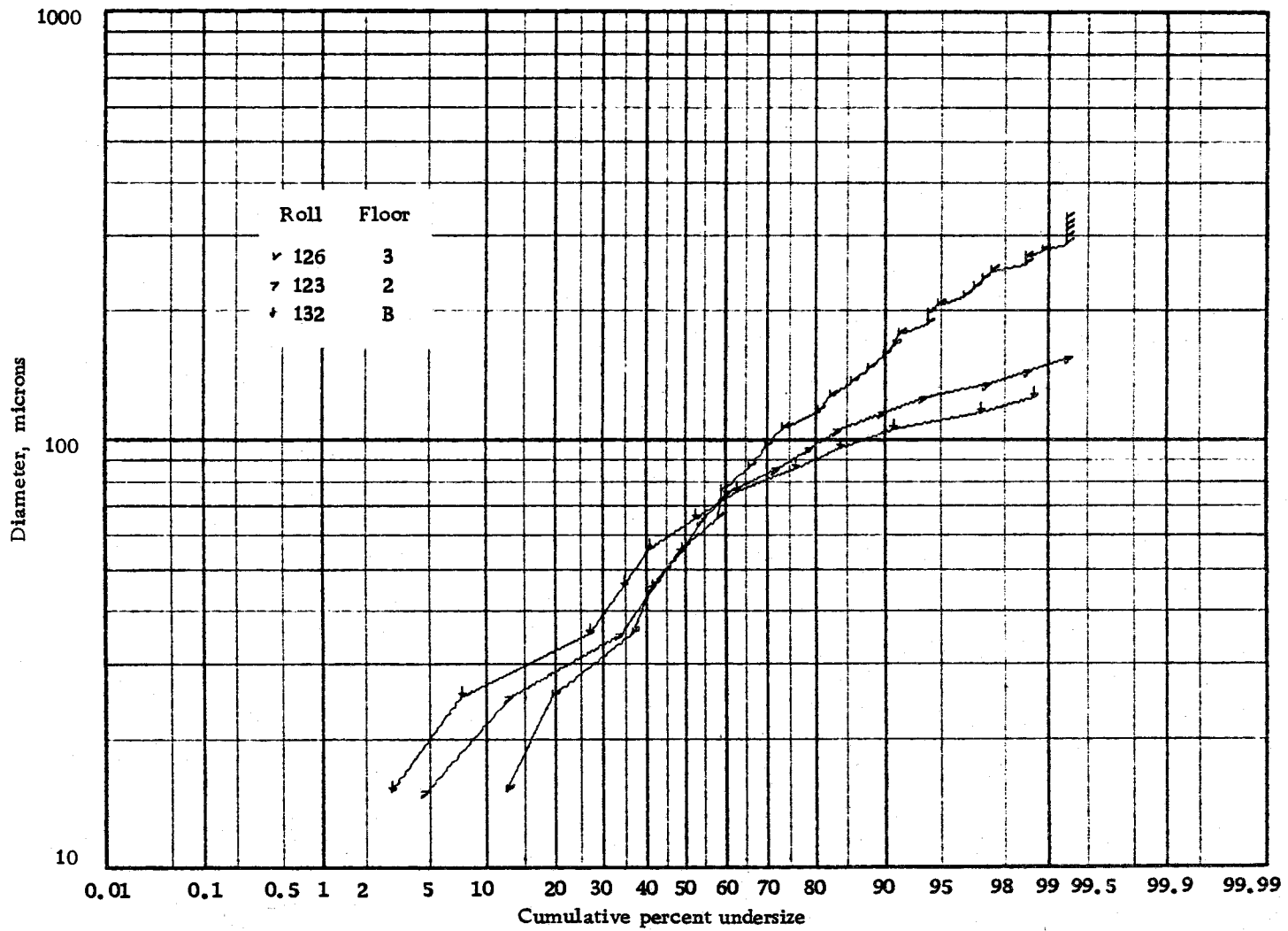


Figure 24. Drop size distributions for 1,3% iso-octyl alcohol, $y/R_w = 0.4$, 16 ft/sec.

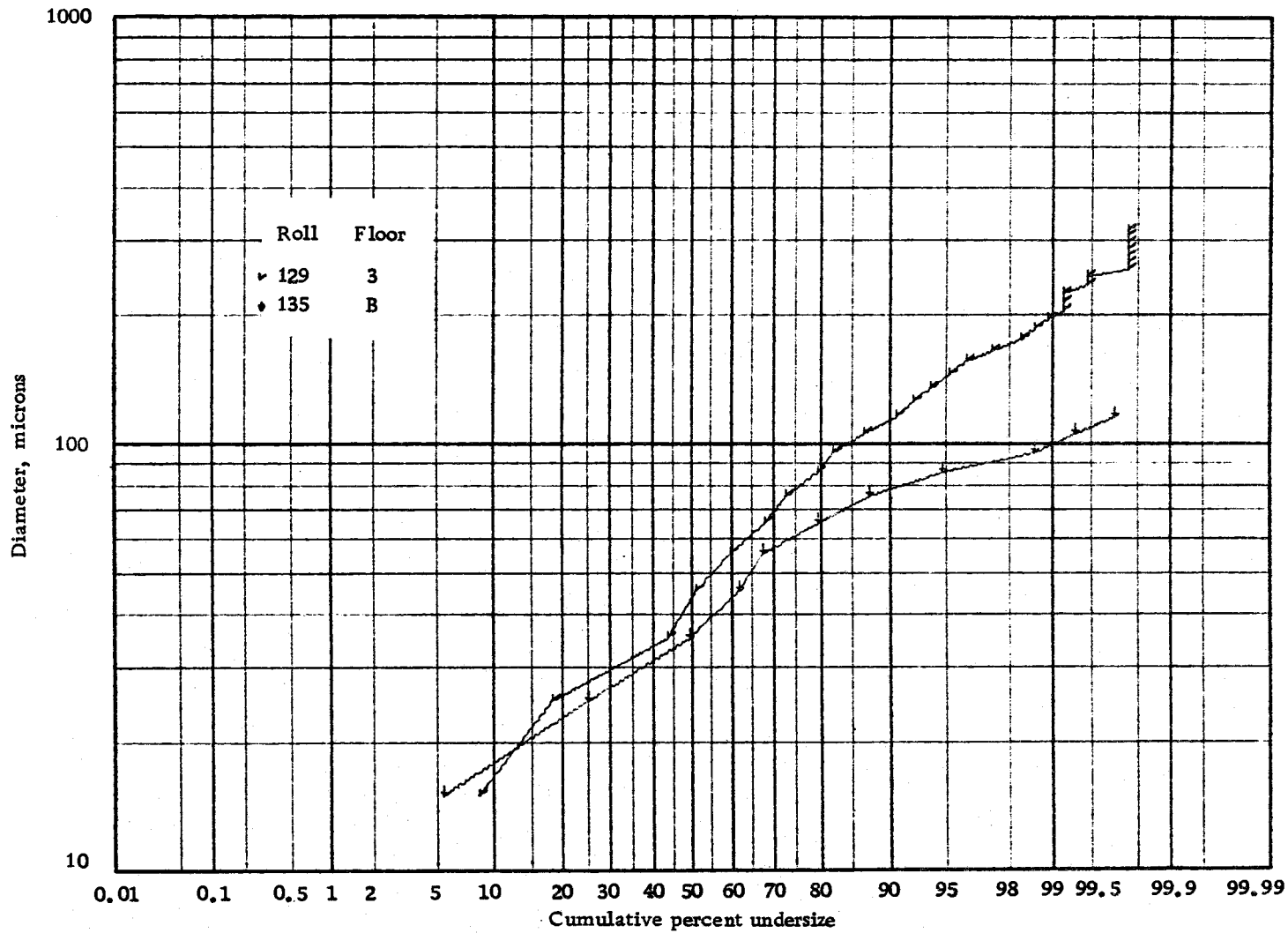


Figure 25. Drop size distributions for 0.6% iso-octyl alcohol, $\gamma/R_w = 0.05$, 16 ft/sec.

DISCUSSION OF RESULTS

Mathematical Model

In order to gain insight into the breakup mechanism responsible for the drop size distributions observed experimentally, possible mechanisms were explored and expressed quantitatively in order to develop a model of the system. The stochastic (or probabilistic) approach as opposed to the deterministic approach to mathematical modeling was indicated by the chaotic nature of the turbulent field responsible for breakup as well as the large number of breakage events leading to the genesis of the observed distributions. As will be seen, the breaking of liquid-liquid dispersions in turbulent pipe flow lends itself well to stochastic modeling.

Because of the low dispersed phase concentrations (less than 10%) used in the experiments and the short time (less than 3 sec) during which the dispersion was in the pipe, it was decided to ignore coalescence effects as compared to breakage effects in the model. It is significant to note that of the nearly 1300 prints examined in the experimental portion of this study no coalescence events were identifiable. In comparison, a significant number of highly deformed drops which appeared ready to fracture and likewise fragments from such fractures were seen. A few examples of such phenomena are shown in Figure 11.

Central to the proposed model is the postulate that the entire process may be considered to take place in independent discrete steps. Epstein (7), in his study of attrition of solids, used this postulate together with the postulates that probability of breakage and the distribution of daughter particles are independent of particle size and showed that a log-normal distribution resulted as a consequence. As described earlier, previous workers (10, and 31) have shown both experimentally and theoretically the existence of a maximum stable drop size for liquid-liquid dispersions in turbulent pipe flow. Thus any model would be expected to include the maximum stable drop size as a parameter. These two ideas together with the requirement that the total mass of the dispersed phase must be conserved were used as starting points in the evolution of the model.

Actual implementation of the model was in the form of a FORTRAN program employing Monte Carlo techniques. A CDC3300 digital computer was used for all of the calculations. The program is detailed in the appendix. The "meat" of the program is to be found in the set of subroutines named MODEL. The balance of the program handles statistical analysis and input/output. Figure 26 shows a generalized flow chart for the subroutine model. Previous to this subroutine, the distribution under consideration has been stored in an array, KFREQ(I), where the value of the Ith array element is the number of drops found in the particular ten micron

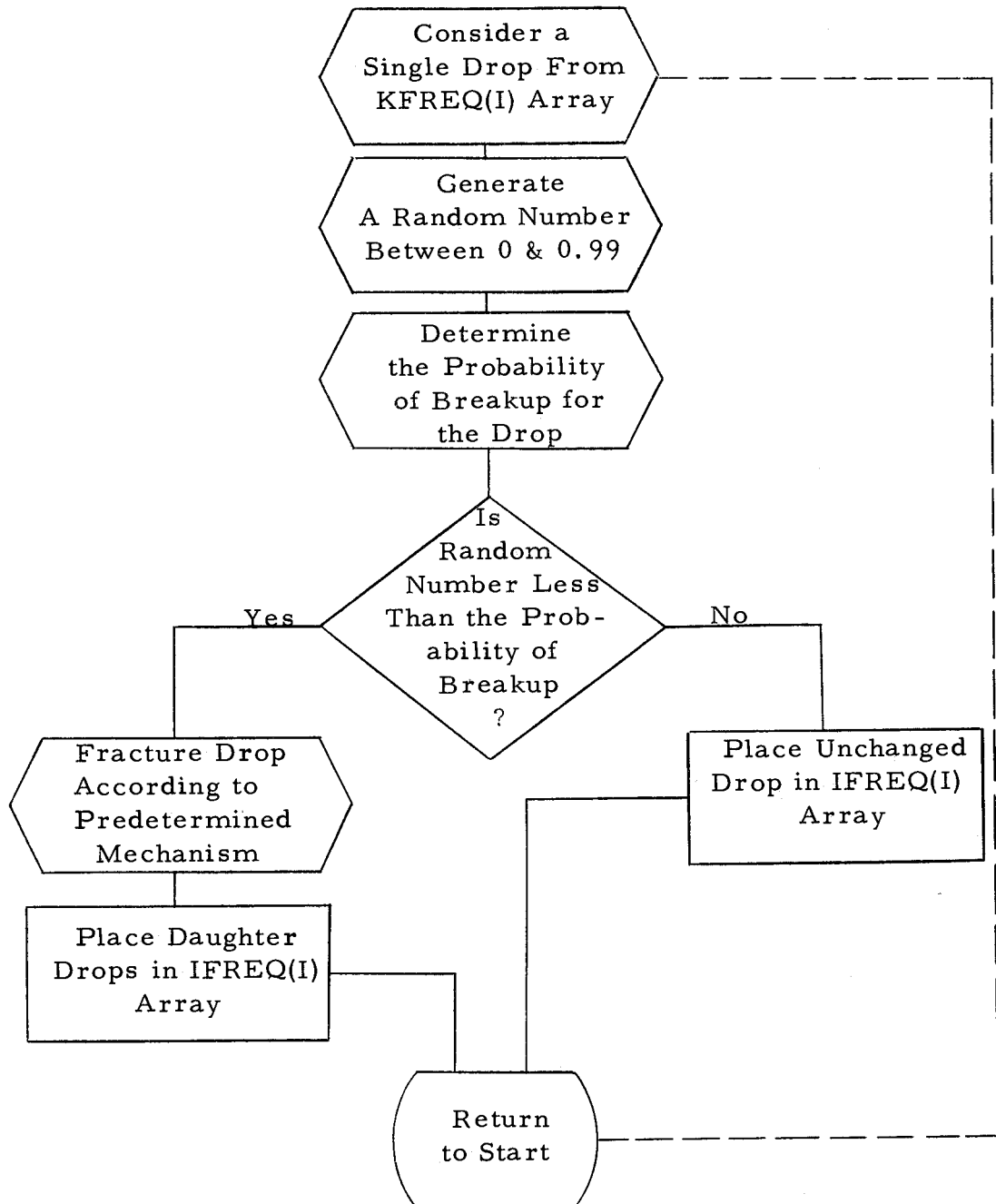


Figure 26. Generalized subroutine MODEL.

interval. The random nature of the breakup process was simulated with the aid of a random number generator. For example, if it was postulated that there was a fifty percent chance of breakup, a random integer between 0 and 99 was generated from a uniform distribution. If the number was greater than or equal to 50, breakup did not occur. If the number was less than 50, breakup occurred. In most of the models a random number generator was also used to randomize the sizes of the daughter drops resulting from breakup. Uniform populations and normal populations were used for this purpose. Drops resulting from the breakup process were placed in an array, IFREQ(I). After all of the elements of the KFREQ(I) array had been considered, the contents of the IFKEQ(I) array were transferred to the KFREQ(I) array, the IFREQ(I) array zeroed and the process repeated for the next breakup step.

A summary of the various breakage mechanisms studied in the effort to simulate the action of the turbulent field are shown in Table IV.

Proposed models were judged by their ability to simulate the experimental distributions observed downstream, when the distribution observed at the top of the pipe was used as data for the program. Experimental distributions were compared graphically in the form of frequency-diameter histograms and log-probability plots and analytically in the form of weighted average diameters.

Table IV. Mathematical models examined.

| Model | Description |
|-------|--------------------------------------------------------------------------------------------------------------------------------------------------------------------------------------------------------------------------------------------|
| 1 | All drops have a 50% probability of breakup into two daughter drops having a uniformly distributed volume ratio. |
| 2 | Same as Model 1 except that the ratio of daughter drop volumes is distributed normally about 0.5. |
| 3 | All drops with a diameter greater than IMAXS have a 50% probability of breakup into two uniformly distributed daughter drops. |
| 4 | Drops with diameters below IMAXS have a 10% chance of breakup; those with diameters above IMAXS have a 50% chance of breakup. A pair of uniformly distributed daughter drops result from each breakup. |
| 5 | Drops with diameters above IMAXS have a 50% chance of breakup into three equal daughter drops. |
| 6 | Drops with diameters above IMAXS have a 50% chance of breakup. Two to six equal-sized daughter drops are produced with equal probability. |
| 7 | Drops with diameters above IMAXS have a 50% chance of breakup into a pair of uniformly distributed daughter drops and a single small satellite drop whose volume is a fixed fraction of one of the daughter drops. |
| 8 | Same as Model 7 except two satellites are formed. |
| 9 | Probability of breakup is zero below a diameter equal to IMAXS and increases linearly to a 1.0 probability at a diameter equal to KPROB. Two uniformly distributed daughter drops and a satellite drop of fixed volume ratio are produced. |
| 10 | Same as Model 9 except probability increases quadratically. |
| 11 | Same as Model 9 except the satellite to daughter drop volume ratio is uniformly distributed over a fixed range. |

Initial trials of the model were compared with distributions observed for the data shown in Figure 7. The observations from Roll 65 (Figure 27) were used as data for the model.

To ascertain the effect of a maximum stable drop size on the genesis of a drop size distribution, Models 1 and 2 were compared with Model 3. As can be seen from Figure 29, Model 1 results in a series of parallel straight lines as the drops broke up. This mechanism then leads to an ever increasing percentage of very small drops in a log normal distribution. Model two, very similar to a case treated theoretically by Epstein (8), gave results almost identical to those of Model 1. Figure 31 shows the effect of the maximum stable drop size on the drop size distributions. In this case, the percentage of small drops decreased and the lines representing the distribution became more curved as the drops broke up. The lines appear to have a common point of intersection.

Comparison of the experimental results shown in Figure 27 with Figures 29 and 31 shows considerable similarity between Figures 27 and 31 and little similarity between Figures 27 and 29. On this basis, the assumption of a maximum stable drop size appears to be a good one. Comparison of the histograms shown in Figures 28, 30, and 32 leads to the opposite conclusion. Figure 32 shows that the assumption of a maximum stable drop size leads to a high peak with a mode close to the maximum stable drop size in addition

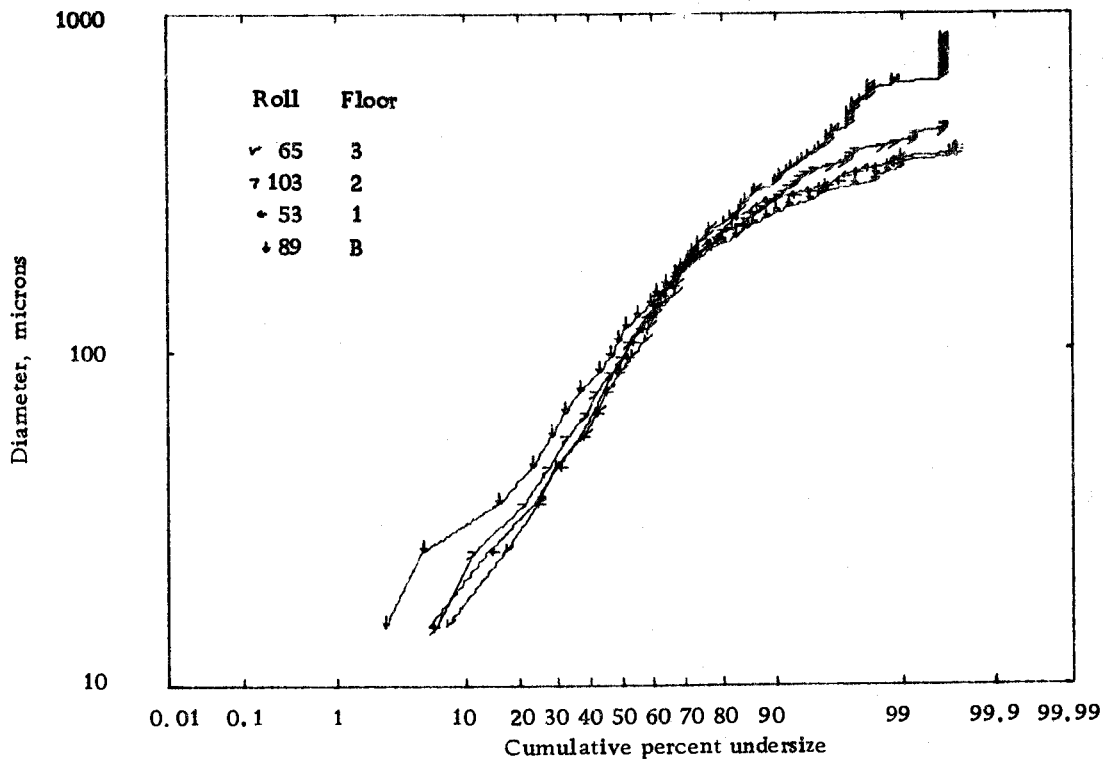


Figure 27. Drop size distribution for 1.3% Shellsolv, $\gamma/R_w = 0.1$, 16 ft/sec.

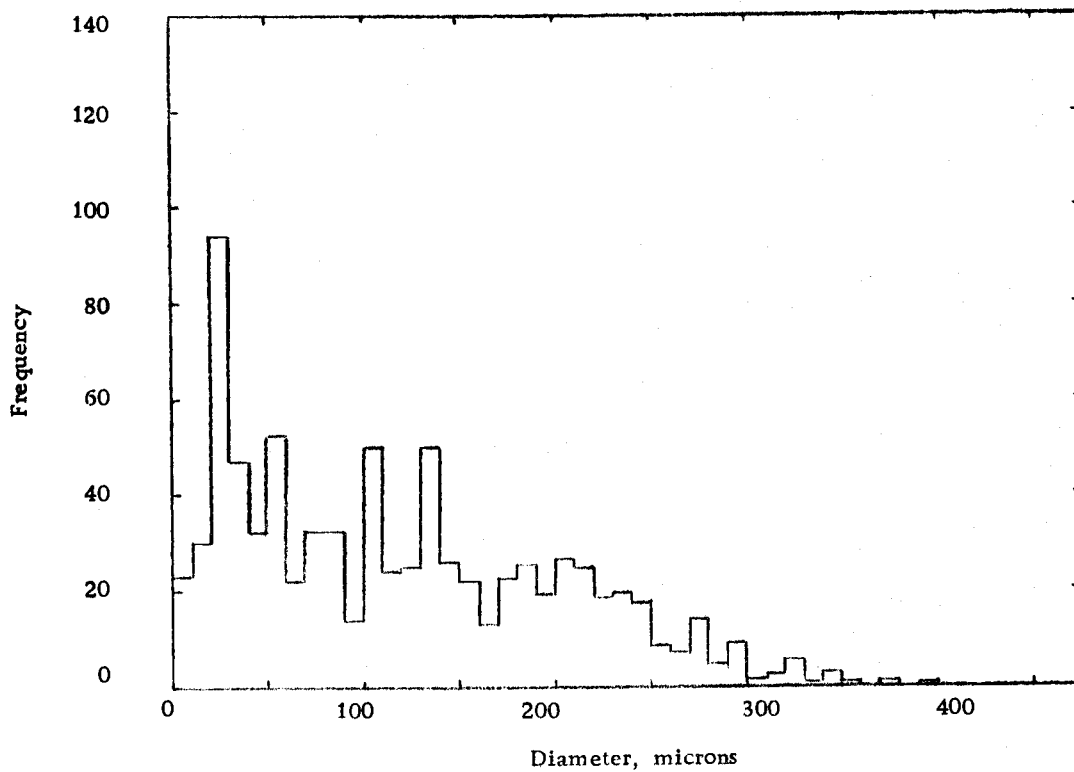


Figure 28. Frequency histogram for Roll 89.

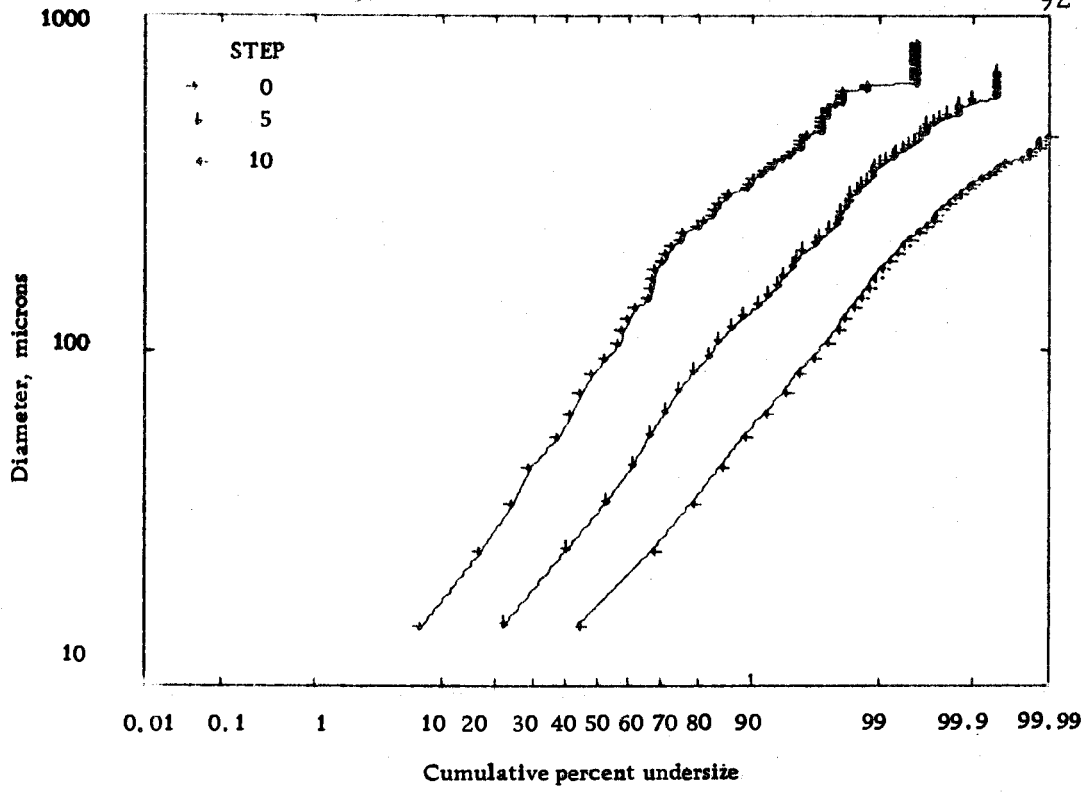


Figure 29. Model 1, log-probability plot.

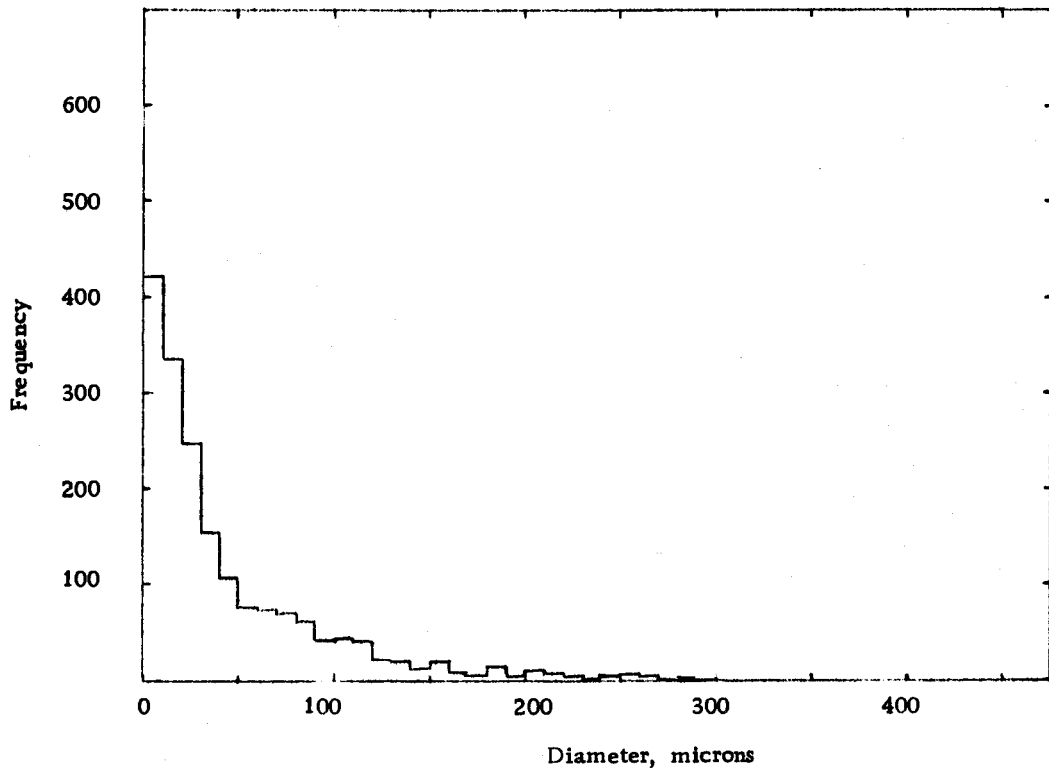


Figure 30. Model 1, frequency histogram, step 5.

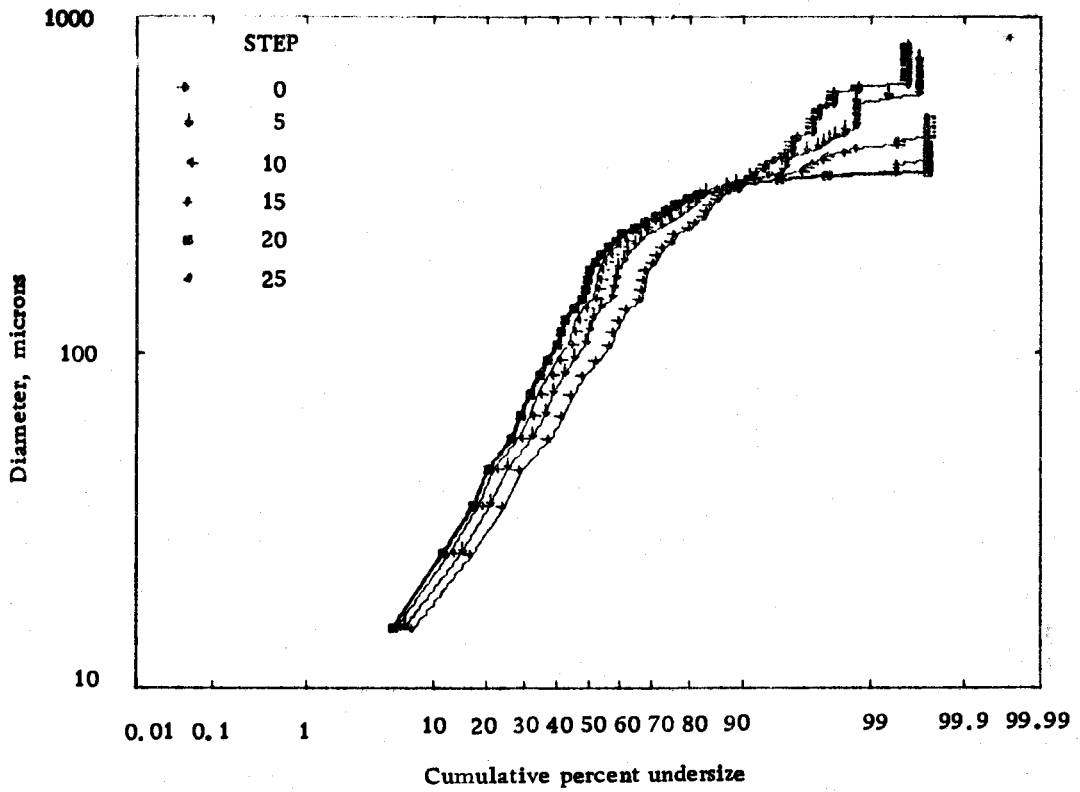


Figure 31. Model 3, log-probability plot.

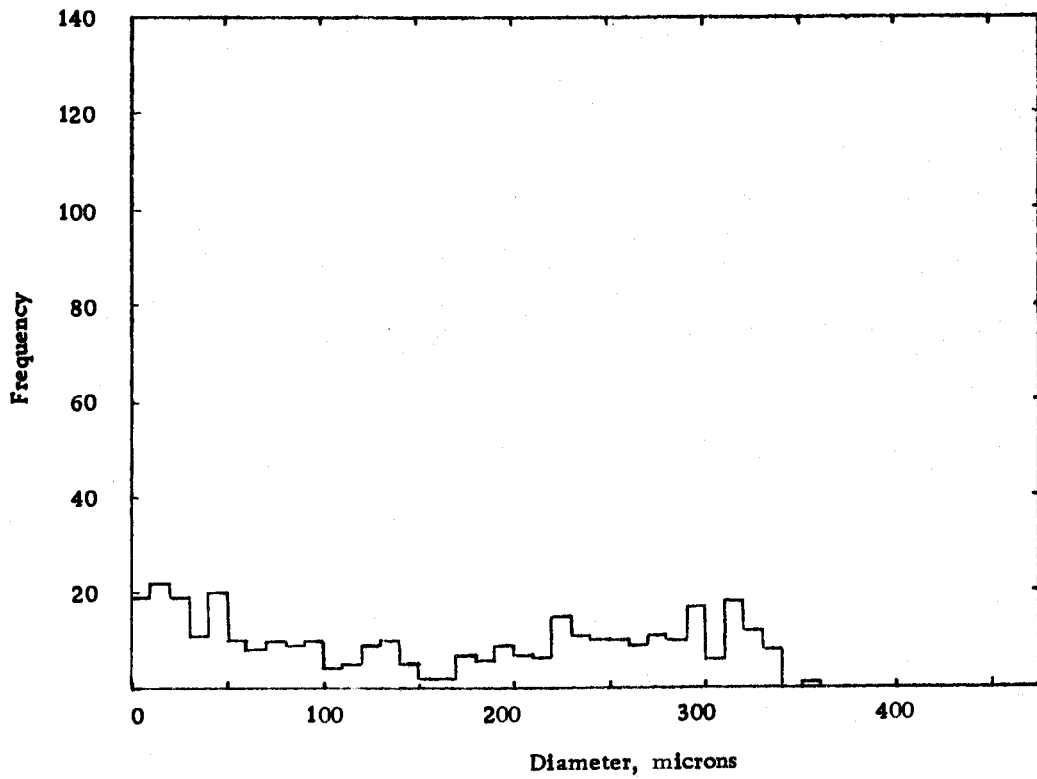


Figure 32. Model 3, frequency histogram, step 25.

to the peak at approximately 30 microns which was present in the initial distribution. Figure 30 shows that Model 1 gives a unimodal distribution similar to that shown in Figure 28 which represents experimental observations.

The result of a compromise between Models 1 and 3 is shown in Figures 33 and 24. Here the probability of breakup was postulated to be 0.1 below the maximum stable drop size and 0.5 above it. Unfortunately this compromise retained the bad features of Models 1 and 3 and not the good ones.

The experimental observations of Rumscheidt and Mason (26) on the modes of breakup in laminar flow fields (Figure 1) indicated that a drop might split into more than two daughter drops. On the basis of the observations of these workers, two mechanisms were postulated. First, in Models 5 and 6, multiple daughter drops of equal size were postulated. Second, in Models 7 and 8, binary breakup with one and two small satellite drops, respectively, were postulated.

The assumption of three equal daughter drops gives little improvement over the assumption of binary breakup as shown by Figures 35 and 36. The limiting curve in Figure 35 breaks much faster than the corresponding curve observed experimentally and there is still a high peak (Figure 36) in the neighborhood of the maximum stable drop size. Similar trials with four, five and six equal daughter

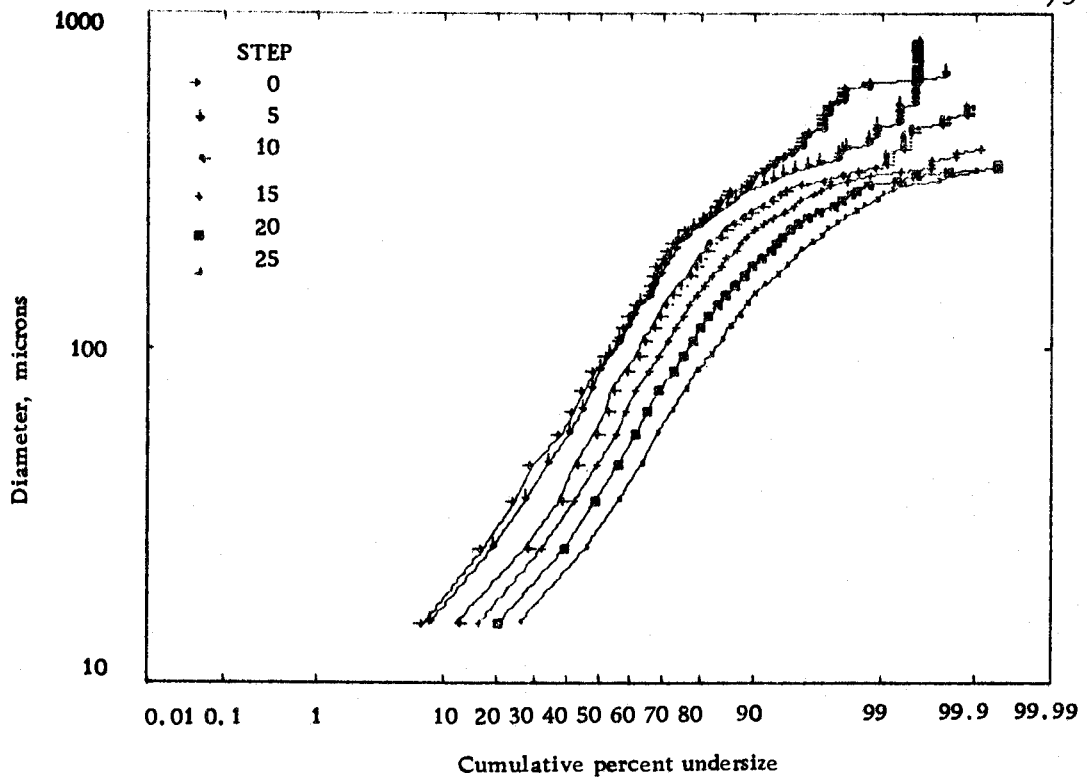


Figure 33. Model 4, log-probability plot.

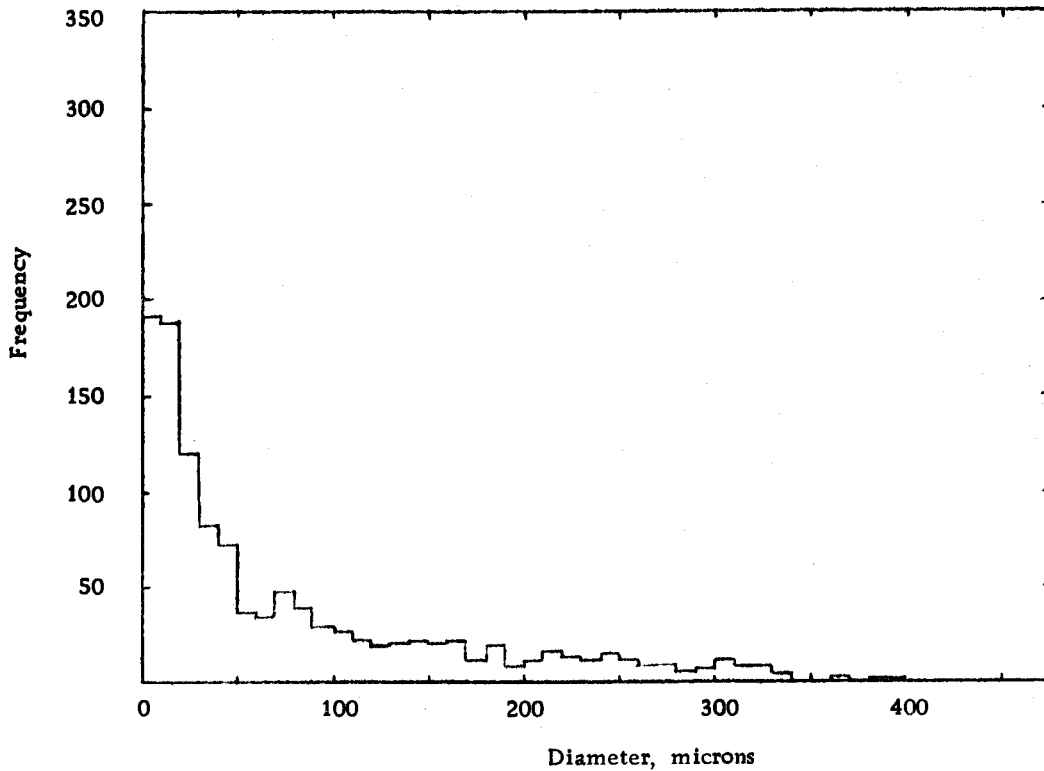


Figure 34. Model 4, frequency histogram, step 15.

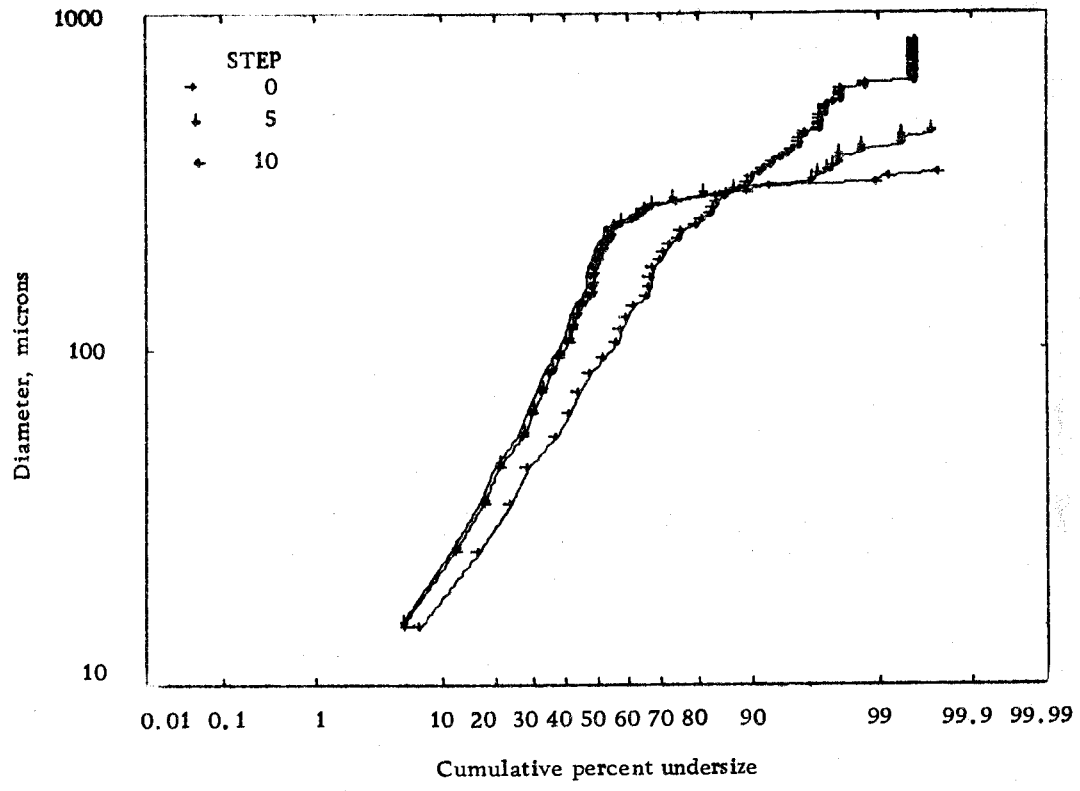


Figure 35. Model 5, log-probability plot.

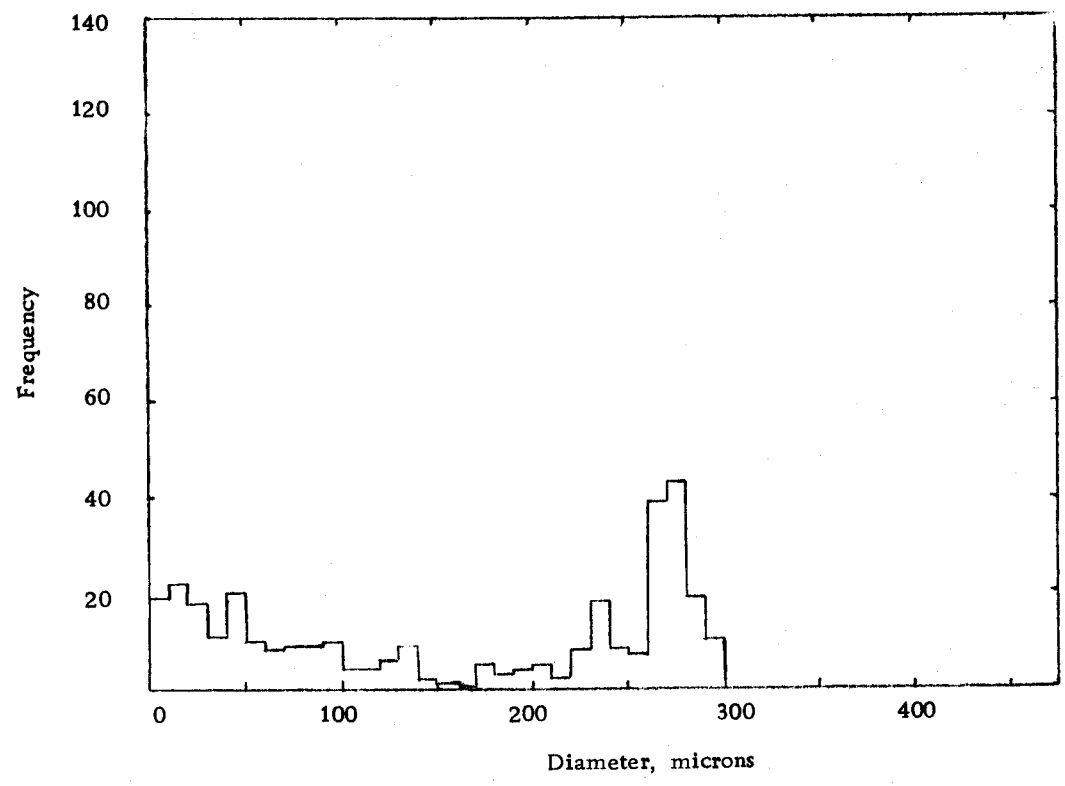


Figure 36. Model 5, frequency histogram, step 10.

drops produced no marked improvement and are not shown. When two to six equal drops were equally probable at each step of the breakup process, results were even worse. For Model 6, Figure 37 shows a very sharply breaking limiting curve.

Models 7 and 8 demonstrate the effect of satellite formation on the drop size distribution. A fixed satellite volume to daughter-drop volume ratio was postulated. The value of this ratio was chosen so as to make the most of the satellites fall into the size range covered by the 30 micron peak found in the initial distribution. Figure 40 shows that Model 8 gives an improved representation of the experimental results as shown in Figure 28. The primary shortcomings of Models 7 and 8 are that they predict a sparsity of drops in the middle range of drop sizes and that it predicts a sharp drop in the number of drops at the maximum stable drop size. The triple crossing predicted by Models 7 and 8 (Figures 38 and 39) indicate that too many small drops are created by both models.

Elimination of the sharp drop in the number of drops predicted in the neighborhood the maximum stable drop size was successfully accomplished by changes which resulted in Model 9. In this case it was postulated that the probability of breakup decreased linearly from 1.0 to 0.0 between two specified drop sizes determined by trial and error. The results are shown in Figures 41 and 42. Model 10 assumed a second order decrease in the probability of breakup.

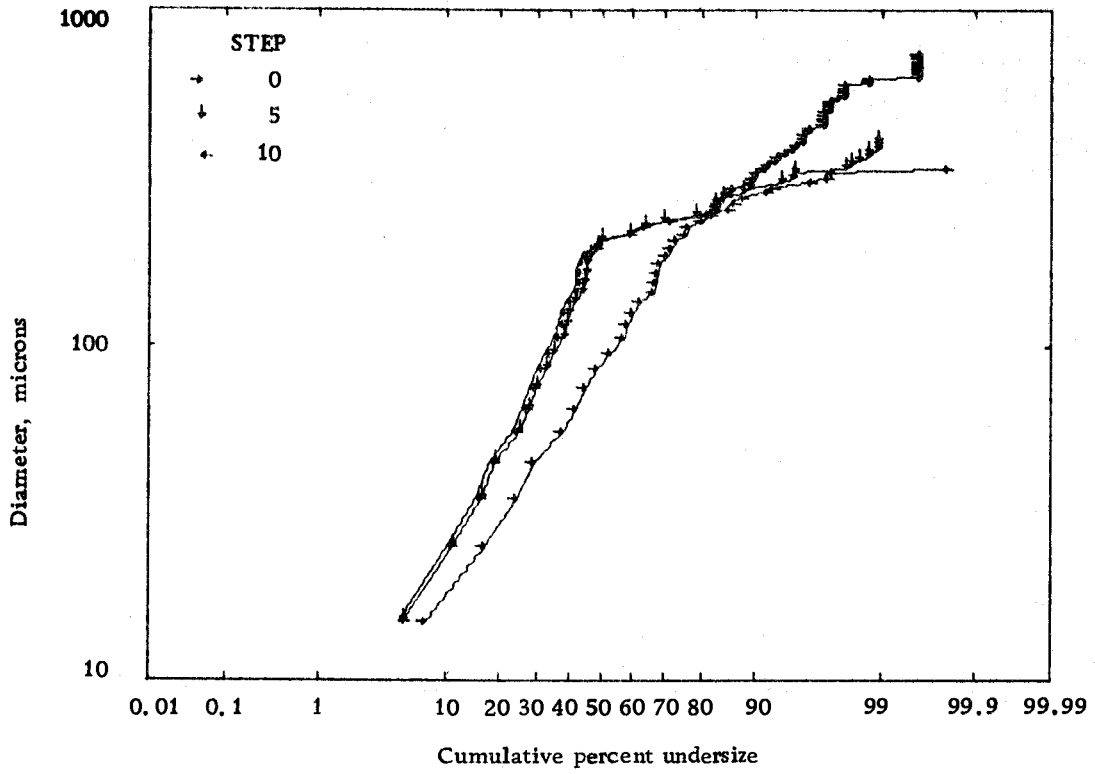


Figure 37. Model 6, log-probability plot.

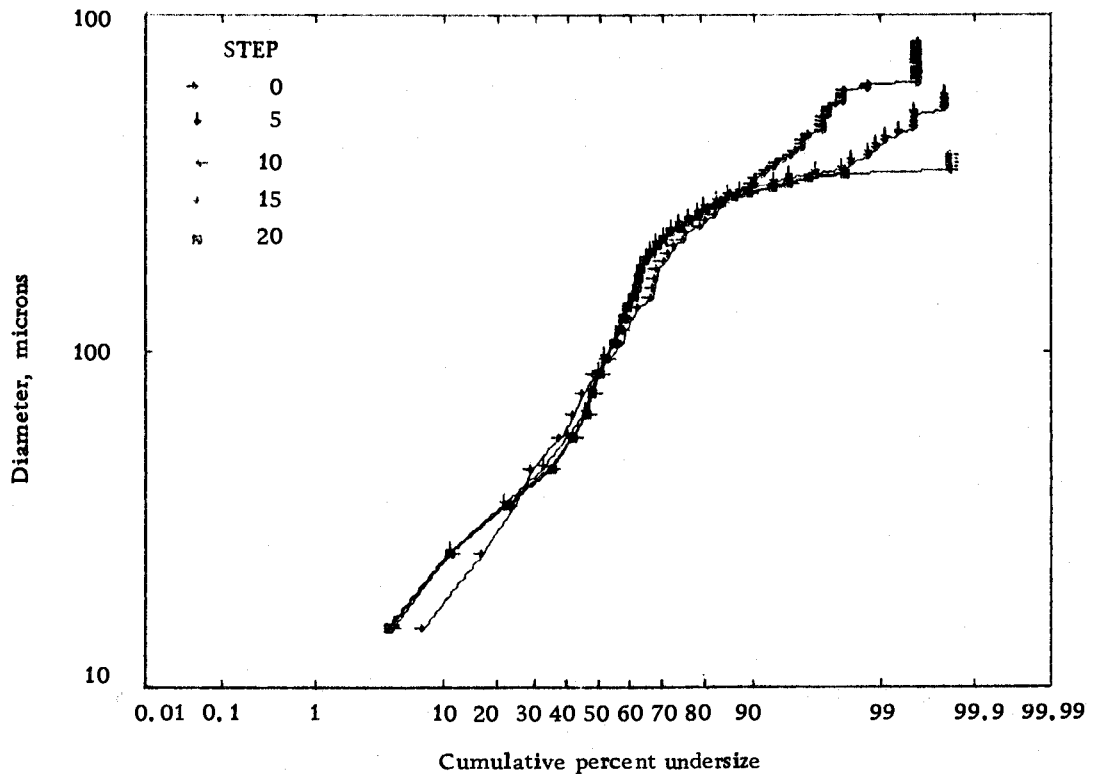


Figure 38. Model 7, log-probability plot.

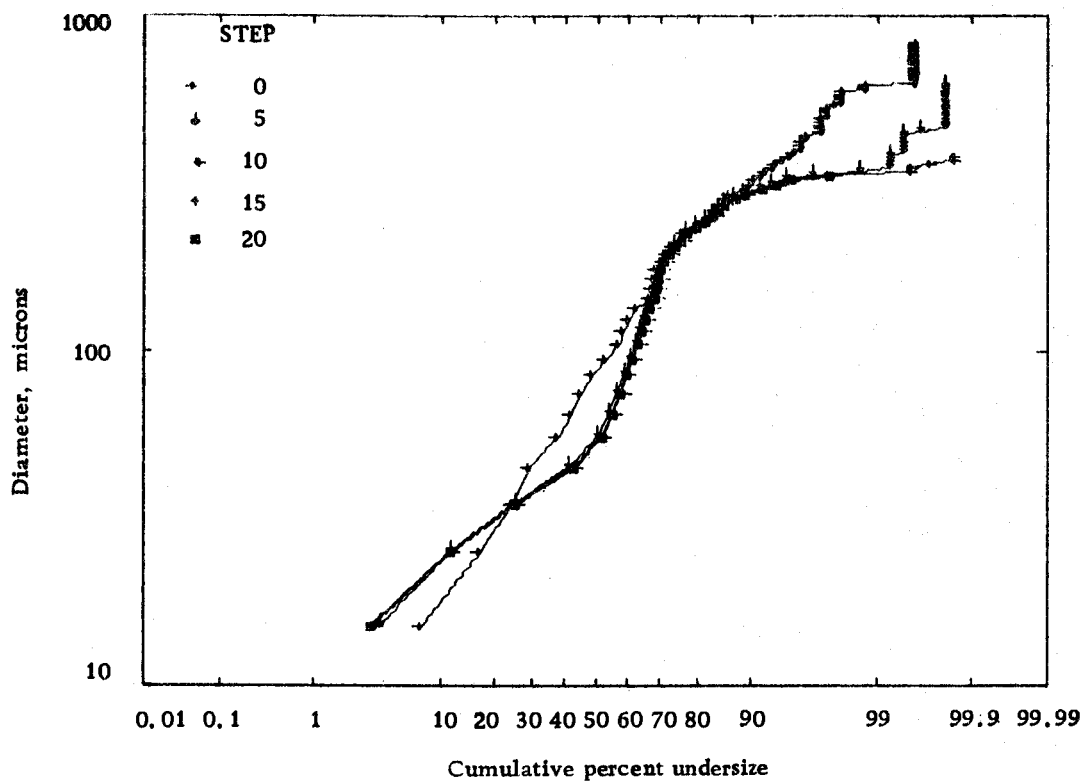


Figure 39. Model 8, log-probability plot.

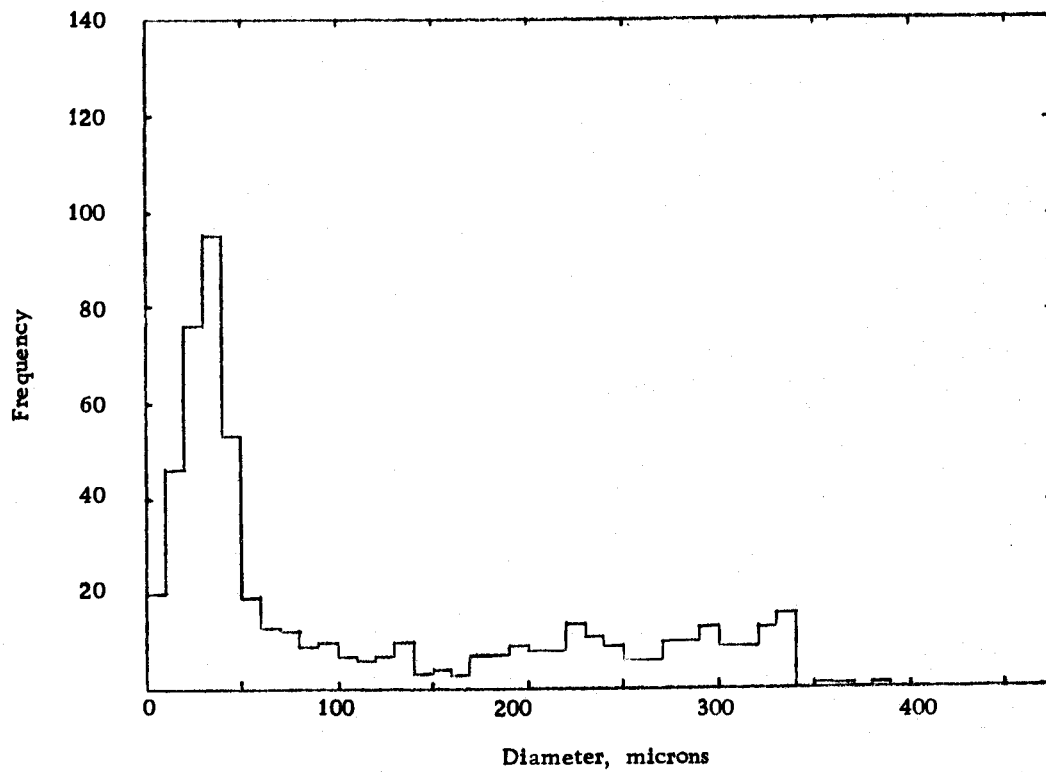


Figure 40. Model 8, frequency histogram, step 20.

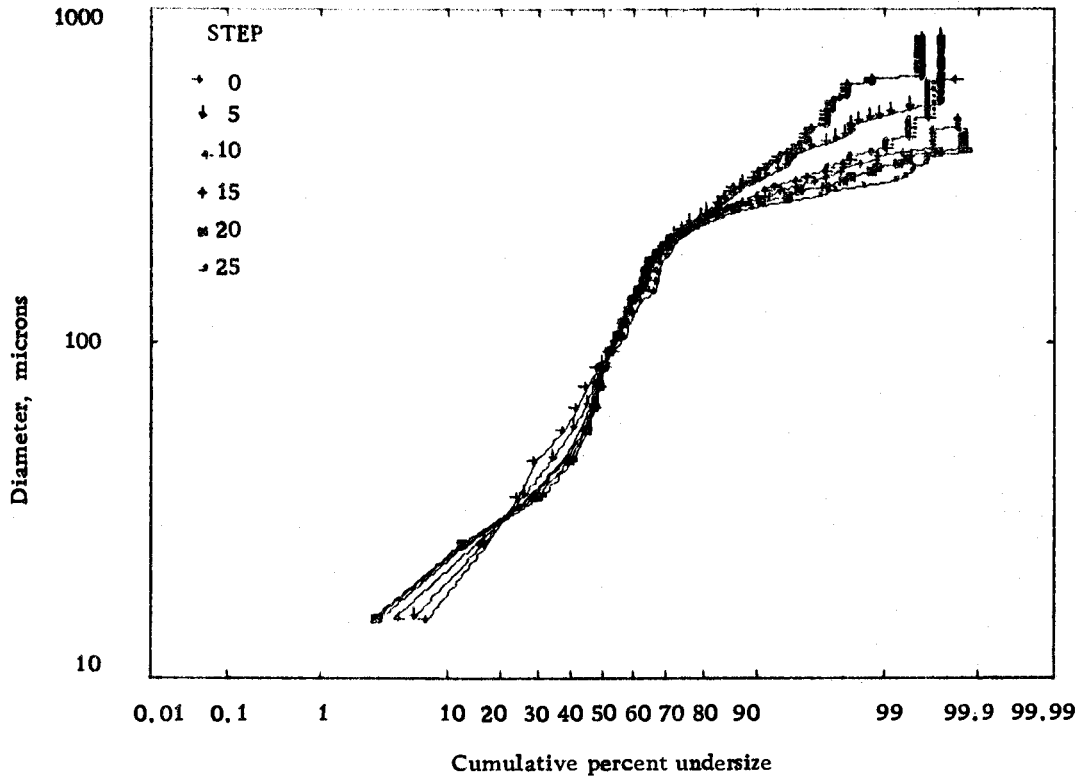


Figure 41. Model 9, log-probability plot.

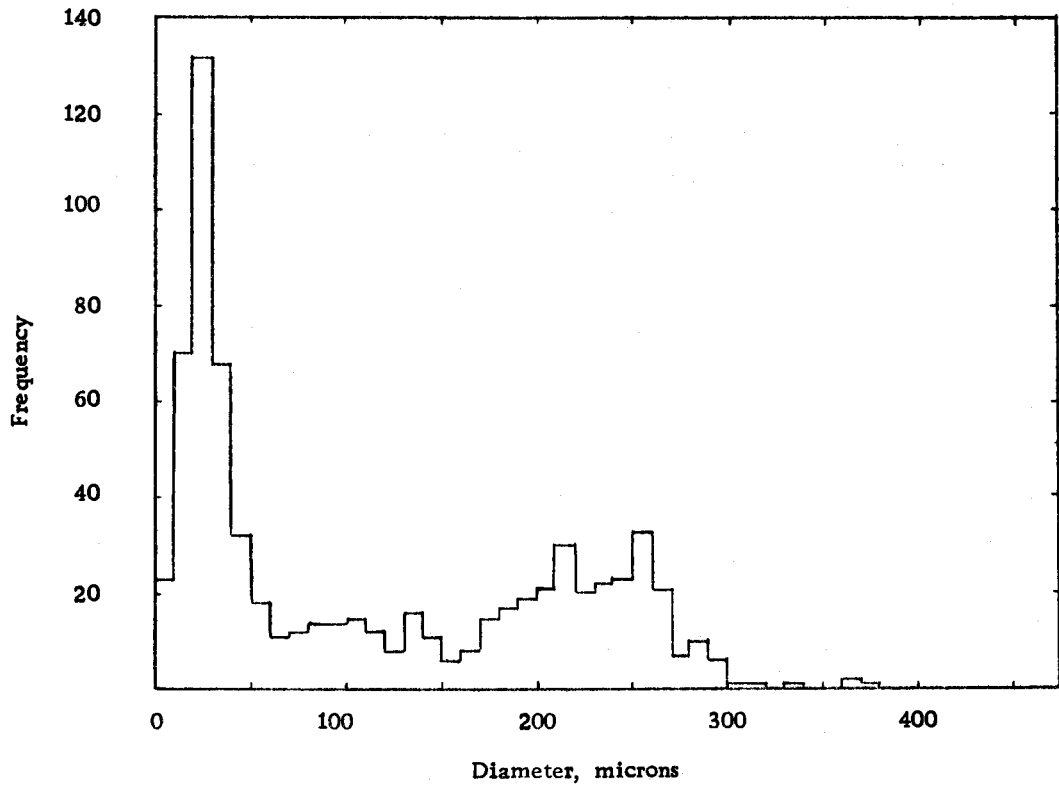


Figure 42. Model 9, frequency histogram, step 25.

Comparison of Figures 42 and 44 indicated that this assumption did not improve the model.

The results of allowing the ratio of satellite volume to daughter volume to vary randomly over a small range are shown in Figures 45 and 46. Comparison with Figures 27 and 28 shows that Model 11 predicts a sequence of distributions very similar in form to those observed experimentally. Not only has the sparsity of drops in the middle range been eliminated (compare Figures 40 and 46), but also the triple crossing predicted by Models 7 and 8 has disappeared (compare Figures 28 and 45). It was concluded that Model 11 gave an adequate qualitative representation of the events occurring in the pipe for the single set of experimental observations shown in Figures 27 and 28.

Comparison of the Model to Experiment

The reason no simple size distribution law could be found to describe the experimentally observed distribution is obvious from the form of the model. The existence of the maximum stable drop size means that that portion of the initial distribution with diameters less than the maximum stable drop size remains unchanged by the action of the turbulence. Thus what was actually measured was a superposition of two distributions, one initially present and the other produced by the turbulence.

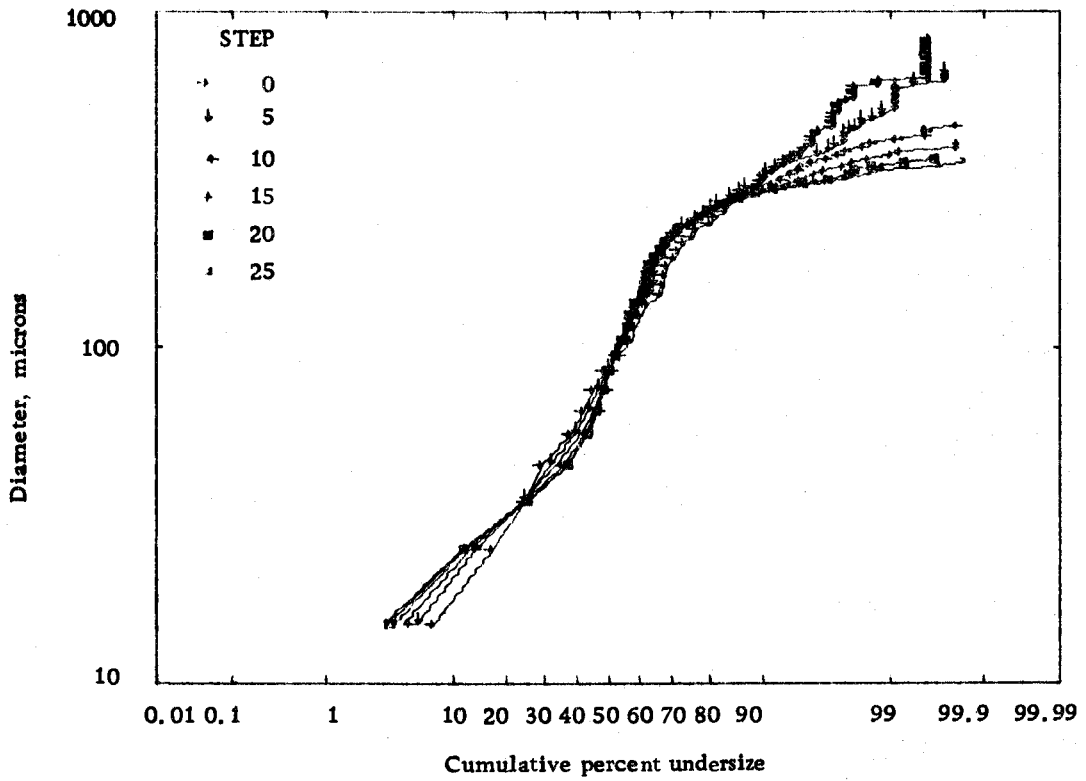


Figure 43. Model 10, log-probability plot.

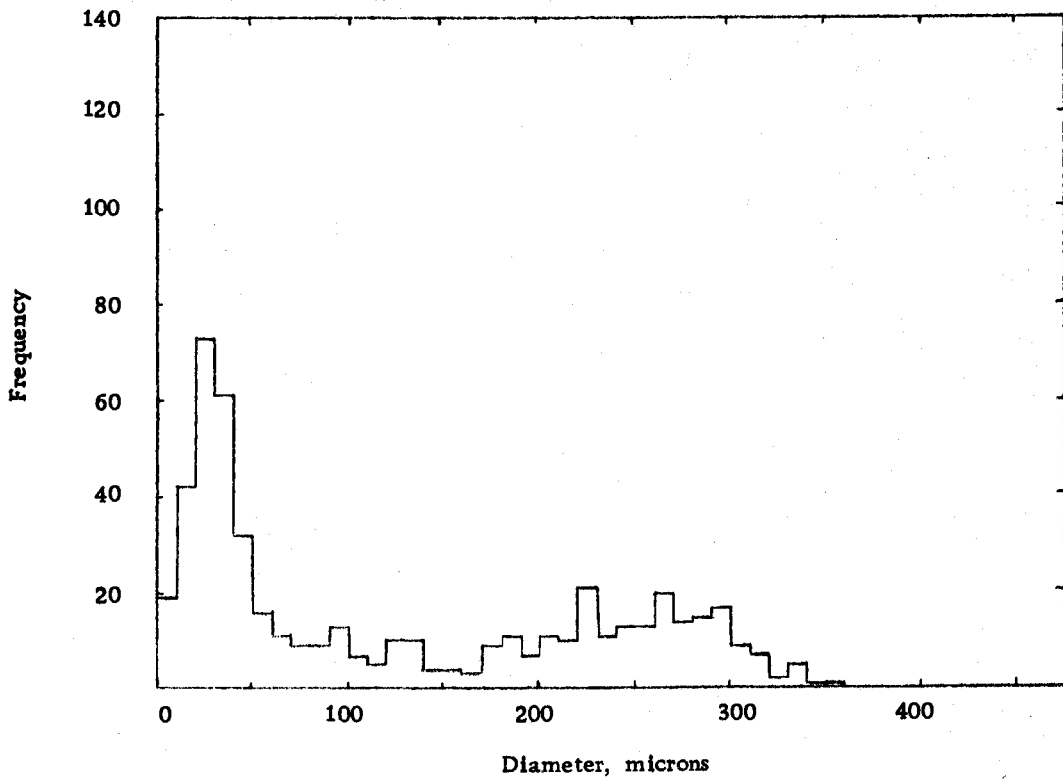


Figure 44. Model 10, frequency histogram, step 25.

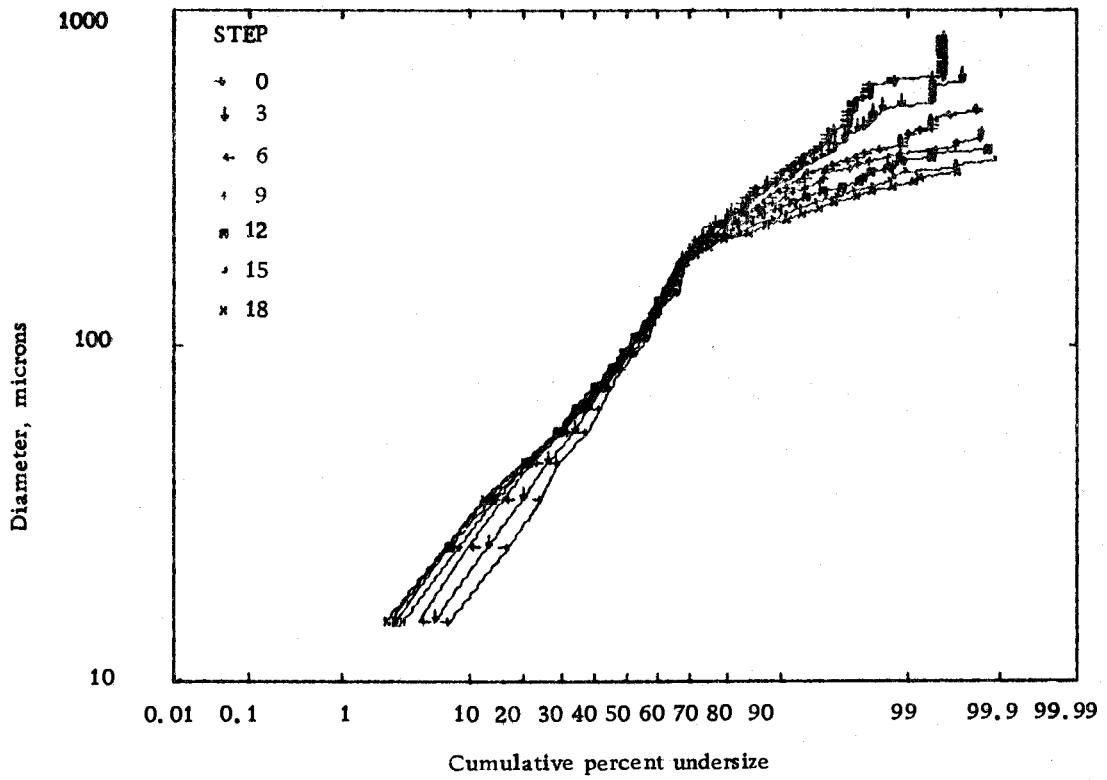


Figure 45. Model 11, log-probability plot, IMAXS = 200, KPROB = 700, SAT = 0.01.

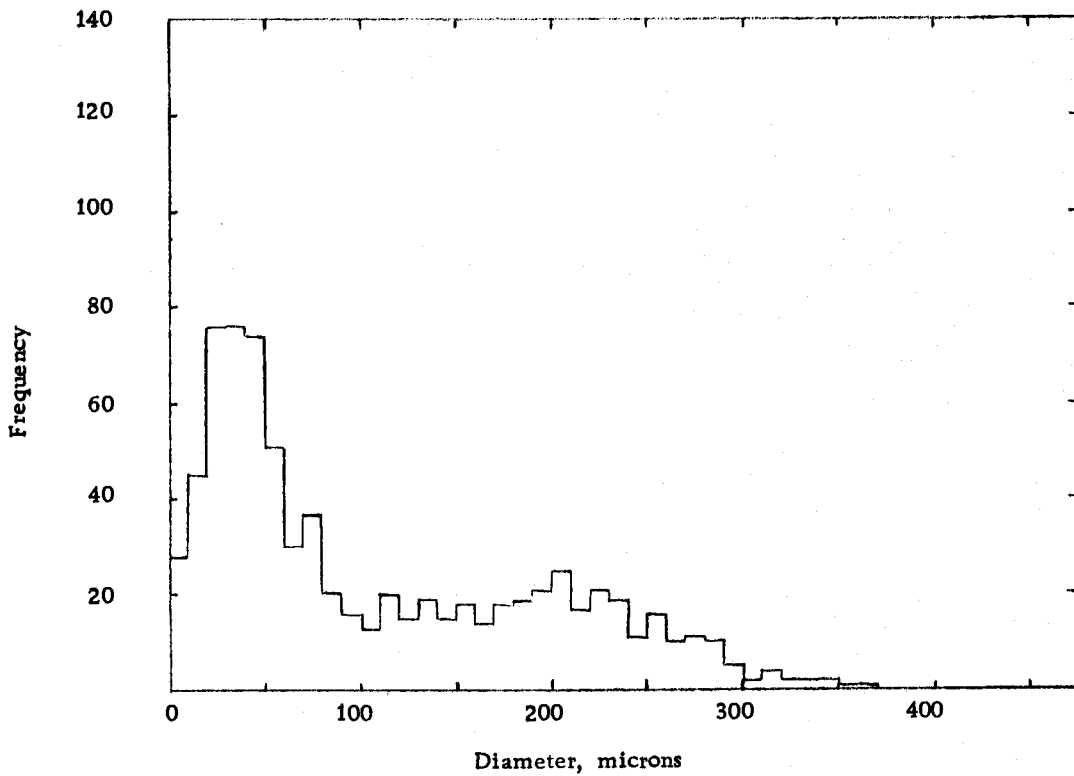


Figure 46. Model 11, frequency histogram, step 15.

Once a qualitatively correct mathematical model had been developed, a quantitative comparison of the weighted averages sizes (Equation 30) calculated from theoretical and experimental distributions was made. Model 11 was a three parameter model; such comparisons allowed the best set of parameters to be found by trial and error. To be acceptable, the model should predict not only the correct individual distributions, but also the proper sequence of distributions or kinetics as the dispersion flows through the pipe. In order to test this aspect of the model a plot of experimental values of D_{32X} vs distance from the nozzle was made as shown in Figure 47. The values of D_{32X} predicted by the model can be compared with the experimental values by constraining the experimental and theoretical curves to match at the nozzle and at a point close to 576 diameters from the nozzle. With these two points fixed, the remaining theoretical points can be plotted by interpolation. The results of such a plot for the data from the 1.3% Shellsolv system used earlier to develop the model is shown in Figure 47 for several sets of parameters. Table V presents both theoretical and experimental weighted average size data for comparative purposes. The model parameters, $IMAXS$, $KPROB$, and SAT are the maximum stable drop size, the point at which the probability of breakup becomes 1.0 and the upper limit on the ratio of satellite volume to daughter drop volume, respectively. Note that the best set of parameters predicts

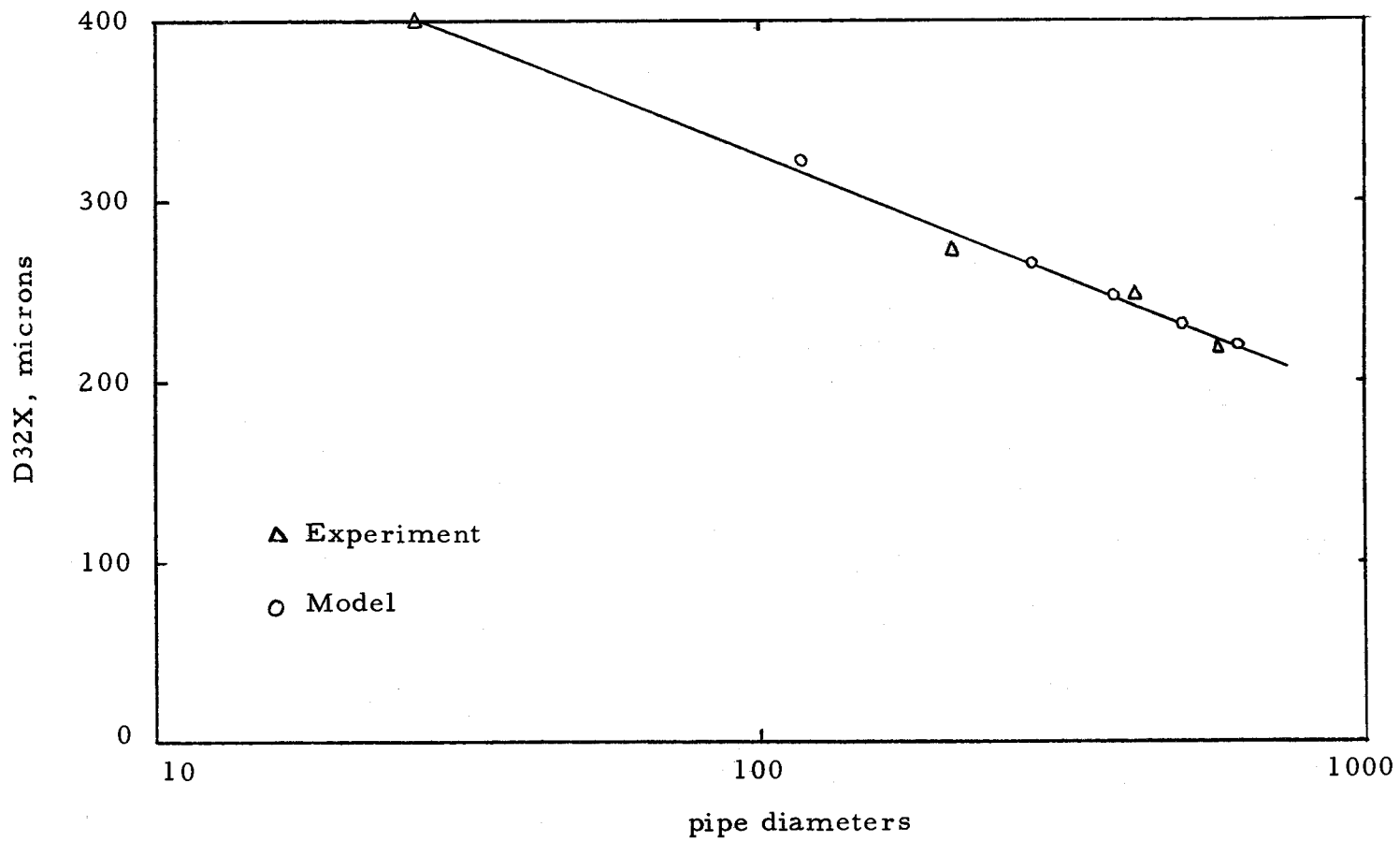


Figure 47. D32X vs. distance from the nozzle, 1.3% Shellsolv, IMAXS = 200, KPROB = 700, SAT = 0.01.

not only the properly timed sequence of distributions but also predicts average sizes which differ no more than ten microns from those measured experimentally. The set of theoretical distribution curves and a theoretical histogram resulting from the best set of parameters are shown in Figures 45 and 46.

Similar analyses of the data from a 5% light oil system (Figure 21) and a 1.3% iso-octyl alcohol system (Figure 22) were also performed. The agreement of the experimental and theoretical kinetics for the light oil case is shown in Figure 48. Similarly Figure 49 illustrates the kinetics for the iso-octyl alcohol system. Average sizes for both systems are presented in Table IV. Theoretical distributions for the light oil and iso-octyl alcohol systems are shown in Figures 50, 51, 52, and 53. The theoretical distributions are in good qualitative agreement with the experimental observations shown in Figures 21 and 22 in both cases. Although no attempt was made to find the optimum parameters for other sets of experimental data, the similarity to those sets which were treated would indicate that no fundamental change in the model would be necessary to achieve a good fit in all cases.

The agreement between the maximum stable drop size as predicted by Sleicher's correlation (Equation 27) and that predicted by the model is very good. Equation 27 gives maximum stable drop sizes of 100, 170 and 230 microns for the Shellsolv, light oil and

Table V. Empirical and theoretical average sizes

| Model Parameters | | | | D10X | D20X | D30X | D21X | D31X | D32X |
|--------------------|-------|-----|------|-------|-------|-------|-------|-------|-------|
| IMAXS | KPROB | SAT | STEP | | | | | | |
| SHELLSOLV ROLL 89 | | | | 121.2 | 149.2 | 183.8 | 170.7 | 202.6 | 223.5 |
| ROLL 140 | | | | 117.2 | 144.9 | 179.1 | 165.8 | 197.2 | 217.0 |
| 150 | 550 | .01 | 6 | 116.4 | 149.5 | 174.1 | 191.9 | 212.9 | 236.2 |
| 150 | 550 | .01 | 9 | 105.3 | 133.6 | 154.5 | 169.6 | 187.1 | 206.4 |
| 150 | 650 | .01 | 9 | 108.1 | 139.1 | 163.3 | 178.9 | 200.7 | 225.2 |
| 150 | 650 | .01 | 12 | 101.8 | 128.9 | 149.4 | 163.2 | 181.0 | 200.0 |
| 150 | 750 | .01 | 9 | 111.9 | 144.2 | 169.2 | 186.0 | 208.2 | 233.0 |
| 150 | 750 | .01 | 12 | 105.3 | 134.4 | 156.9 | 171.5 | 191.5 | 213.9 |
| 200 | 600 | .01 | 9 | 116.4 | 148.8 | 172.5 | 190.2 | 209.4 | 231.7 |
| 200 | 600 | .01 | 12 | 113.2 | 143.2 | 164.7 | 181.2 | 198.7 | 217.9 |
| 200 | 700 | .01 | 9 | 117.3 | 149.8 | 174.0 | 191.5 | 211.9 | 234.5 |
| 200 | 700 | .01 | 12 | 112.6 | 142.5 | 164.2 | 180.4 | 198.3 | 218.0 |
| 200 | 800 | .01 | 15 | 114.9 | 145.9 | 169.1 | 185.2 | 205.2 | 227.3 |
| 200 | 800 | .01 | 18 | 111.8 | 141.2 | 163.0 | 178.3 | 196.8 | 217.3 |
| 200 | 600 | .02 | 9 | 119.7 | 149.8 | 172.4 | 184.4 | 206.9 | 228.5 |
| 200 | 600 | .02 | 12 | 116.6 | 144.2 | 164.6 | 178.4 | 195.6 | 214.5 |
| 200 | 700 | .02 | 12 | 120.6 | 150.6 | 173.3 | 188.0 | 207.7 | 229.4 |
| 200 | 700 | .02 | 15 | 116.3 | 143.6 | 164.1 | 177.3 | 194.8 | 214.0 |
| 200 | 800 | .02 | 15 | 118.6 | 147.0 | 168.9 | 182.1 | 201.6 | 223.2 |
| 200 | 800 | .02 | 18 | 115.0 | 142.2 | 162.8 | 175.1 | 193.2 | 213.1 |
| LIGHT OIL ROLL115 | | | | 110.9 | 145.0 | 189.6 | 172.9 | 215.9 | 245.8 |
| 150 | 1250 | .02 | 15 | 122.9 | 156.1 | 183.2 | 198.2 | 223.6 | 252.3 |
| 150 | 1250 | .02 | 20 | 117.4 | 146.9 | 170.7 | 183.9 | 205.7 | 230.2 |
| OCTYL ALC ROLL 130 | | | | 43.8 | 51.2 | 60.0 | 57.7 | 66.3 | 73.3 |
| 100 | 180 | .05 | 10 | 46.7 | 54.4 | 61.0 | 63.3 | 69.8 | 76.9 |
| 100 | 180 | .05 | 15 | 44.1 | 50.8 | 56.5 | 58.6 | 64.0 | 69.9 |

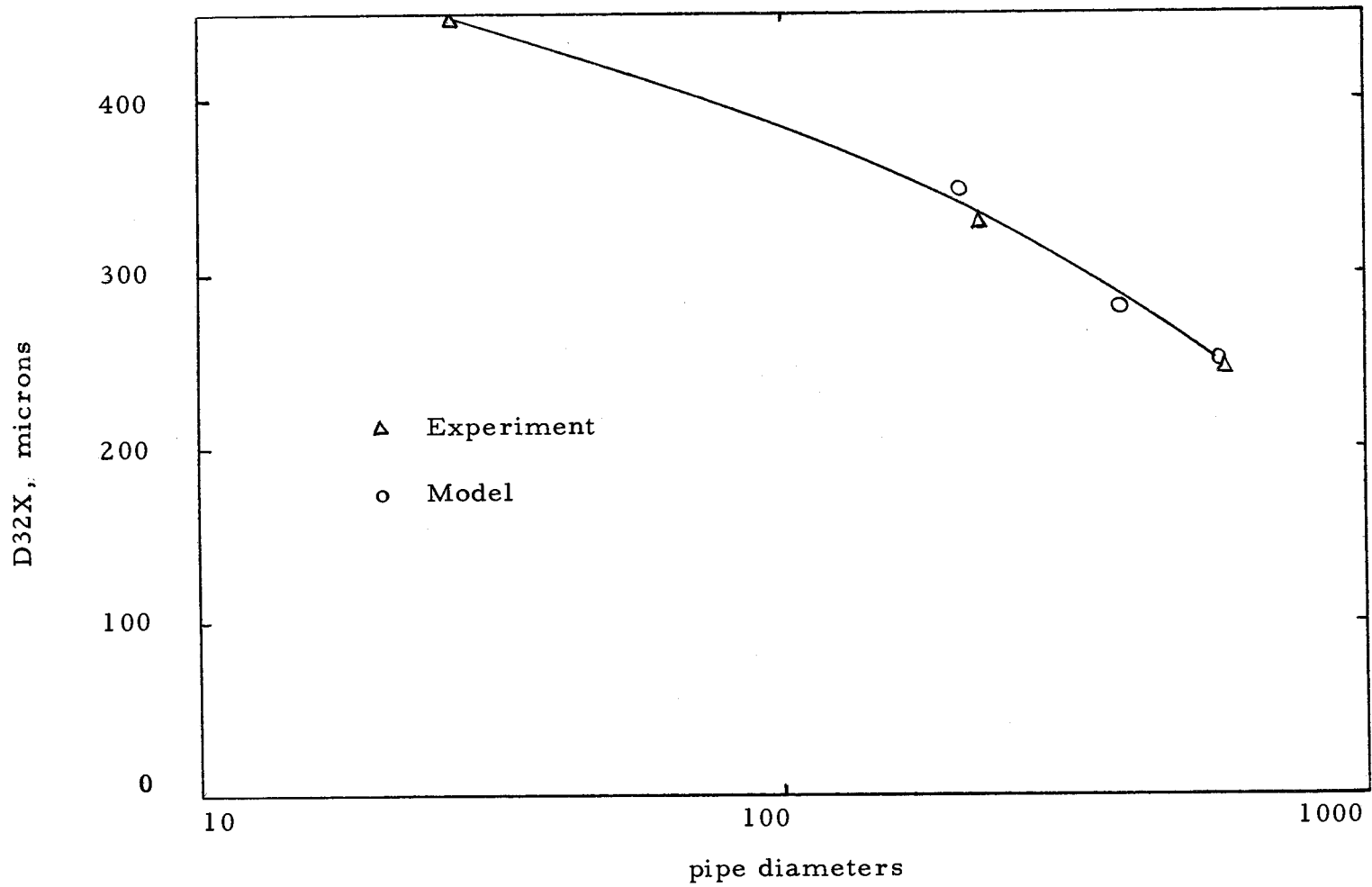


Figure 48. D32X vs. distance from the nozzle, 5% light oil, IMAXS = 150, KPROB = 1250, SAT = 0.02.

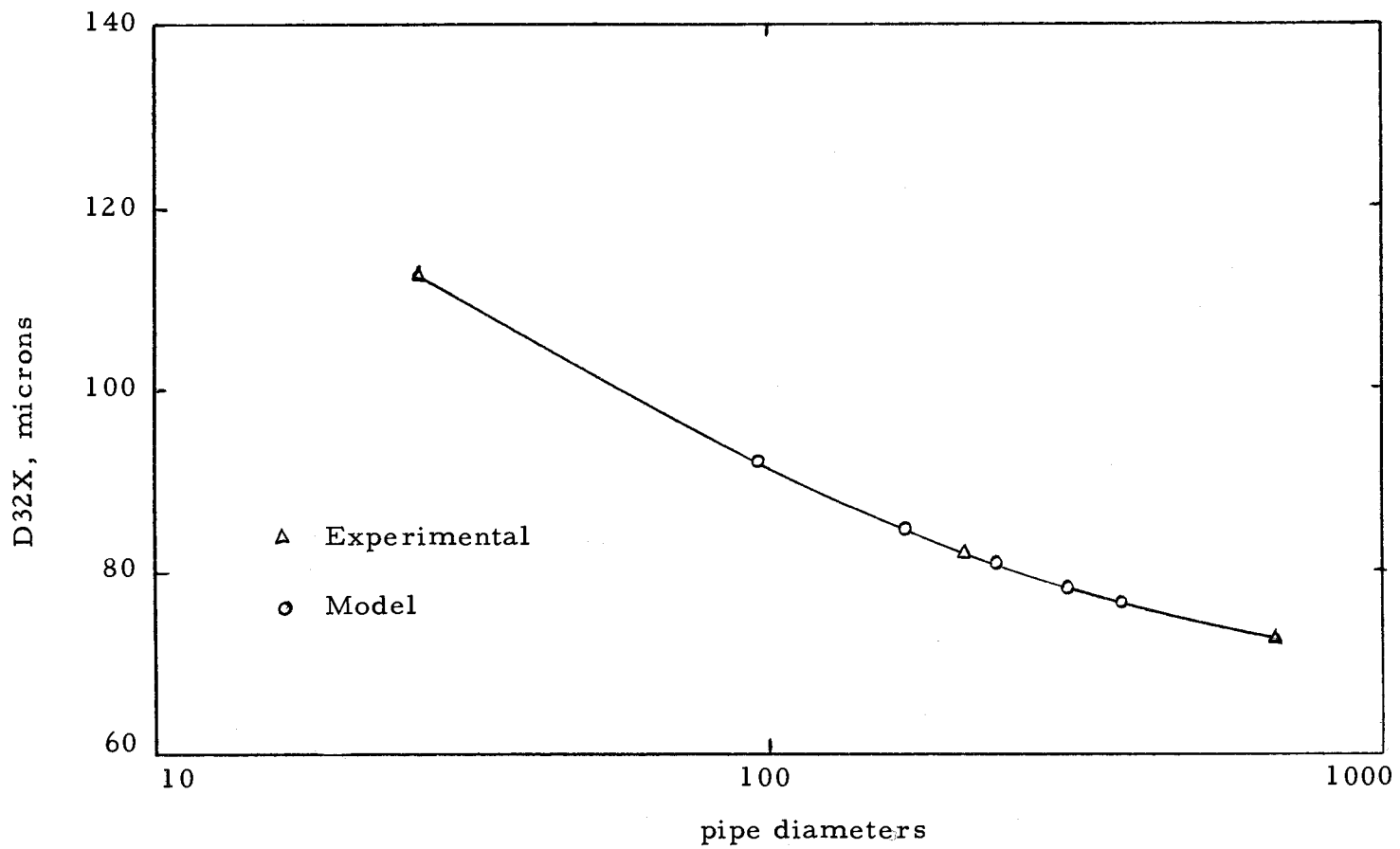


Figure 49. D32X vs. distance from the nozzle, 1.3% iso-octyl alcohol, IMAXS = 100, KPROB = 140, SAT = 0.05.

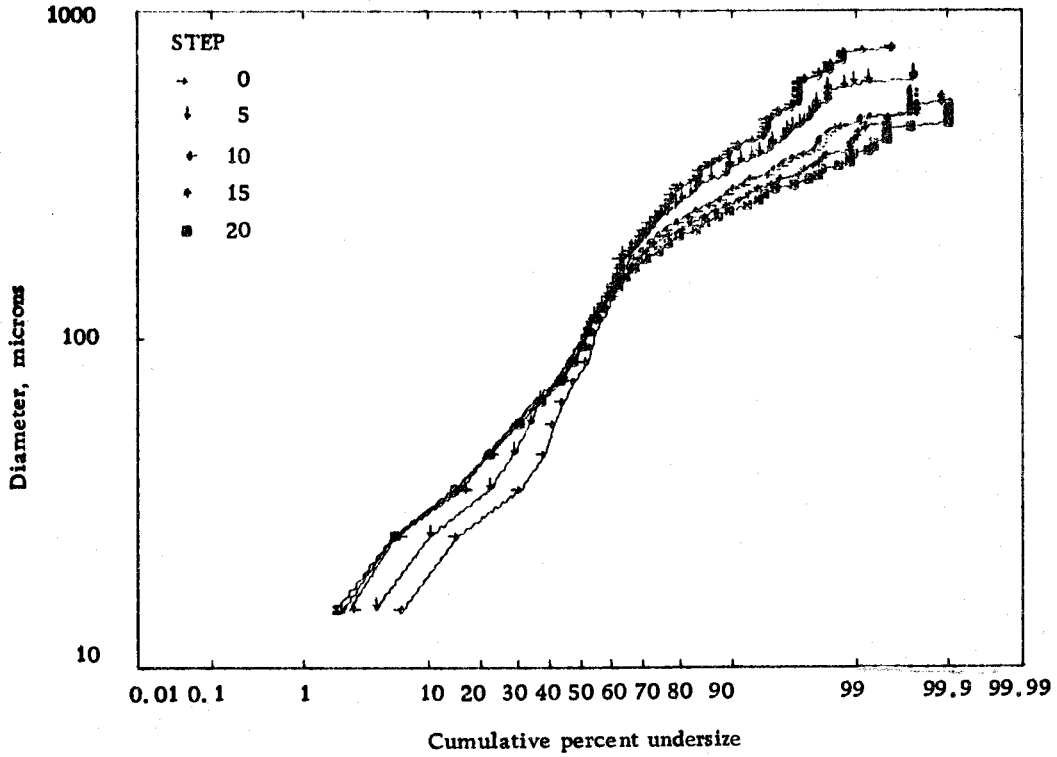


Figure 50. Theoretical distributions for 5% light oil, IMAXS = 150, KPROB = 1250, SAT = 0.02, Model 11.

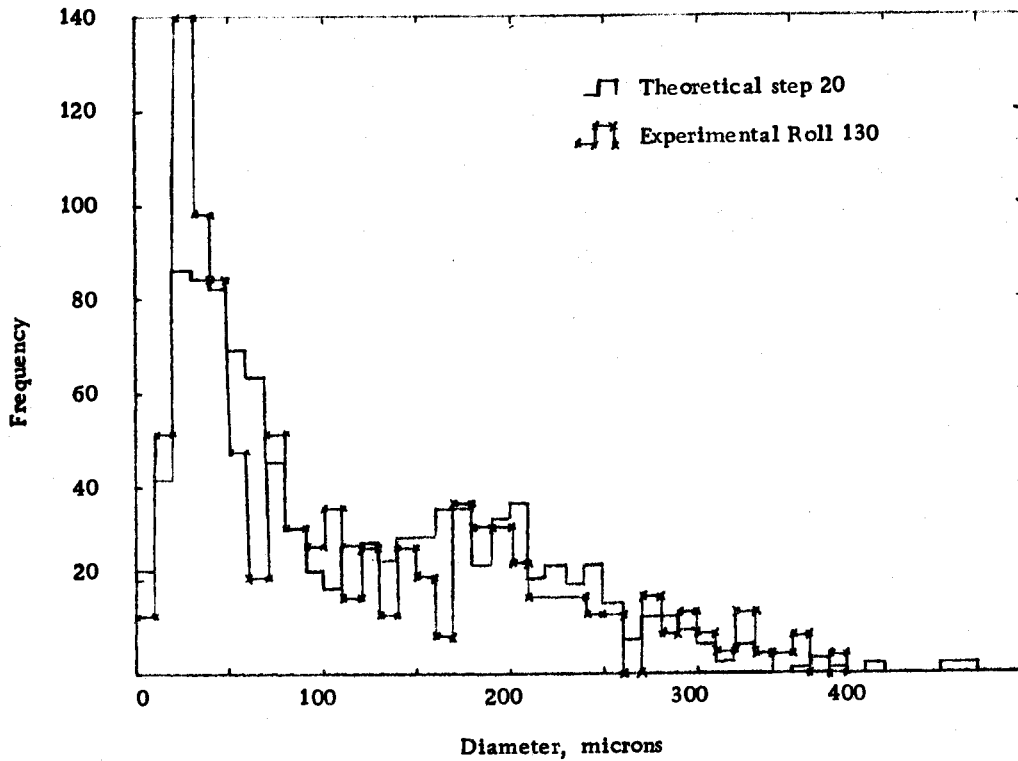


Figure 51. Theoretical and experimental frequency histograms for 5% light oil, IMAS = 150, KPROB = 1250, SAT = 0.02, Model 11.

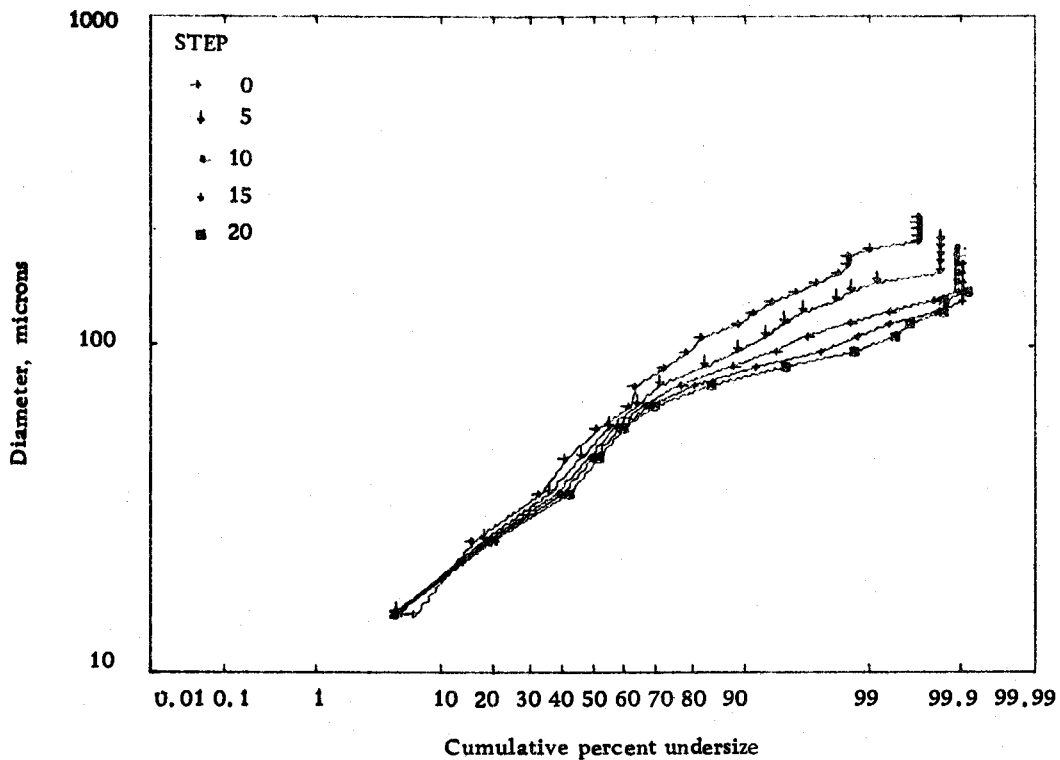


Figure 52. Theoretical distributions for 1.3% iso-octyl alcohol, IMAXS = 100, KPROB = 180, SAT = 0.05, Model 11.

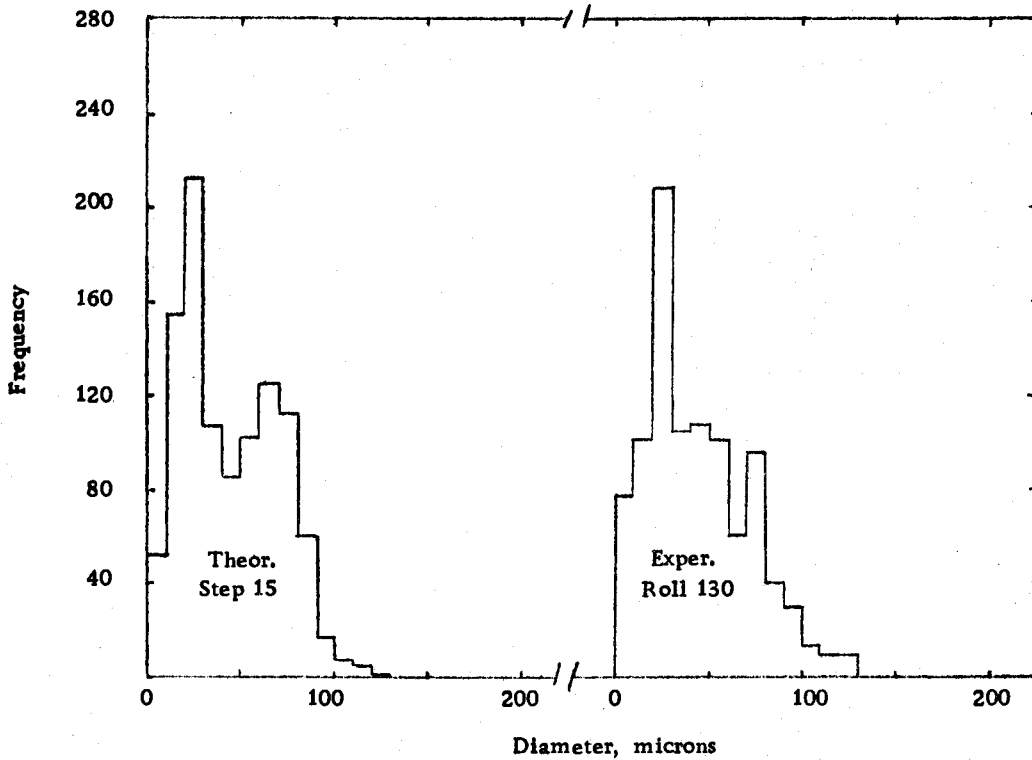


Figure 53. Theoretical and experimental frequency histograms, 1.3% iso-octyl alcohol, IMAXS = 100, KPROB = 180, SAT = 0.05, Model 11.

iso-octyl alcohol systems respectively. Best results with the model were obtained with corresponding maximum stable drop sizes of 100, 150 and 200 microns. The differences are within the $\pm 35\%$ claimed for the correlation. No correlation exists for the prediction of the other two parameters of the model, the ratio of satellite to daughter drop volume and the rate of change of breakup probability with diameter.

Although uniqueness of the breakup mechanism proposed in the model developed during the course of the present work cannot be proven, the agreement between theory and experiment are a strong indication that the proposed mechanism is responsible for breakup in the turbulent field of a pipe. Thus it seems safe to conclude that when drops break up in the turbulent field of a pipe, two daughter drops are produced which have uniformly distributed volume ratios. On the average one very small satellite drop is also produced by each breakage event. The effects of a maximum stable drop size were clearly present in the experimental data by comparing the predictions of Models 1 and 3 which did and did not postulate the existence of a maximum stable drop size. Pure binary and higher order breakup mechanisms were also eliminated as possible mechanisms.

The breakup mechanism resulting from a turbulent flow field corresponds closely to the laminar breakup mechanism B-1 shown in Figure 1. The model indicates that in the turbulent case only one

satellite drop and not three satellite drops as in the laminar case are produced by each breakup event. The general applicability of the model to the three systems examined in the present work indicates that this type of breakup occurs over a wider range of viscosity ratios ($1 \leq \mu_d/\mu_c \leq 18$) for the turbulent case than in the laminar flow case ($1 \leq \mu_d/\mu_c \leq 2.2$).

CONCLUSIONS

1. The distributions shown in the experimental results section are representative of drop size distributions produced by the turbulent field of liquids flowing in a pipe. The distributions are not described by any known distribution law.
2. A mathematical model of the breakup process has been developed which allows both the form of the experimentally observed distribution and the kinetics of the breakup process to be simulated. The model indicates that each breakup event leads to two daughter drops with uniformly distributed volume ratios and a very small satellite droplet.
3. The existence of a maximum stable drop size is clearly indicated by comparison of Models 1 and 3 to experimental data.
4. Tertiary and higher orders of breakup do not appear to be present as evidenced by the results of Models 5 and 6.
5. Highly-distorted drops and breakup appear to be restricted to the neighborhood of the pipe wall.
6. Average drop size increases slowly with distance from the pipe wall.
7. The mathematical model contains three parameters. Sleicher's relationship (Equation 27) gives a good prediction of the maximum stable drop size. No correlations exist to predict the

slope of the straight line which describes the probability of breakup above the maximum stable drop size or to predict the ratio of satellite volume to daughter drop volume. Both of these parameters appear to be system dependent and must be determined by trial and error fit of more extensive experimental data than obtained in this work. In the limit of a very long pipe, the breakup process reaches completion and the form of the model indicates that the slope of the breakup probability function would no longer be a parameter of the distribution at this limit. The ratio of satellite volume to daughter drop volume sets the position of the high peak observed at small drop sizes. In the present work, best results were obtained if this ratio was set so as to give the mode of the peak at approximately 30 microns for all systems studied.

RECOMMENDATIONS FOR FURTHER WORK

High-speed motion pictures of the dispersion flowing in the apparatus used in the present work would provide better information on the breakup process itself. With a synchronous strobe light for a light source, adequate illumination with a sufficiently short duration to stop the motion of the drop would be obtainable. Such photographs would allow the breakup process to be followed in stages and provide a firmer basis for formulating a model of the breakup process.

Further studies of the two uncorrelated parameters of the model should be undertaken. A direct measurement of the shape of the curve describing the probability of breakup could be accomplished by a technique similar to that which Sleicher (30) used to measure the maximum stable drop size. He measured the velocity necessary to give 20% breakup after the dispersion had been exposed to a turbulent field for 176 pipe diameters. Measurements of higher percent breakup closer to the entrance would allow other points on the breakup probability curve to be determined.

Drop size distributions resulting from turbulence should be measured for a wider range of physical properties and experimental conditions. The position of the high peak in each case is of particular interest because it is formed by the satellite drops and indicates their size. In the present work, the mode of the peak was always

observed to be close to 30 microns, but the range of experimental conditions was limited.

It would also be very informative to study the distributions produced when different types of nozzles are used to produce a variety of initial distributions. In present form of the model, the parameters proposed are independent of initial distribution. A change of the initial distribution without a change in any other experimental conditions would provide a good test of this aspect of the model.

BIBLIOGRAPHY

1. Adler, C. R. et al. A scanning device for determining the size distribution of spray droplet images. *Chemical Engineering Progress* 50:14-24. 1954.
2. Baranaev, M. K., E. N. Teverovskii and E. L. Tregubova. The dimension of minimum pulsations in turbulent flow. *Akademiia Nauk, U. S. S. R. Doklady* 66:821-824. (Translated by Special Libraries Association)
3. Bromfield, F. S. and C. A. Sleicher, Jr. An investigation of the maximum stable drop size in turbulent flow between rotating cylinders. *The Trend in Engineering at the University of Washington*, July, 1962, p. 24-29.
4. Brown, R. A. S. and G. W. Govier. High speed photography in the study of two phase flow. *Canadian Journal of Chemical Engineering* 39:159-164. 1961.
5. Cengel, J. A. et al. An apparatus for the measurement of light transmittance of emulsions. *Canadian Journal of Chemical Engineering* 39:189-191. 1961.
6. Clay, P. H. Mechanism of emulsion formulation in turbulent flow. *Koninklijke Nederlandsche Akademie van Wetenschappen* 43:852-865, 979-990. 1940.
7. Epstein, B. The mathematical description of certain breakage mechanisms leading to the logarithmico-normal distribution. *Journal of the Franklin Institute* 244:471-477. 1947.
8. _____ . Logarithmico-normal distribution in breakage of solids. *Industrial and Engineering Chemistry* 40:2289-2291. 1948.
9. Green, H. A photomicrographic method for the determination of particle size of paint and rubber pigments. *Journal of the Franklin Institute* 192:637-666. 1921.
10. Hinze, J. O. Fundamentals of the hydrodynamic mechanism of splitting in dispersion processes. *Journal of the American Institute of Chemical Engineers* 1:289-295. 1955.

11. _____ . Turbulence. New York, McGraw-Hill, 1959. 586p.
12. Kessie, R. W. and J. H. Rushton. Dispersion caused by turbulence in pipes. Paper presented at the American Institute of Chemical Engineers meeting, Kansas City, 1959. (As cited in: Sleicher, C. A., Jr. Maximum stable drop size in turbulent flow. Journal of the American Institute of Chemical Engineers 8:471-477. 1962.)
13. Kinter, R. C. et al. Photography in bubble and drop research. Canadian Journal of Chemical Engineering 39:235-241. 1961.
14. Kolmogorov, A. N. The breakdown of drops in turbulent flow. Akademiia Nauk, U. S. S. R. Doklady 66:825-828. 1949. (Translated from the Russian)
15. Kottler, F. The distribution of particle sizes, pts. I and II. Journal of the Franklin Institute 250:339-356, 419-441. 1950.
16. Langloise, Gordon E., Jonas E. Gullberg and Theodore Vermeulen. Determination of interfacial area in unstable emulsions by light transmission. Review of Scientific Instruments 25:360-363. 1954.
17. Levich, V. G. Physicochemical hydrodynamics. Englewood Cliffs, N.J., Prentice-Hall, 1962. 700p. (Translated from the Russian)
18. Lloyd, N. E. Determination of surface average particle diameter of colored emulsions by reflectance. Journal of Colloid Science 14:441-451. 1959.
19. Marshall, W. R., Jr. Atomization and spray drying. New York, 1954. 122p. (American Institute of Chemical Engineers. Chemical engineering progress monograph series no. 2)
20. Mugele, R. A. and H. D. Evans. Droplet size distribution in sprays. Industrial and Engineering Chemistry 43:1317-1324. 1951.
21. Paul, H. I. and C. A. Sleicher, Jr. The maximum stable drop size in turbulent flow; effect of pipe diameter. Chemical Engineering Science 20:57-59. 1965.

22. Rajagopal, E. S. Statistical theory of particle size distribution in emulsions and suspensions. *Kolloid Zeitschrift* 162:7-17. 1959.
23. Rayleigh, J. W. S. (Lord) On the instability of jets. *Proceedings of the London Mathematical Society* 10:4-13. 1878.
24. Rodger, W. S., V. G. Trice, Jr. and J. H. Rushton. Effect of fluid motion on interfacial area of dispersions. *Chemical Engineering Progress* 52:515-520. 1956.
25. Rosin, R. and E. Z. Rammler. The laws governing the fineness of powdered coal. *Institution of Fuel Journal, London* 7:29-36. 1933.
26. Rumscheidt, F. D. and S. G. Mason. Particle motions in sheared suspensions. XII. Deformation and burst of drops in shear and hyperbolic flow. *Journal of Colloid Science* 16:238-261. 1961.
27. Schwarz, N. and C. Bezemer. A new equation for the size distribution of emulsion particles. *Kolloid Zeitschrift* 146:139-151. 1956.
28. Scott, L. S., W. B. Hayes, III and C. D. Holland. The formation of interfacial area in immiscible liquids by orifice mixers. *Journal of the American Institute of Chemical Engineers* 4:346-350. 1958.
29. Shinnar, R. On the behavior of liquid dispersions in mixing vessels. *Journal of Fluid Mechanics* 10:259-275. 1961.
30. Shinnar, R. and J. M. Church. Statistical theories of turbulence in predicting particle size in agitated dispersions. *Industrial and Engineering Chemistry* 52:253-256. 1960.
31. Sleicher, C. A., Jr. Maximum stable drop size in turbulent flow. *Journal of the American Institute of Chemical Engineers* 8:471-477. 1962.
32. Sullivan, D. M. and E. E. Lindsey. An approach to characterizing agitation by dispersion particle size. *Industrial and Engineering Chemistry Fundamentals* 1:87-93. 1962.

33. Tate, R. W. and W. R. Marshall, Jr. Atomization by centrifugal pressure nozzels. *Chemical Engineering Progress* 49: 226-233. 1953.
34. Taylor, G. I. The formation of emulsions in definable fields of flow. *Proceedings of the Royal Society of London, Ser. A*, 146:501-523. 1934.
35. Tomotika, S. On the instability of a cylindrical thread of a viscous liquid surrounded by another viscous liquid. *Proceedings of the Royal Society of London, Ser. A*, 150:322-337. 1935.
36. _____ . Breaking up of a drop of viscous liquid immersed in another viscous fluid which is extending at a uniform rate. *Proceedings of the Royal Society of London, Ser. A*, 153:302-318. 1936.
37. Valentas, K. J., O. Bilous and N. R. Amundson. Analysis of breakage in dispersed phase systems. *Industrial and Engineering Chemistry Fundamentals* 5:271-279. 1966.
38. Ward, J. P. Turbulent flow of liquid-liquid dispersions; drop size, friction losses, and velocity distributions. Ph.D. thesis. Corvallis, Oregon State University, 1964. 353 numb. leaves.
39. Wise, M. E. Converting a number distribution of particle size into one of volume or surface area. *Philips Research Laboratory Report* 9:231-237. 1954.

APPENDICES

APPENDIX I

SUPPLEMENTARY DROP SIZE DISTRIBUTIONS

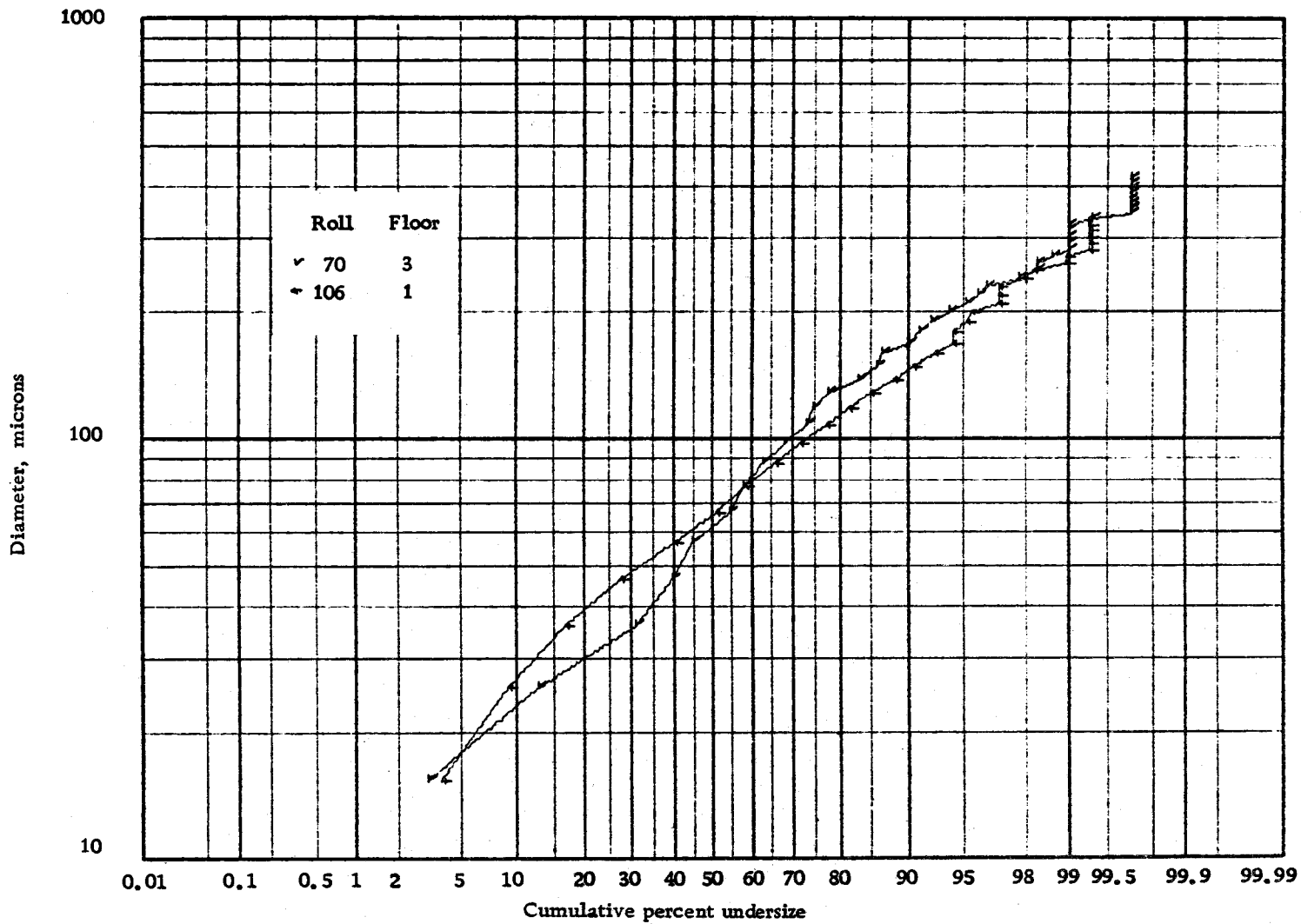


Figure 54. Drop size distribution for 0.6% Shellsolv, $\gamma/R_w = 0.05$, 16 ft/sec.

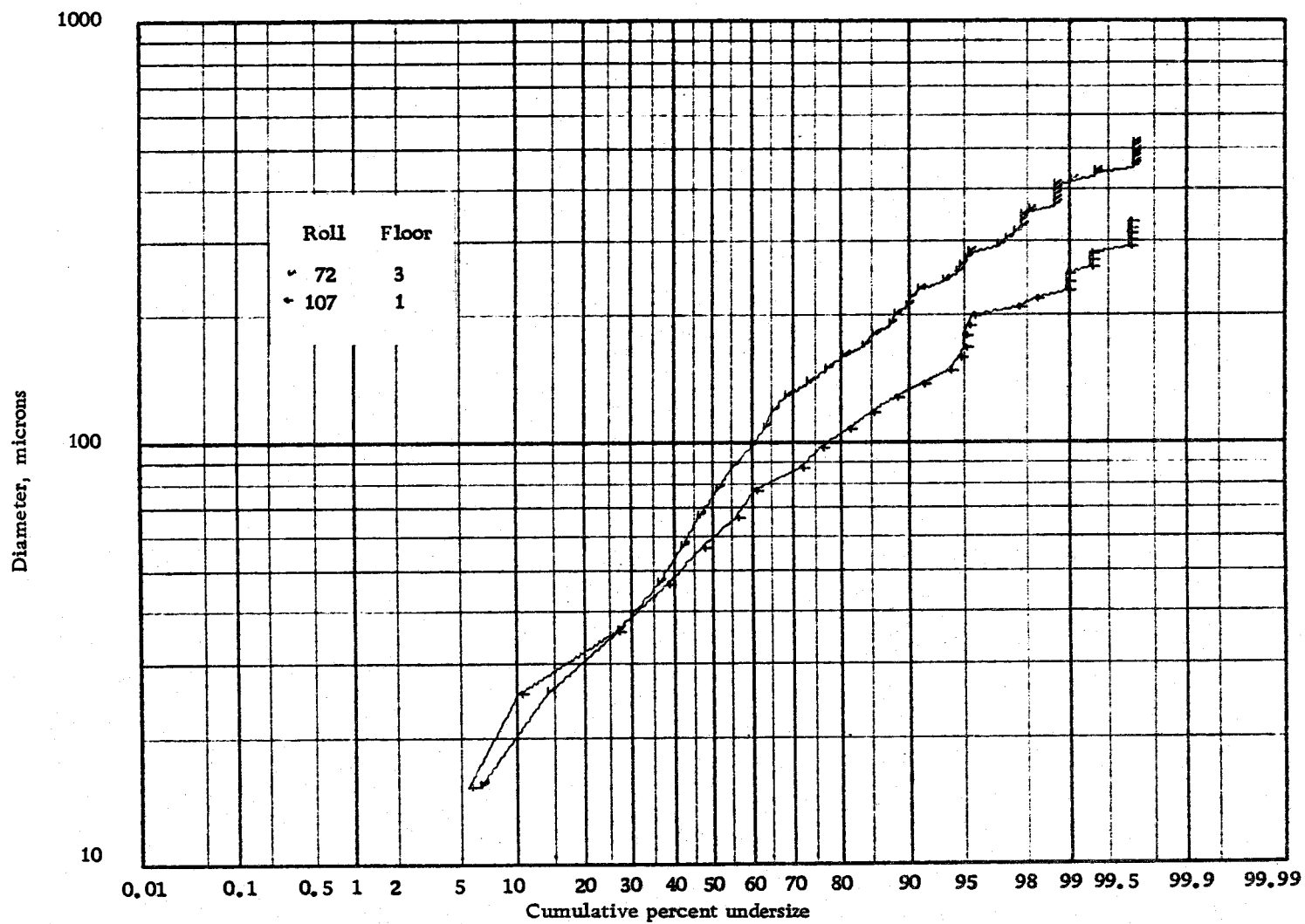


Figure 55. Drop size distribution for 0.6% Shellsolv, $\gamma/R_w = 0.4$, 16 ft/sec.

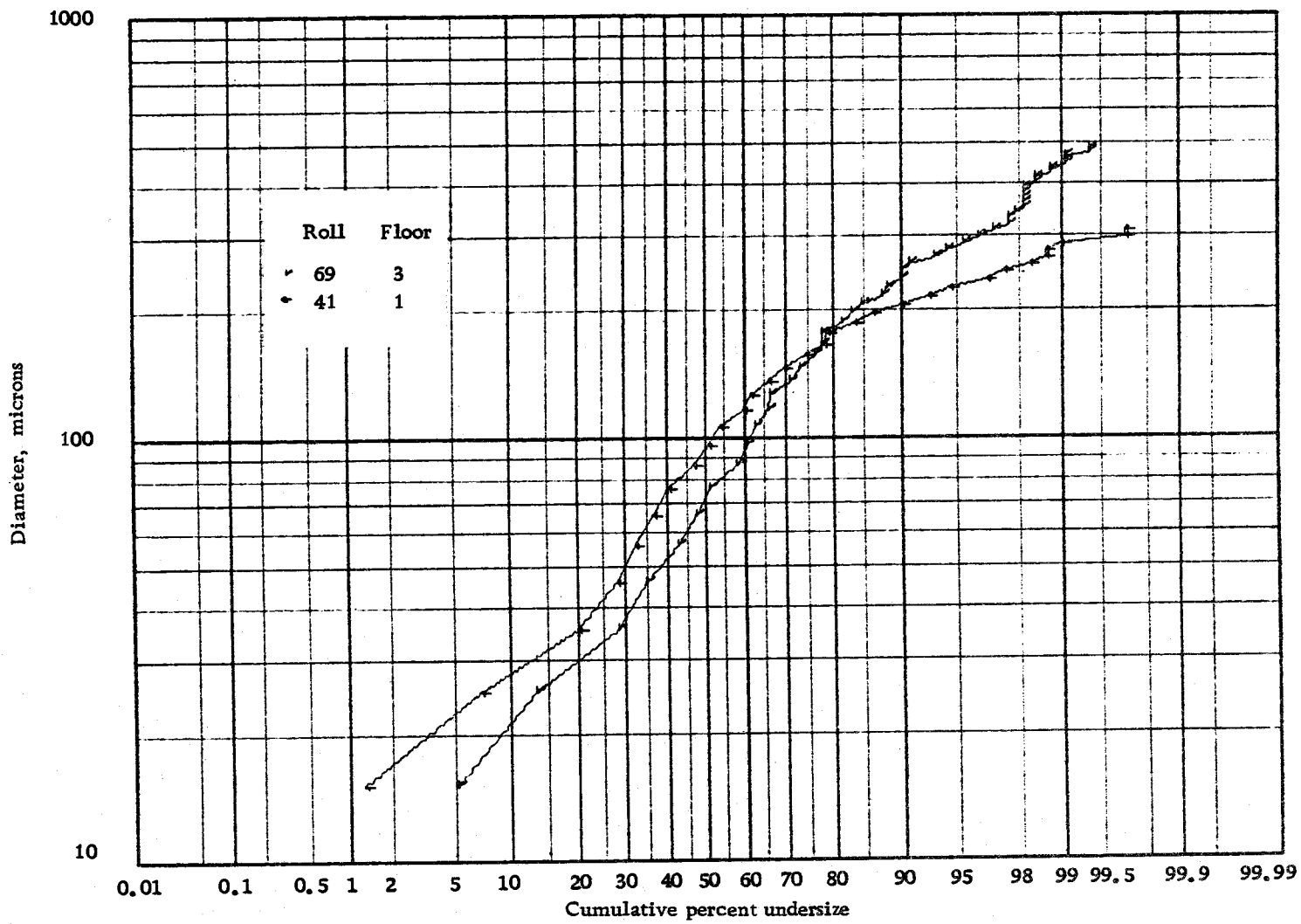


Figure 56. Drop size distribution for 1.3% Shellsolv, $\gamma/R_w = 0.4$, 20 ft/sec.

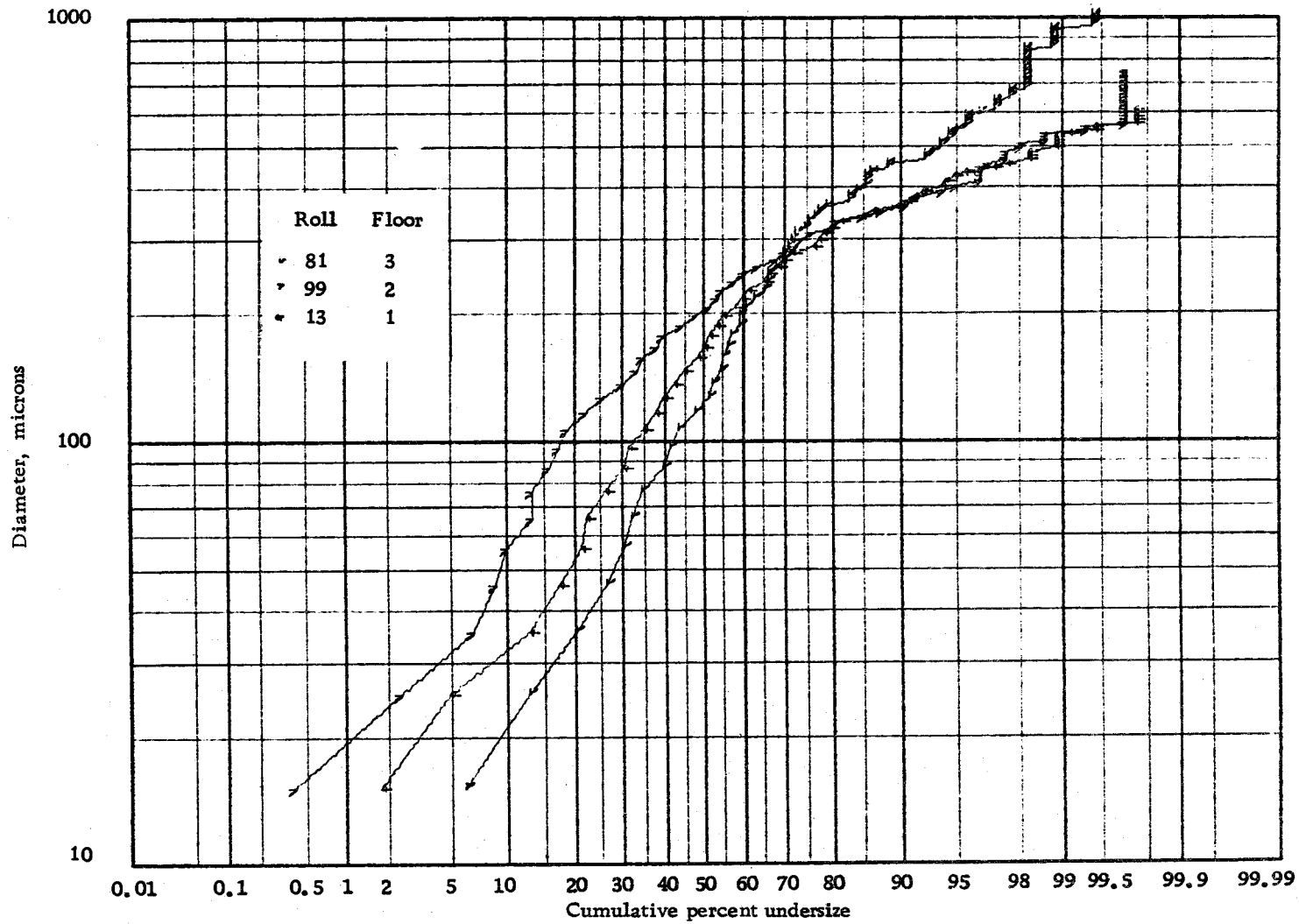


Figure 57. Drop size distribution for 10% Shellsolv, $\gamma/R_w = 0.1$, 16 ft/sec.

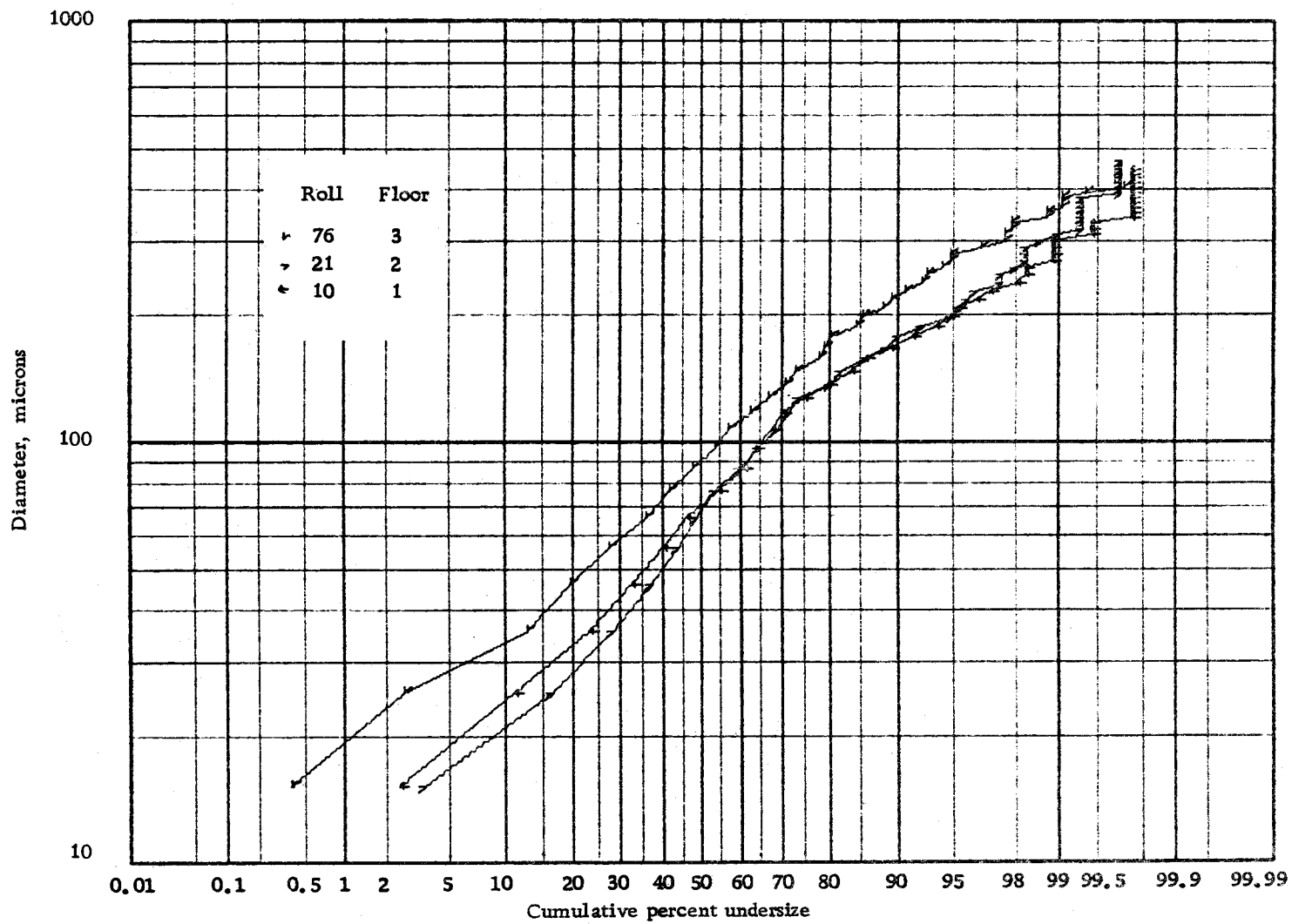


Figure 58. Drop size distribution for 1.3% Shellsolv, $y/R_w = 0.1$, 16 ft/sec.

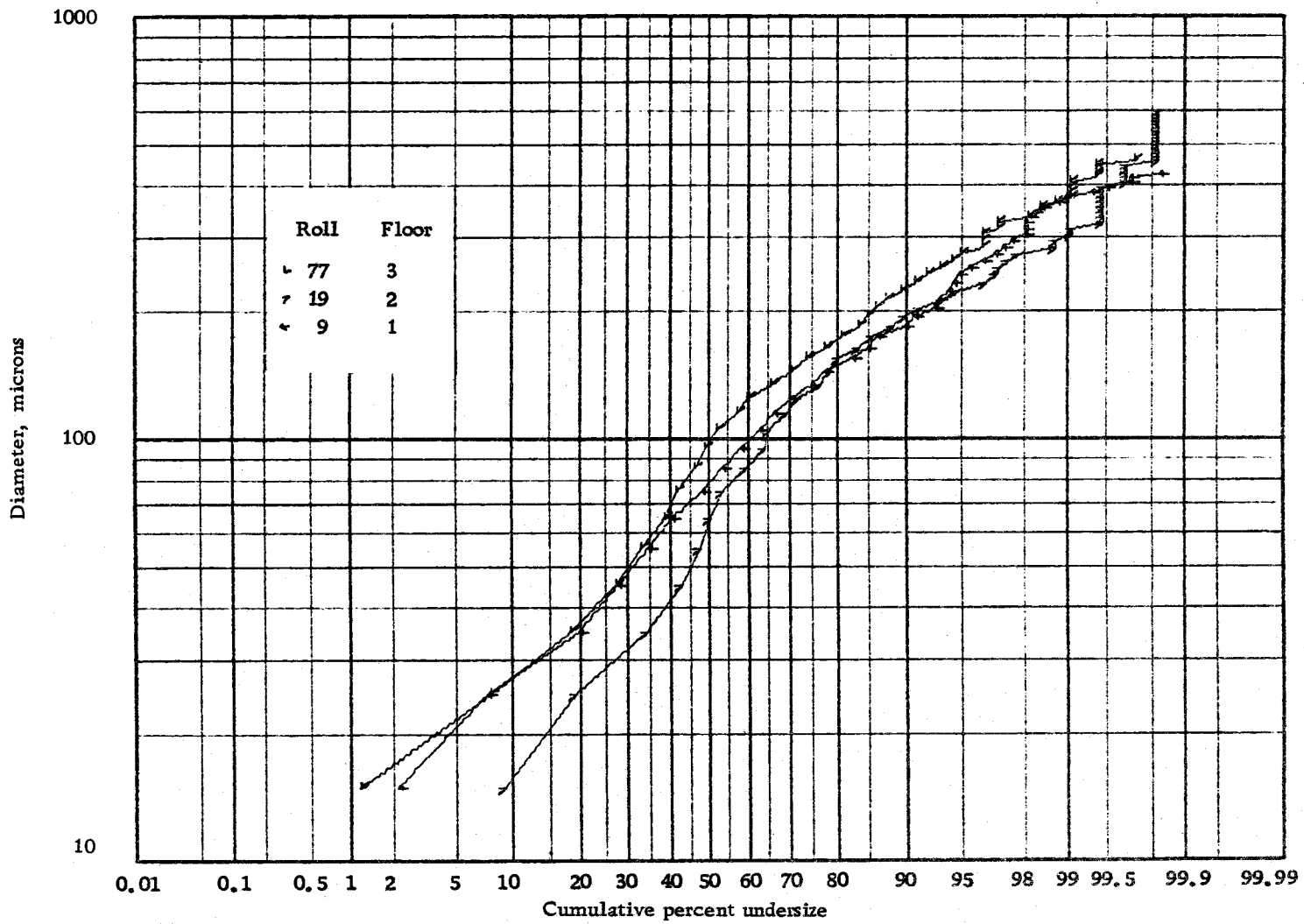


Figure 59. Drop size distribution for 1.3% Shellsoolv, $\gamma/R_w = 0.4$, 16 ft/sec.

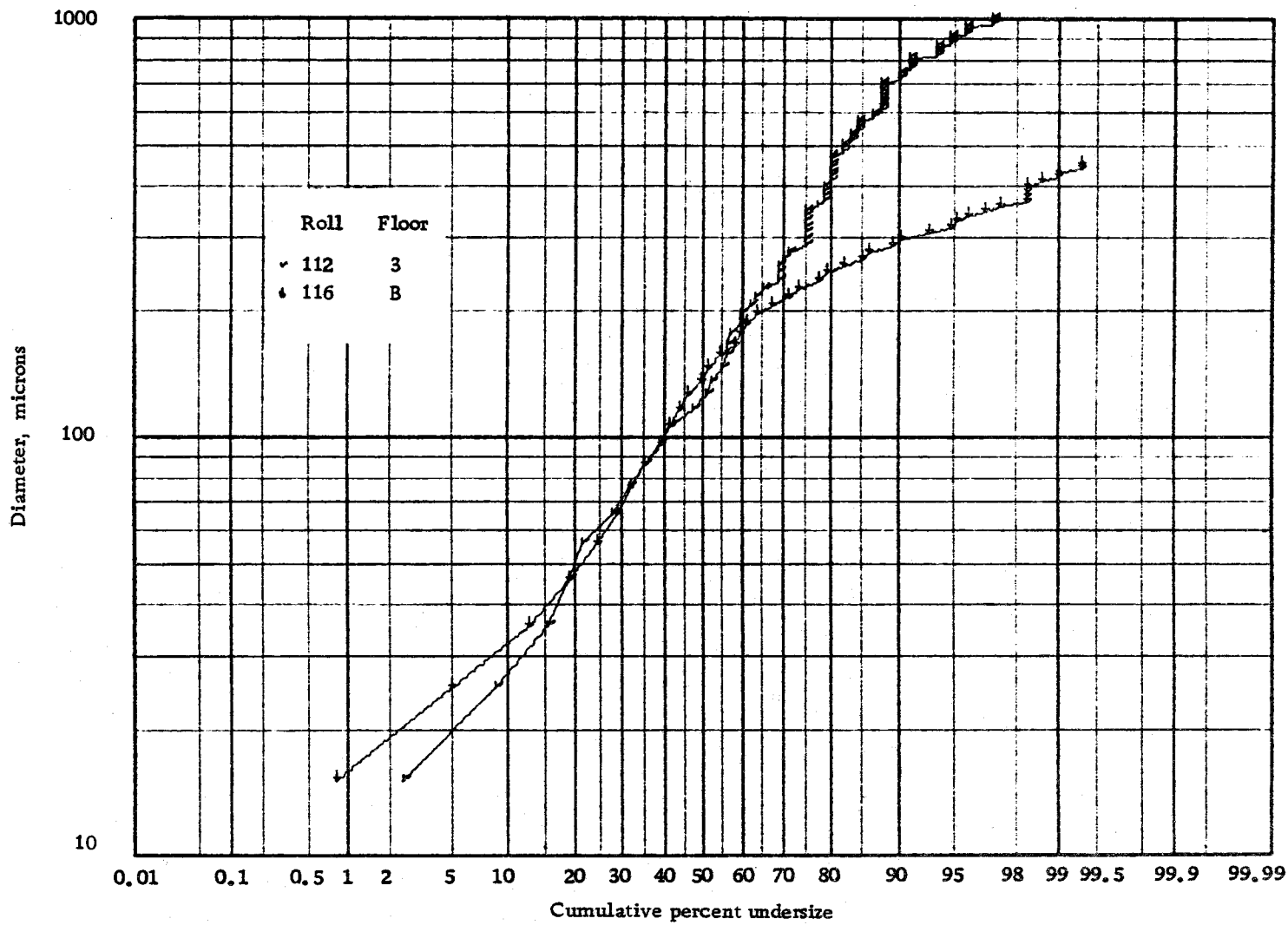


Figure 60. Drop size distribution for 5% light oil, $y/R_w = 0.1$, 16 ft/sec.

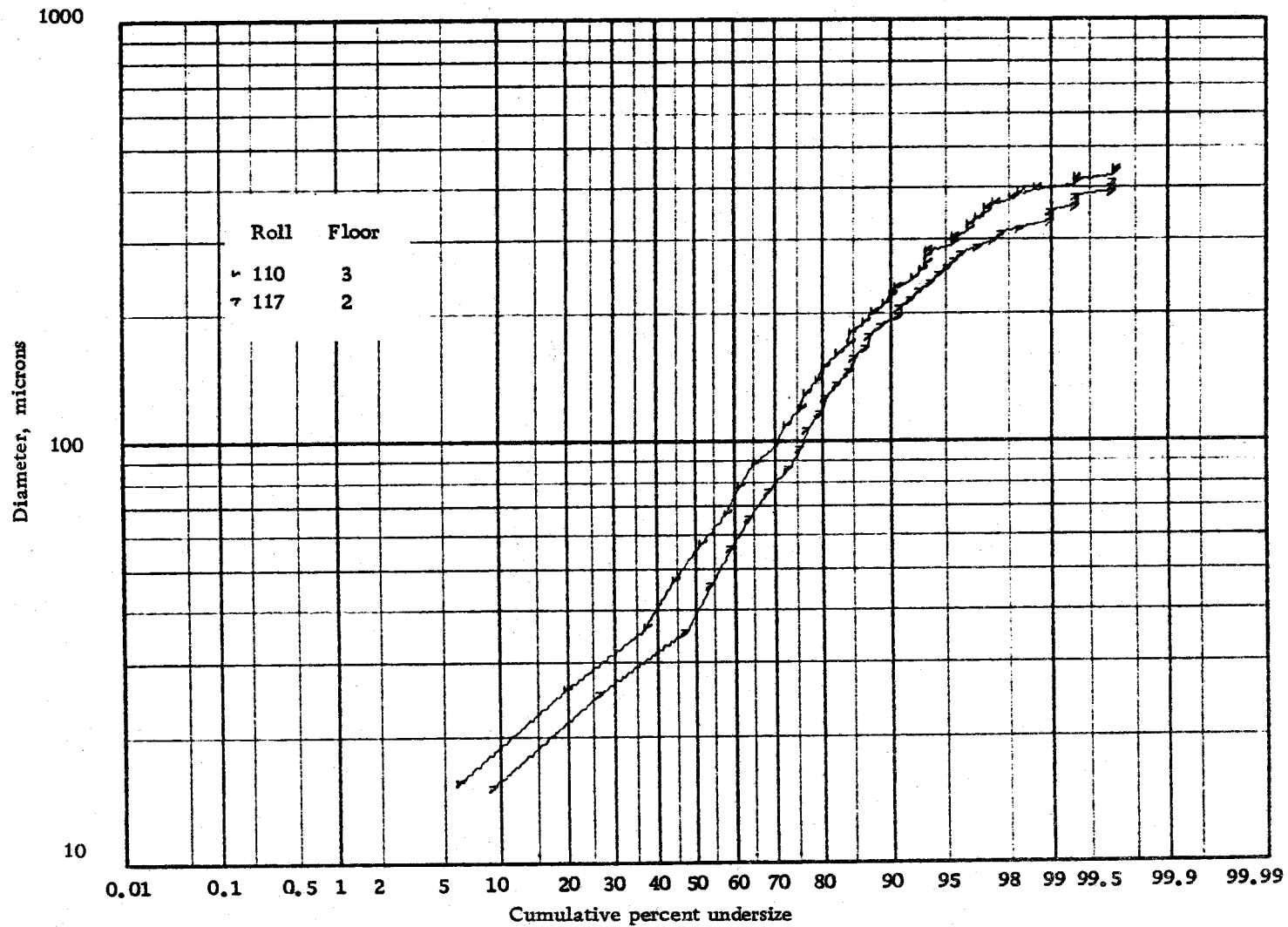


Figure 61. Drop size distribution for 0.6% light oil, $\gamma/R_w = 0.4$, 16 ft/sec.

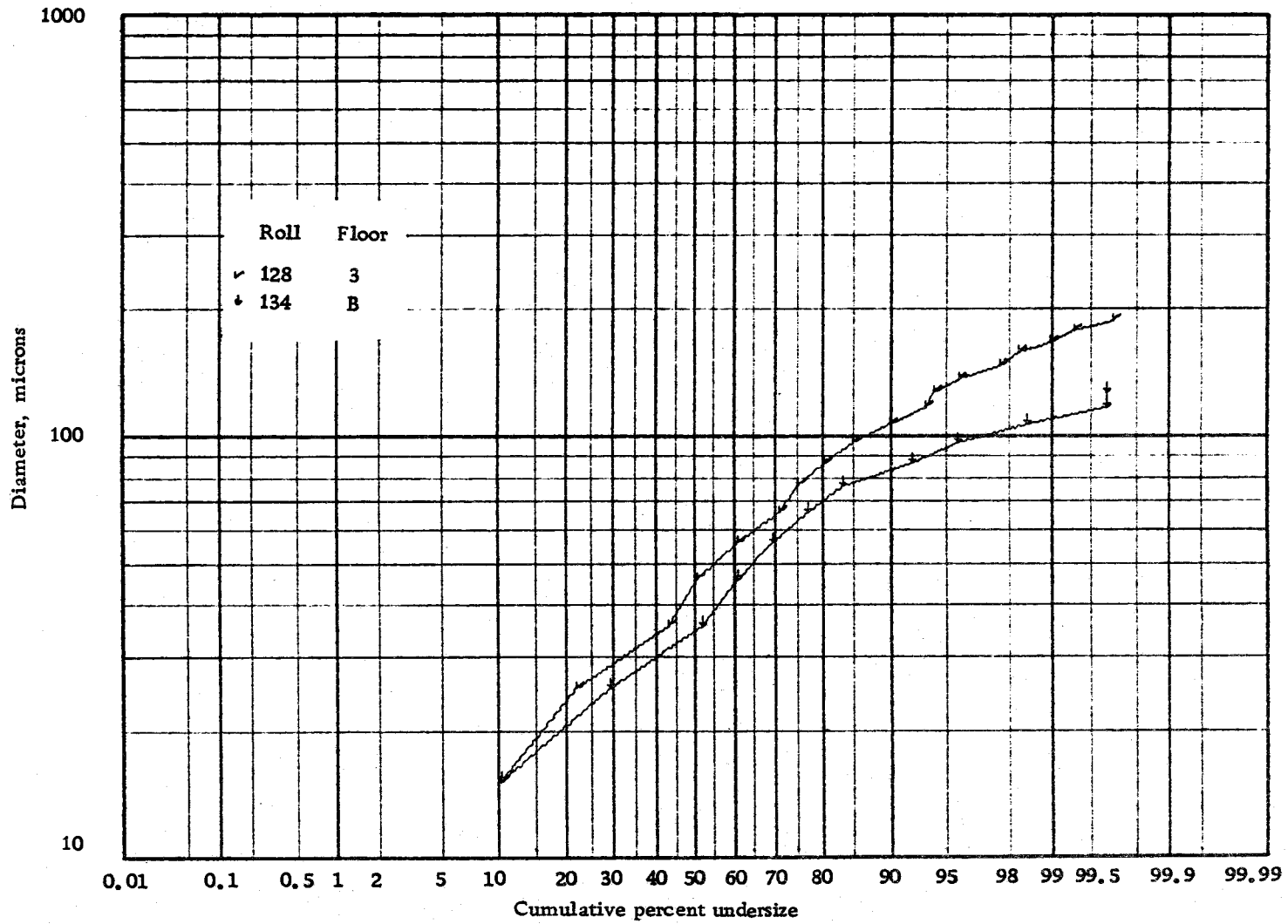


Figure 62. Drop size distribution for 0.6% iso-octyl alcohol, $y/R_w = 0.1$, 16 ft/sec.

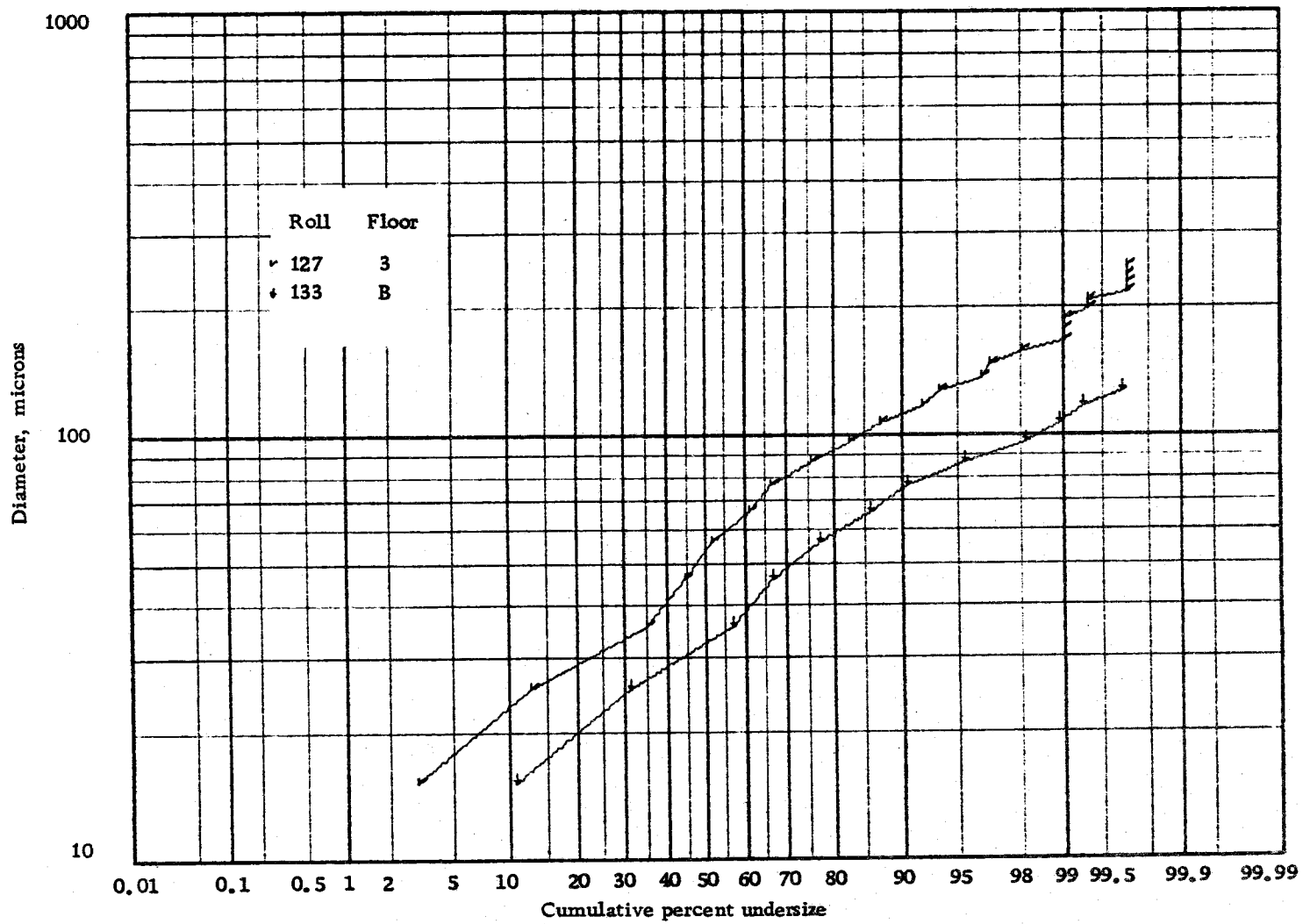


Figure 63. Drop size distribution for 0.6% iso-octyl alcohol, $\gamma/R_w = 0.4$, 16 ft/sec.

APPENDIX II

COMPLETE PICTURE QUALITY, DROPLET
DISTORTION AND AVERAGE SIZE DATA

Table VI. Complete picture quality, droplet distortion and average size data

| ROLL NO. | RUN CODE | QUAL. | DISTORT. | SAMPLE SIZE | D10X | D20X | D30X | D21X | D31X | D32X |
|----------|-----------|-------|----------|-------------|-------|-------|-------|-------|-------|--------|
| 3 | 10SS-1-05 | A | 3 | | | | | | | |
| 4 | 10SS-1-1 | A | 4 | 254 | 184.5 | 243.4 | 320.9 | 280.8 | 346.4 | 373.9 |
| 5 | 10SS-1-05 | C | 3 | | | | | | | |
| 6 | 10SS-1-1 | B | 2 | 544 | 166.3 | 214.7 | 277.2 | 249.3 | 305.2 | 336.1 |
| 7 | 10SS-1-1 | C | 2-3 | | | | | | | |
| 9 | 9SS-1-4 | B | 1 | 501 | 96.7 | 123.1 | 156.8 | 148.3 | 183.7 | 215.3 |
| 10 | 9SS-1-1 | A | 1 | 300 | 84.0 | 105.5 | 132.6 | 125.9 | 154.1 | 179.1 |
| 11 | 9SS-1-4 | D | 2 | 251 | 95.2 | 122.5 | 157.7 | 147.9 | 184.3 | 215.4 |
| 12 | 11SS-1-4 | D | 2 | 204 | 189.2 | 234.8 | 291.5 | 265.6 | 314.7 | 339.8 |
| 13 | 11SS-1-1 | B | 2 | 300 | 187.6 | 228.8 | 279.1 | 258.9 | 304.1 | 331.3 |
| 14 | 11SS-1-05 | A | 4 | 350 | 106.7 | 135.5 | 172.0 | 158.6 | 193.3 | 217.3 |
| 16 | 10SS-2-1 | B | 2 | 141 | 199.8 | 256.6 | 329.5 | 296.0 | 360.4 | 394.1 |
| 17 | 10SS-2-4 | B | 2-3 | | | | | | | |
| 18 | 10SS-2-1 | A | 3 | 295 | 134.7 | 186.9 | 259.4 | 227.3 | 295.4 | 336.3 |
| 19 | 9SS-2-4 | A | 2 | 478 | 86.1 | 116.5 | 157.5 | 143.8 | 185.9 | 219.4 |
| 20 | 9SS-2-4 | A | 1 | | | | | | | |
| 21 | 9SS-2-1 | A | 2-3 | 257 | 83.0 | 107.9 | 140.2 | 131.5 | 165.5 | 195.4 |
| 22 | 10SS-4-1 | A | 4 | | | | | | | |
| 28 | 9SS-4-1 | A | 4 | 250 | 95.4 | 128.8 | 174.0 | 156.8 | 200.9 | 232.0 |
| 29 | 9SS-4-4 | A | 1 | 250 | 97.7 | 150.5 | 231.7 | 196.0 | 277.7 | 332.8 |
| 30 | 9SS-4-4 | A | 1 | 297 | 56.2 | 78.2 | 108.8 | 96.9 | 127.1 | 148.5 |
| 31 | 5SS-4-1 | B | 3 | | | | | | | |
| 32 | 5SS-4-4 | B | 2 | 55 | 195.2 | 257.9 | 340.8 | 305.6 | 382.4 | 429.0 |
| 33 | 5SS-4-10 | B | 2 | | | | | | | |
| 35 | 12SS-4-4 | A | 2 | | | | | | | |
| 36 | 12SS-4-4 | B | 2 | | | | | | | |
| 37 | 5SS-1-4 | A | 2 | | | | | | | |
| 38 | 5SS-1-10 | B | 1 | | | | | | | |
| 39 | 12SS-1-10 | B | 2 | | | | | | | |
| 40 | 12SS-1-4 | B | 2 | | | | | | | |
| 41 | 7SS-1-4 | A | 1 | 250 | 104.6 | 125.9 | 151.7 | 142.1 | 165.7 | 180.9 |
| 42 | 7SS-1-10 | C | 1 | | | | | | | |
| 43 | 6SS-1-4 | B | 2 | 177 | 120.9 | 148.7 | 183.1 | 169.6 | 200.9 | 220.5 |
| 44 | 6SS-1-1 | A | 2-3 | 252 | 103.2 | 132.3 | 169.6 | 154.2 | 188.5 | 209.5 |
| 46 | 7SS-1-1 | A | 2 | 500 | 85.7 | 105.5 | 129.8 | 121.4 | 144.5 | 160.9 |
| 47 | 3SS-1-1 | A | 2 | 250 | 70.3 | 87.0 | 107.6 | 100.7 | 120.5 | 135.0 |
| 48 | 3SS-1-4 | C | 1 | | | | | | | |
| 49 | 4SS-1-1 | A | 2 | 150 | 158.7 | 210.9 | 280.5 | 248.4 | 310.8 | 344.5 |
| 50 | 4SS-1-4 | A | 1 | 108 | 165.4 | 214.5 | 278.2 | 250.8 | 308.9 | 343.0 |
| 51 | 1SS-1-4 | A | 1 | 195 | 121.2 | 167.4 | 231.3 | 206.0 | 268.5 | 311.6 |
| 52 | 5SS-1-4 | A | 1 | 200 | 145.8 | 180.5 | 223.5 | 206.4 | 245.6 | 269.9 |
| 53 | 5SS-1-1 | A | 3 | 300 | 119.7 | 156.2 | 203.7 | 182.3 | 225.0 | 248.5 |
| 54 | 2SS-1-1 | A | 2 | 250 | 85.0 | 111.7 | 146.8 | 133.1 | 166.7 | 189.2 |
| 64 | 5SS-3-05 | A | 4 | 235 | 129.8 | 181.1 | 252.6 | 224.8 | 295.9 | 346.6 |
| 65 | 5SS-3-1 | A | 4 | 237 | 132.9 | 192.8 | 279.6 | 246.2 | 335.1 | 401.7 |
| 66 | 5SS-3-4 | A | 2 | 217 | 127.9 | 184.4 | 266.0 | 232.7 | 313.8 | 370.3 |
| 67 | 5SS-3-05 | A | 4 | 267 | 87.6 | 112.6 | 144.7 | 133.9 | 165.6 | 189.5 |
| 68 | 5SS-3-1 | A | 3 | 251 | 102.4 | 131.7 | 169.3 | 155.8 | 192.1 | 218.1 |
| 69 | 5SS-3-4 | A | 2 | 272 | 103.6 | 140.8 | 191.3 | 172.7 | 223.0 | 260.0 |
| 70 | 2SS-3-05 | A | 2 | 256 | 78.3 | 101.9 | 132.6 | 123.9 | 155.9 | 183.3 |
| 71 | 2SS-3-1 | A | 2 | 253 | 81.4 | 107.5 | 141.8 | 131.2 | 166.6 | 195.7 |
| 72 | 2SS-3-4 | A | 2 | 264 | 96.6 | 129.2 | 172.9 | 158.8 | 203.6 | 239.8 |
| 73 | 2SS-3-10 | C | 1 | 280 | 84.1 | 116.3 | 160.9 | 145.3 | 191.1 | 226.9 |
| 74 | 5SS-3-00 | A | 4 | | | | | | | |
| 75 | 5SS-3-1 | A | 4 | 211 | 135.7 | 183.7 | 248.5 | 220.9 | 281.8 | 319.5 |
| 76 | 9SS-3-1 | A | 2 | 272 | 108.7 | 134.1 | 165.5 | 157.3 | 189.2 | 216.2 |
| 77 | 9SS-3-4 | A | 1 | 275 | 111.9 | 141.4 | 178.7 | 167.3 | 204.5 | 234.0 |
| 78 | 10SS-3-05 | A | 4 | 206 | 136.7 | 178.5 | 233.0 | 214.9 | 269.3 | 311.3 |
| 80 | 11SS-3-05 | A | 4 | 86 | 152.2 | 227.3 | 339.5 | 306.1 | 434.2 | 555.2 |
| 81 | 11SS-3-1 | B | 4 | 141 | 202.6 | 287.7 | 408.5 | 366.0 | 492.0 | 592.5 |
| 82 | 8SS-3-05 | A | 4 | 229 | 118.6 | 170.2 | 244.2 | 215.9 | 291.4 | 347.7 |
| 83 | 8SS-3-1 | B | 4 | 94 | 191.4 | 354.1 | 655.0 | 516.1 | 847.4 | 1096.3 |
| 84 | 8SS-3-4 | A | 4 | 192 | 146.1 | 229.4 | 360.3 | 315.7 | 464.0 | 597.5 |
| 88 | 5SS-B-05 | A | 2 | 269 | 133.8 | 162.1 | 196.3 | 182.8 | 213.7 | 232.6 |
| 89 | 5SS-B-1 | A | 2 | 278 | 121.2 | 149.2 | 183.8 | 170.7 | 202.6 | 223.5 |
| 90 | 5SS-B-4 | A | 1 | 266 | 131.7 | 165.0 | 206.8 | 189.3 | 226.9 | 249.0 |
| 92 | 8SS-B-1 | B | 4 | 251 | 96.3 | 122.3 | 155.3 | 145.7 | 179.1 | 206.6 |
| 94 | 10SS-B-05 | B | 3 | | | | | | | |
| 95 | 10SS-B-1 | A | 3-4 | 270 | 135.6 | 156.7 | 181.2 | 173.7 | 196.6 | 213.3 |
| 96 | 11SS-B-05 | D | 4 | 252 | 109.3 | 134.9 | 166.4 | 153.6 | 182.1 | 199.2 |
| 97 | 10SS-1-05 | A | 4 | 251 | 181.7 | 205.5 | 232.4 | 225.1 | 250.6 | 270.2 |
| 98 | 10SS-2-1 | B | 2-3 | 270 | 163.0 | 202.4 | 251.2 | 233.1 | 278.7 | 309.2 |
| 99 | 11SS-2-1 | C | 2 | 263 | 212.4 | 244.4 | 280.7 | 270.4 | 305.0 | 331.5 |
| 100 | 11SS-2-05 | C | 4 | 276 | 188.6 | 220.0 | 256.8 | 245.1 | 279.3 | 303.9 |
| 101 | 8SS-2-4 | C-D | 2 | 201 | 214.5 | 257.2 | 308.4 | 294.0 | 344.3 | 384.4 |
| 102 | 5SS-2-05 | A | 3 | 260 | 125.0 | 156.5 | 196.0 | 182.1 | 219.8 | 246.6 |
| 103 | 5SS-2-1 | A | 3-4 | 266 | 122.7 | 162.0 | 213.8 | 192.8 | 241.7 | 273.2 |
| 104 | 5SS-2-4 | A | 1 | 252 | 133.5 | 174.1 | 227.0 | 203.9 | 252.0 | 279.7 |
| 105 | 5SS-1-05 | B | 3-4 | 254 | 128.3 | 157.3 | 192.9 | 181.5 | 215.9 | 241.1 |
| 106 | 2SS-1-05 | A | 1 | 240 | 75.7 | 93.4 | 115.4 | 111.8 | 135.9 | 160.1 |
| 107 | 2SS-1-4 | A | 1 | 240 | 67.9 | 85.1 | 106.5 | 102.4 | 125.8 | 148.6 |
| 108 | 11SS-1-1 | D | 2 | | | | | | | |
| 109 | 1LO-3-05 | A | 2 | 264 | 13.8 | 16.0 | 18.5 | 20.8 | 25.6 | 35.5 |
| 110 | 1LO-3-4 | A | 1 | 251 | 87.5 | 126.2 | 182.1 | 160.0 | 216.5 | 257.3 |
| 111 | 2LO-2-05 | A | 4 | 236 | 147.7 | 219.8 | 327.2 | 278.9 | 383.2 | 448.9 |
| 115 | 2LO-B-05 | A | 4 | 251 | 110.9 | 145.0 | 189.6 | 172.9 | 215.9 | 245.8 |
| 116 | 2LO-B-1 | C | 2 | 255 | 150.5 | 182.3 | 220.8 | 205.9 | 240.8 | 262.5 |
| 117 | 1LO-2-4 | B | 1 | 266 | 72.1 | 107.7 | 160.9 | 138.6 | 192.2 | 229.7 |
| 118 | 2LO-2-05 | C | 3 | 342 | 165.7 | 211.0 | 268.7 | 245.0 | 297.9 | 330.3 |
| 119 | 2LO-2-4 | D | 2 | 241 | 178.2 | 223.8 | 281.1 | 256.8 | 308.3 | 338.1 |
| 122 | 2OA-2-4 | A | 4 | 256 | 41.1 | 51.2 | 63.9 | 60.1 | 72.7 | 82.7 |
| 123 | 2OA-2-4 | B-C | 1 | 257 | 59.1 | 69.5 | 81.8 | 77.8 | 89.2 | 97.3 |
| 125 | 2OA-3-1 | B | 2 | 233 | 69.1 | 86.2 | 107.6 | 99.5 | 119.3 | 132.4 |
| 126 | 1OA-3-4 | B | 2 | 235 | 71.9 | 96.1 | 128.5 | 117.4 | 150.1 | 175.2 |
| 127 | 1OA-3-4 | B | 2-3 | 263 | 57.5 | 69.2 | 83.4 | 80.4 | 95.1 | 108.4 |
| 128 | 1OS-3-1 | B | 1 | 261 | 49.5 | 62.0 | 77.6 | 73.0 | 88.6 | 101.1 |
| 129 | 1OA-3-05 | B-C | 1 | 318 | 54.1 | 70.1 | 91.0 | 86.3 | 109.0 | 130.6 |
| 130 | 2OA-3-05 | A | 3 | 771 | 43.8 | 51.2 | 60.0 | 57.7 | 66.3 | 73.3 |
| 131 | 2OA-B-1 | A | 1-2 | 255 | 40.4 | 48.1 | 57.3 | 55.2 | 64.5 | 72.5 |
| 132 | 2OA-B-4 | C-D | 1 | 203 | 58.7 | 65.6 | 73.4 | 71.2 | 78.4 | 83.7 |
| 133 | 1OA-B-4 | A | 2-4 | 237 | 34.9 | 41.8 | 50.0 | 48.3 | 56.8 | 64.6 |
| 134 | 1OA-B-1 | A | 1 | 234 | 39.0 | 47.0 | 56.6 | 53.8 | 63.1 | 70.5 |
| 135 | 1OA-B-05 | B | 1 | 256 | 39.1 | 45.4 | 52.8 | 51.1 | 58.4 | 64.5 |
| 136 | 5SS-B-1 | B | 2 | 454 | 124.7 | 152.0 | 185.3 | 172.6 | 203.0 | 222.4 |
| 137 | 5SS-B-1 | B | 2 | 446 | 117.3 | 144.7 | 178.5 | 165.3 | 196.2 | 215.6 |
| 138 | 5SS-B-1 | B | 2 | 409 | 108.7 | 136.7 | 172.0 | 158.1 | 190.7 | 211.4 |
| 140 | 5SS-B-1 | B | 2 | 1309 | 117.2 | 144.9 | 179.1 | 165.8 | 197.2 | 217.0 |

APPENDIX III

PHYSICAL PROPERTIES

PHYSICAL PROPERTIES

The physical properties of the three organic phases are listed in Table VII. Values of viscosity and density determined by Ward (38, p. 193) for Shellsolv and light oil were used after checking the values at 68^oF. The density of the iso-octyl alcohol (2-ethyl-1-hexanol) was determined by weighing 100 milliliter samples to within 0.001 gram. The viscosity of the iso-octyl alcohol was measured with a Kinematic viscometer of the Cannon-Fenske type which had been calibrated by the Bureau of Standards. Interfacial tensions were measured with a direct reading CENCO-DuNouy ring tensiometer according to ASTM method D971-50.

Table VII. Physical properties.

| Temperature (°F) | Shellsolv | | Light Oil | | Iso-Octyl Alcohol | |
|--------------------------------------------|----------------------------------|-------------------|----------------------------------|-------------------|----------------------------------|-------------------|
| | Density (lb/ft ³) | Viscosity (cp) | Density (lb/ft ³) | Viscosity (cp) | Density (lb/ft ³) | Viscosity (cp) |
| 64 | 49.01 | 1.037 | 51.85 | 17.2 | 53.10 | 10.02 |
| 66 | 48.96 | 1.019 | 54.05 | 16.4 | 53.07 | 9.73 |
| 68 | 48.81 | 1.005 | 54.25 | 15.6 | 53.04 | 8.59 |
| 70 | 48.85 | 0.908 | 53.81 | 14.7 | 53.01 | 8.76 |
| 74 | 48.80 | 0.967 | 53.66 | 13.9 | 53.00 | 8.31 |
| Interfacial tension Dynes/cm 68°F | | 40.3 | | 17.6 | | 13.0 |

APPENDIX IV

COMPUTER PROGRAMS

```

$JOB,6858,SBC,020,DUMP
$EQUIP,16=MTCIEDU01
$REWIND,16
$FORTRAN,L,X
PROGRAM MAIN
DIMENSION IFREQ(100),KFREQ(100),D(4),FREQ(201),
I(33),PRØB(33),PERCT(100),LIST(4)
COMMON IFREQ,FREQ,KMAX,IRØLL,ENTER,WIDTH,NUM,T,PRØB,
IPERCT,IMARK,YMN,YMX,I,EXIT,FREQY,SAT,FRAC,IPRØB,
2KPRØB,IMAXS,KFREQ
100 FØRMAI(2I4,10F7.2/(8X,10F7.2))
101 FØRMAI(4I5,4F5.0)
102 FØRMAI(5F7.3)
103 FØRMAI(5F7.2)
104 FØRMAI(1H,15,2F10.5)
READ 102,(I(I),I=1,33)
READ 103,(PRØB(I),I=1,33)
ISET=-1
4 DØ 5 I=1,100
5 IFREQ(I)=KFREQ(I)=DELTA=0.
READ 101,IMAXS,KPRØB,IPRØB,NUM,WIDTH,TIME,EXIT,ENTER
GØ TØ(91,6)EØFCKF(60)
6 CALL RESET(ISET,16)
READ 104,MØD,FRAC,SAT
IMARK=3
PØS=ALØG(800.)
YMN=ALØG(10.)
YMX=ALØG(1000.)
DEL=YMX-YMN
READ 100,IRØLL,KMAX,(FREQ(I),I=1,KMAX)
C *****
C PRØDUCE 3.5X4.7 PLØT ØUTLINE
CALL AXISXY(16,5,6,7.5,7.829,DEL*6./3.5,-3.719,YMN,
1-3.719,YMN,DEL+0.5)
CALL PLØTXY(I(3),YMN,1,22)
CALL PLØTXY(I(6),YMN,1,22)
DØ 7 I=9,25,2
7 CALL PLØTXY(I(I),YMN,1,22)
CALL PLØTXY(I(28),YMN,1,22)
CALL PLØTXY(I(31),YMN,1,22)
CALL PLØTXY(I(33),YMN,1,0)
CALL PLØTXY(I(33),DEL/2.,1,24)
CALL PLØTXY(I(33),YMX,1,0)
CALL PLØTXY(I(31),YMX,1,24)
CALL PLØTXY(I(28),YMX,1,24)
DØ 27 I=9,25,2
II=34-I
27 CALL PLØTXY(I(II),YMX,1,24)
CALL PLØTXY(I(6),YMX,1,24)
CALL PLØTXY(I(3),YMX,1,24)
CALL PLØTXY(I(1),YMX,1,0)
CALL PLØTXY(I(1),DEL/2.,1,22)
CALL PLØTXY(I(1),YMN,1,0)
C *****
C PRINT DATA
300 FØRMAI(6H MØDEL,13/6H RØLL,15,5X,15,11H INTERVALS,
19HINITIALLY)
301 FØRMAI(7H IMAXS=,15,7H KPRØB=,15,7H IPRØB=,15,
15H NUM=,15)
302 FØRMAI(6H FRAC=,F10.5,5H SAT=,F10.5)
303 FØRMAI(1H,4HSTEP,F4.0,9H AT START,F4.0,9H AT END.,
112HØUTPUT EVERY,F4.0,6H STEPS)
304 FØRMAI(1H,20HINITIAL DISTRIBUTIØN)
PRINT 300,MØD,IRØLL,KMAX
PRINT 301,IMAXS,KPRØB,IPRØB,NUM
PRINT 302,FRAC,SAT
PRINT 303,ENTER,EXIT,TIME
PRINT 304
DØ 8 I=1,KMAX
8 IFREQ(I)=FREQ(I)
CALL ØUTPUT
CALL ØGIVE

```

```

P0S=P0S-.263
CALL PL0TXY(T(2),P0S,0,IMARK)
305 F0RMA T(6H SUMV=,F11.0,6H SUMA=,F11.0,6H SUMD=,F11.0)
307 F0RMA T(1H ,7F8.1)
308 F0RMA T(13H V0LUME DISTR)
309 F0RMA T(1H ,10F7.2)
310 F0RMA T(1H-)
CALL DISTR(PERCT,2.,SUMA)
CALL DISTR(PERCT,1.,SUMD)
CALL DISTR(PERCT,3.,SUMV)
PRINT 305,SUMV,SUMA,SUMD
D10X=SUMD/FREQY
D20X=(SUMA/FREQY)**.5
D30X=(SUMV/FREQY)**(1./3.)
D21X=SUMA/SUMD
D31X=(SUMV/SUMD)**.5
D32X=(SUMV/SUMA)
PRINT 307,ENTER,D10X,D20X,D30X,D21X,D31X,D32X
PRINT 308
D0 35 II=1,KMAX,10
JMAX=II+9
35 PRINT 309,(PERCT(JJ),JJ=II,JMAX)
PRINT 310
PRINT 310
IMARK=IMARK+2
D0 10 I=1,KMAX
KFREQ(I)=IFREQ(I)
10 IFREQ(I)=0
9 C0NTINUE
C *****
C ST0CASTIC M0DEL
CALL M0DEL
C *****
C TERMINATION AND 0UTPUT C0NTR0L
DELTA=DELTA+1.
ENTER=ENTER+1.
IF(EXIT.GT.ENTER)39,40
39 IF(TIME.GT.DELTA)90,40
40 DELTA=0.
C *****
C 0UTPUT RESULTS
CALL 0UTPUT
CALL 0GIVE
P0S=P0S-.263
CALL PL0TXY(T(2),P0S,0,IMARK)
CALL DISTR(PERCT,2.,SUMA)
CALL DISTR(PERCT,1.,SUMD)
CALL DISTR(PERCT,3.,SUMV)
PRINT 305,SUMV,SUMA,SUMD
D10X=SUMD/FREQY
D20X=(SUMA/FREQY)**.5
D30X=(SUMV/FREQY)**(1./3.)
D21X=SUMA/SUMD
D31X=(SUMV/SUMD)**.5
D32X=(SUMV/SUMA)
PRINT 307,ENTER,D10X,D20X,D30X,D21X,D31X,D32X
PRINT 308
D0 36 II=1,KMAX,10
JMAX=II+9
36 PRINT 309,(PERCT(JJ),JJ=II,JMAX)
PRINT 310
PRINT 310
88 IMARK=IMARK+2
IF(EXIT.GT.ENTER)90,89
89 ISET=20
CALL PL0TXY(T(1),YMX+1.,0,0)
110 F0RMA T(I4)
ENC0DE(4,110,M0DL)M0D
CALL LABEL(4,1,0,M0DL)
G0 T0 4
90 D0 30 J=1,KMAX

```



```

KFREQ(J)=IFREQ(J)
IF(IFREQ(J).GT.0)21,30
21 JMAX=J
30 IFREQ(J)=0
   KMAX=JMAX
   GO TO 9
91 CALL AXISXY(00,5,6,7.5,7.829,DEL*6./3.5,-3.719, YMN,
1-3.719, YMN, DEL+.5)
401 FØRMAT(9H /ØSUEØF/)
   WRITE(16,401)
402 FØRMAT(37H BKGD DUMP TAPE ØN UNIT 01 ØN PLØTTER)
   WRITE(59,402)
   CALL UNLØAD(16)
   END

SUBRØUTINE ØUTPUT
DIMENSØN IFREQ(100),KFREQ(100),D(4),FREQ(201),
IT(33),PRØB(33),PERCT(100),LIST(4)
CØMMØN IFREQ,FREQ,KMAX,IRØLL,ENTER,WIDTH,NUM,T,PRØB,
IPERCT,IMARK,YMN,YMX,I,EXIT,FREQY,SAT,FRAC,IPRØB,
2KPRØB,IMAXS,KFREQ
DØ 10 I=1,200
10 FREQ(I)=0.
   DØ 15 I=1,KMAX
15 FREQ(I)=IFREQ(I)
   DØ 20 I=1,KMAX
   J=KMAX-I
   FREQ(J+1)=FREQ(J+1)+FREQ(J+2)
20 FREQ(J+101)=FREQ(J+1)
   FREQ(KMAX+101)=0.
   FREQY=FREQ(I)
   DØ 30 I=1,KMAX
30 PERCT(I)=FREQ(I)*100./FREQY
110 FØRMAT(2I4,1ØF7.2,2H 1)
111 FØRMAT(23H FREQUENCY DISTRIBUTØN)
112 FØRMAT(28H PERCENT CUMULATIVE FREQ FØR,F7.0,5HDRØPS,
1F4.0,26H MICRØN INTERVALS STEP,F5.0)
113 FØRMAT(2I4,1ØF7.2,2H 2)
   PRINT 112,FREQY,WIDTH,ENTER
   DØ 40 I=1,KMAX,10
   JMAX=I+9
40 PRINT 110,IRØLL,KMAX,(PERCT(J),J=1,JMAX)
   PRINT 111
   DØ 45 I=1,KMAX
45 FREQ(I)=IFREQ(I)
   DØ 50 I=1,KMAX,10
   JMAX=I+9
50 PRINT 113,IRØLL,KMAX,(FREQ(J),J=1,JMAX)
   IF(FREQY.GT.10000.)61,62
61 EXIT=ENTER-1.
62 CØNTINUE
   RETURN
   END

SUBRØUTINE RANDØM(RAND)
DIMENSØN IFREQ(100),FREQ(100)
CØMMØN IFREQ,FREQ,KMAX,IRØLL,ENTER,WIDTH,NUM
RAND=1.E-300
CALL UNIFØRMI(NUM)
XN=NUM
RAND=RAND+XN/8388608.
RETURN
END

SUBRØUTINE FRAGMENT(RAND)
DIMENSØN IFREQ(100),FREQ(201)
CØMMØN IFREQ,FREQ,KMAX,IRØLL,ENTER,WIDTH,NUM
RAND=1.E-300
CALL UNIFØRMI(NUM)
XN=NUM
RAND=XN/83886080.+RAND
RETURN
END

```

```

SUBROUTINE OGIVE
  DIMENSION IFREQ(100),KFREQ(100),D(4),FREQ(201),
  IT(33),PRØB(33),PERCT(100),LIST(4)
  COMMON IFREQ,FREQ,KMAX,IRØLL,ENTER,WIDTH,NUM,T,PRØB,
  1PERCT,IMARK,YMN,YMX,I,EXIT,FREQY,SAT,FRAC,IPRØB,
  2KPRØB,IMAXS,KFREQ
  IPØS=0
50 DØ 20 I=1,KMAX
  J=1
  A=I
  Y=ALØG((A*10.)-5.)
43 IF(Y-YMN)4,2,2
  2 IF(Y-YMX)3,3,4
  4 J=2
  3 IF(PERCT(I)-PRØB(I))5,5,7
  5 IF(PERCT(I)-PRØB(33))7,12,12
  7 J=2
12 GØ TØ(8,21)J
  8 P=PERCT(I)
  CALL INTERP(X)
  GØ TØ(9,10)IMARK
100 FØRMAT(2E11.4)
  9 PRINT 100,P,X
  10 CALL PLØTXY(X,Y,IPØS,IMARK)
  IPØS=1
  GØ TØ 20
  21 PRINT 101,Y,PERCT(I)
101 FØRMAT(1H ,2HY=,E11.4,10H PERCT(I)=,E11.4)
  20 CØNTINUE
102 FØRMAT(1H-)
  PRINT 102
  RETURN
  END

```

```

SUBROUTINE DISTR(W,Q,SUMW)
  DIMENSION W(1)
  DIMENSION IFREQ(100),KFREQ(100),D(4),FREQ(201),
  IT(33),PRØB(33),PERCT(100),LIST(4)
  COMMON IFREQ,FREQ,KMAX,IRØLL,ENTER,WIDTH,NUM,T,PRØB,
  1PERCT,IMARK,YMN,YMX,I,EXIT,FREQY,SAT,FRAC,IPRØB,
  2KPRØB,IMAXS,KFREQ
  W(KMAX+1)=0.
  DØ 10 I=1,KMAX
  A=KMAX-I
  D1=WIDTH*(A+1.E-300)
  D2=WIDTH*(A+1.)
  P=Q-1.
  J=KMAX-I
  W(J+1)=Q*WIDTH*((D1**P)*FREQ(J+101)+(D2**P)*FREQ(J+
  1102))/2.+W(J+2)
10 CØNTINUE
  DØ 20 I=1,KMAX
  A=KMAX-I
  D1=WIDTH*A
  J=KMAX-I
  20 W(J+1)=(D1**Q)*FREQ(J+101)+W(J+1)
  SUM=W(KMAX+1)
  DØ 30 I=1,KMAX
  J=KMAX-I
  SUMW=W(J+1)
  W(J+1)=W(J+1)-SUM
  30 SUM=SUMW
  DØ 40 I=1,KMAX
  J=KMAX-I
  40 W(J+1)=W(J+1)+W(J+2)
  WW=W(1)
  DØ 50 I=1,KMAX
  50 W(I)=W(I)*100./WW
  RETURN
  END

```

```

SUBROUTINE INTERP(VAL)
  DIMENSION IFREQ(100),KFREQ(100),D(4),FREQ(201),
  IT(33),PRØB(33),PERCT(100),LIST(4)
  COMMON IFREQ,FREQ,KMAX,IRØLL,ENTER,WIDTH,NUM,T,PRØB,
  IPERCT,IMARK,YMN,VMX,I,EXIT,FREQY,SAT,FRAC,IPRØB,
  2KPRØB,IMAXS,KFREQ
  DO 10 K=1,33
  IF(PERCT(I)-PRØB(K))10,12,11
100 FORMAT(15H VALUE ØFF PLØT,F7.2)
  10 CONTINUE
  PRINT 100,PERCT(I)
  RETURN
  12 VAL=T(K)
  RETURN
  11 VAL=(T(K-1)-T(K))*(PERCT(I)-PRØB(K-1))/(PRØB(K-1)
  I-PRØB(K))+T(K-1)
  RETURN
END

```

```

$COMPASS,L,X,P
  IDENT      UNIFØRMI
  ENTRY      UNIFØRMI
UNIFØRMI    UJP      **
            LDA      UNIFØRMI
            SWA      URNADD
            INA      I
            SWA      UNIFØRMI
            ENA      O
            LDQ,I    URNADD
            AQA
            LPA      MASKU3
            SHA      4
            AQA
            LPA      MASKUI
            ADA      C
            LPA      MASKUI
URNADD     STA,I    **
            INTS    1000B,0
            UJP     UNIFØRMI
            UJP     UNIFØRMI
MASKU3     ØCT     07777777
MASKUI     ØCT     37777777
C          DEC     1772721
            END
            FINIS

```

```

SUBROUTINE MØDEL 1,2,3,4
DIMENSION IFREQ(100),KFREQ(100),D(4),FREQ(201),
1 T(33),PRØB(33),PERCT(100),LIST(4)
COMMON IFREQ,FREQ,KMAX,IRØLL,ENTER,WIDTH,NUM,T,PRØB,
1 PERCT,IMARK,YMN,YMX,I,EXIT,FREQY,SAT,FRAC,IPRØB,
2 KPRØB,IMAXS,KFREQ
DØ 20 I=1,KMAX
KFRE=KFREQ(I)
DØ 20 J=1,KFRE
CALL UNIFØRMI(NUM)
ANUM=NUM
LUCK=ANUM*100./8388608.
IF(I.LE.IMAXS)17,18
17 IF(LUCK.LT.KPRØB)11,19
18 IF(LUCK.LT.IPRØB)12,19
19 IFREQ(I)=IFREQ(I)+1
GØ TØ 20
11 CALL RANDØM(RATIØ)
GØ TØ 13
12 CALL FRAGMENT(RATIØ)
13 DIA=I
DIA=DIA-.475
D(1)=((RATIØ)**(0.333333333))*DIA
D(2)=((1.-RATIØ)**(0.333333333))*DIA
DØ 20 K=1,2
ID=D(K)+1.
IFREQ(ID)=IFREQ(ID)+1
20 CONTINUE
RETURN
END

```

```

SUBROUTINE MØDEL 5
DIMENSION IFREQ(100),KFREQ(100),D(4),FREQ(201),
1 T(33),PRØB(33),PERCT(100),LIST(4)
COMMON IFREQ,FREQ,KMAX,IRØLL,ENTER,WIDTH,NUM,T,PRØB,
1 PERCT,IMARK,YMN,YMX,I,EXIT,FREQY,SAT,FRAC,IPRØB,
2 KPRØB,IMAXS,KFREQ
DØ 20 I=1,KMAX
KFRE=KFREQ(I)
DØ 20 J=1,KFRE
CALL UNIFØRMI(NUM)
ANUM=NUM
LUCK=ANUM*10./8388608.
IF(I.LE.IMAXS)17,18
17 IF(LUCK.LT.KPRØB)12,19
18 IF(LUCK.LT.IPRØB)11,19
19 IFREQ(I)=IFREQ(I)+1
GØ TØ 20
11 CALL RANDØM(RATIØ)
GØ TØ 13
12 CALL FRAGMENT(RATIØ)
13 DIA=I
DIA=DIA-.475
D(1)=((1./FRAC)**(1./3.))*DIA
IFRAC=FRAC
DØ 20 K=1,IFRAC
ID=D(1)+1.
IFREQ(ID)=IFREQ(ID)+1
20 CONTINUE
RETURN
END

```

```

SUBROUTINE MØDEL 6
DIMENSION IFREQ(100),KFREQ(100),D(4),FREQ(201),
IT(33),PRØB(33),PERCT(100),LIST(4)
COMMON IFREQ,FREQ,KMAX,IRØLL,ENTER,WIDTH,NUM,I,PRØB,
IPERCT,IMARK,YMN,YMX,I,EXIT,FREQY,SAT,FRAC,IPRØB,
2KPRØB,IMAXS,KFREQ
DØ 20 I=1,KMAX
KFRE=KFREQ(I)
DØ 20 J=1,KFRE
CALL UNIFØRMI(NUM)
ANUM=NUM
LUCK=ANUM*10./8388608.
IF(I.LE.IMAXS)17,18
17 IF(LUCK.LT.KPRØB)12,19
18 IF(LUCK.LT.IPRØB)11,19
19 IFREQ(I)=IFREQ(I)+1
GØ TØ 20
11 CALL RANDØM(RATIØ)
GØ TØ 13
12 CALL FRAGMENT(RATIØ)
13 DIA=I
DIA=DIA-.475
IFRAC=IPRØB-LUCK+1
FRAC=IFRAC
D(1)=((1./FRAC)**(1./3.))*DIA
DØ 20 K=1,IFRAC
ID=D(K)+1.
IFREQ(ID)=IFREQ(ID)+1
20 CONTINUE
RETURN
END

```

```

SUBROUTINE MØDEL 7
DIMENSION IFREQ(100),KFREQ(100),D(4),FREQ(201),
IT(33),PRØB(33),PERCT(100),LIST(4)
COMMON IFREQ,FREQ,KMAX,IRØLL,ENTER,WIDTH,NUM,I,PRØB,
IPERCT,IMARK,YMN,YMX,I,EXIT,FREQY,SAT,FRAC,IPRØB,
2KPRØB,IMAXS,KFREQ
DØ 20 I=1,KMAX
KFRE=KFREQ(I)
DØ 20 J=1,KFRE
CALL UNIFØRMI(NUM)
ANUM=NUM
LUCK=ANUM*10./8388608.
IF(I.LE.IMAXS)17,18
17 IF(LUCK.LT.KPRØB)12,19
18 IF(LUCK.LT.IPRØB)11,19
19 IFREQ(I)=IFREQ(I)+1
GØ TØ 20
11 CALL RANDØM(RATIØ)
GØ TØ 13
12 CALL FRAGMENT(RATIØ)
13 DIA=I
DIA=DIA-.475
D(1)=((RATIØ)**(0.33333333))*DIA
D(2)=((1.-RATIØ)**(0.33333333))*DIA
D(3)=((FRAC)**(1./3.))*D(1)
D(1)=((1.-FRAC)**(1./3.))*D(1)
DØ 20 K=1,3
ID=D(K)+1.
IFREQ(ID)=IFREQ(ID)+1
20 CONTINUE
RETURN
END

```

```

SUBROUTINE MØDEL 8
DIMENSION IFREQ(100),KFREQ(100),D(4),FREQ(201),
1 T(33),PRØB(33),PERCT(100),LIST(4)
CØMMØN IFREQ,FREQ,KMAX,IRØLL,ENTER,WIDTH,NUM,T,PRØB,
1 PERCT,IMARK,YMN,YMX,I,EXIT,FREQY,SAT,FRAC,IPRØB,
2 KPRØB,IMAXS,KFREQ
DØ 20 I=1,KMAX
KFRE=KFREQ(I)
DØ 20 J=1,KFRE
CALL UNIFØRMI(NUM)
ANUM=NUM
LUCK=ANUM*10./8388608.
IF(1.LE.IMAXS)17,18
17 IF(LUCK.LT.KPRØB)12,19
18 IF(LUCK.LT.IPRØB)11,19
19 IFREQ(I)=IFREQ(I)+1
GØ TØ 20
11 CALL RANDØM(RATIØ)
GØ TØ 13
12 CALL FRAGMENT(RATIØ)
13 DIA=I
DIA=DIA-.475
D(1)=((RATIØ)**(0.333333333))*DIA
D(2)=((1.-RATIØ)**(0.333333333))*DIA
D(3)=((FRAC)**(1./3.))*D(1)
D(4)=((FRAC)**(1./3.))*D(2)
D(1)=((1.-FRAC)**(1./3.))*D(1)
D(2)=((1.-FRAC)**(1./3.))*D(2)
DØ 20 K=1,4
ID=D(K)+1.
IFREQ(ID)=IFREQ(ID)+1
20 CØNTINUE
RETURN
END

```

```

SUBROUTINE MØDEL 9
DIMENSION IFREQ(100),KFREQ(100),D(4),FREQ(201),
1 T(33),PRØB(33),PERCT(100),LIST(4)
CØMMØN IFREQ,FREQ,KMAX,IRØLL,ENTER,WIDTH,NUM,T,PRØB,
1 PERCT,IMARK,YMN,YMX,I,EXIT,FREQY,SAT,FRAC,IPRØB,
2 KPRØB,IMAXS,KFREQ
DØ 20 I=1,KMAX
KFRE=KFREQ(I)
DØ 20 J=1,KFRE
CALL UNIFØRMI(NUM)
ANUM=NUM
LUCK=ANUM*100./8388608.
IF(1.LE.IMAXS)17,18
17 IF(1.GT.KPRØB)16,19
16 KKPRØB=IPRØB*(1-KPRØB)/(IMAXS-KPRØB)
IF(LUCK.LT.KKPRØB)12,19
18 IF(LUCK.LT.IPRØB)11,19
19 IFREQ(I)=IFREQ(I)+1
GØ TØ 20
11 CALL RANDØM(RATIØ)
GØ TØ 13
12 CALL FRAGMENT(RATIØ)
13 DIA=I
DIA=DIA-.475
D(1)=((RATIØ)**(0.333333333))*DIA
D(2)=((1.-RATIØ)**(.333333333))*DIA
D(3)=((FRAC)**(.333333333))*D(1)
D(1)=((1.-FRAC)**(.333333333))*D(1)
DØ 20 K=1,3
ID=D(K)+1.
IFREQ(ID)=IFREQ(ID)+1
20 CØNTINUE
RETURN
END

```

```

SUBROUTINE MØDEL 10
DIMENSION IFREQ(100),KFREQ(100),D(4),FREQ(201),
I(33),PRØB(33),PERCT(100),LIST(4)
COMMON IFREQ,FREQ,KMAX,IRØLL,ENTER,WIDTH,NUM,I,PRØB,
I PERCT,IMARK,YMN,VMX,I,EXIT,FREQY,SAT,FRAC,IPRØB,
2KPRØB,IMAXS,KFREQ
DØ 20 I=1,KMAX
KFRE=KFREQ(I)
DØ 20 J=1,KFRE
CALL UNIFORMI(NUM)
ANUM=NUM
LUCK=ANUM*100./8388608.
IF(I.LE.IMAXS)17,18
17 IF(I.GT.KPRØB)16,19
16 NUMER=I-KPRØB
DENØM=IMAXS-KPRØB
RAT=(NUMER/DENØM)**SAT
KKPRØB=IPRØB*RAT
IF(LUCK.LT.KKPRØB)12,19
18 IF(LUCK.LT.IPRØB)11,19
19 IFREQ(I)=IFREQ(I)+1
GØ TØ 20
11 CALL RANDØM(RATIØ)
GØ TØ 13
12 CALL FRAGMENT(RATIØ)
13 DIA=I
DIA=DIA-.475
D(1)=((RATIØ)**(0.333333333))*DIA
D(2)=((1.-RATIØ)**(.333333333))*DIA
D(3)=((FRAC)**(.333333333))*D(1)
D(1)=((1.-FRAC)**(.333333333))*D(1)
DØ 20 K=1,3
ID=D(K)+1.
IFREQ(ID)=IFREQ(ID)+1
20 CONTINUE
RETURN
END

```

```

SUBROUTINE MØDEL 11
DIMENSION IFREQ(100),KFREQ(100),D(4),FREQ(201),
I(33),PRØB(33),PERCT(100),LIST(4)
COMMON IFREQ,FREQ,KMAX,IRØLL,ENTER,WIDTH,NUM,I,PRØB,
I PERCT,IMARK,YMN,VMX,I,EXIT,FREQY,SAT,FRAC,IPRØB,
2KPRØB,IMAXS,KFREQ
DØ 20 I=1,KMAX
KFRE=KFREQ(I)
DØ 20 J=1,KFRE
CALL UNIFORMI(NUM)
ANUM=NUM
LUCK=ANUM*100./8388608.
IF(I.LE.IMAXS)17,18
17 IF(I.GT.KPRØB)16,19
16 KKPRØB=IPRØB*(I-KPRØB)/(IMAXS-KPRØB)
IF(LUCK.LT.KKPRØB)11,19
18 IF(LUCK.LT.IPRØB)11,19
19 IFREQ(I)=IFREQ(I)+1
GØ TØ 20
11 CALL RANDØM(RATIØ)
GØ TØ 13
13 DIA=I
DIA=DIA-.475
D(1)=((RATIØ)**(0.333333333))*DIA
D(2)=((1.-RATIØ)**(.333333333))*DIA
CALL FRAGMENT(RATIØ)
FRAC=RATIØ*SAT
D(3)=((FRAC)**(.333333333))*D(1)
D(1)=((1.-FRAC)**(.333333333))*D(1)
DØ 20 K=1,3
ID=D(K)+1.
IFREQ(ID)=IFREQ(ID)+1
20 CONTINUE
RETURN
END

```

NOMENCLATURE

The fundamental dimensions are represented by the following letters: F = force, L = length, M = mass, T = time.

| <u>Symbol</u> | <u>Meaning</u> | <u>Dimensions</u> |
|------------------------------------|---------------------------------------------------------------------|-------------------|
| B | Length of the minor axis of an ellipsoid, constant in Equation 41 | L |
| C, C _a , C _p | Experimentally determined constants | |
| D | Diameter | L |
| D _{—X} | Weighted average drop size as described in Equation 30 | L |
| D _{max} | Maximum stable drop diameter | L |
| D ₉₅ | Diameter below which 95% of the volume of the distribution is found | L |
| D _{min} | Minimum drop diameter resulting from breakup | L |
| E | Spectrum function for turbulent fluctuations | |
| f | Arbitrary function in Equation 30 | |
| F | Arbitrary function in Equation 37 | |
| G | Velocity gradient | T ⁻¹ |
| k | Wave number | |
| KPROB | Diameter at which probability of breakup becomes 100% | L |
| L | Length of major axis of an ellipsoid | L |

| <u>Symbol</u> | <u>Meaning</u> | <u>Dimensions</u> |
|---------------|------------------------------------------------------------------------|-------------------|
| m | Parameter of Equation 36 | |
| N_{Ta} | Taylor number (defined by Equation 28) | |
| N_{Re} | Reynolds number based on pipe diameter and continuous phase properties | |
| N_{We} | Weber number | |
| N_{vi} | Viscosity group (defined by Equation 10) | |
| P | Pressure | F/L^2 |
| p' | Pressure fluctuation | F/L^2 |
| p | Order of weighted average drop size | |
| q | Order of weighted average drop size | |
| R | Radius, reflectance in Equation 42 | L |
| s | Geometric standard deviation | L |
| SAT | Range of satellite to daughter drop volume ratios | L |
| t | Width of the annular space between two coaxial cylinders | L |
| U | Average velocity | L/T |
| u' | Fluctuating component of velocity | L/T |
| U_* | Friction velocity | L/T |
| V | Total volume | L^3 |
| v | Cumulative volume fraction of drops | L^3 |
| $W_p(r_1)$ | Cumulative fraction of the total number of drops above size r_1 | |

| <u>Symbol</u> | <u>Meaning</u> | <u>Dimensions</u> |
|----------------------|------------------------------------------------|-------------------|
| x | Coordinate | L |
| \bar{x} | Mean value of x | L |
| y | Coordinate, radial distance from the pipe wall | L |
| <u>Greek Symbols</u> | | |
| α | Constant found in Equation 17 | |
| δ | Parameter of Equation 36 | |
| δ_o | Thickness of the laminar sublayer | L |
| Δ | Difference operator | |
| ϵ | Energy dissipation per unit mass | FL/M |
| λ | Scale of turbulence | L |
| μ | Coefficient of viscosity | M/LT |
| ν | Kinematic viscosity | L ² /T |
| σ | Standard deviation, interfacial tension | L |
| τ_w | Shear stress at the wall | F/L ² |
| ρ | Density | M/L ³ |
| ϕ | Angle in Equation 1 | |
| ψ | Arbitrary function in Equation 11 | |
| ω | Angular velocity | T ⁻¹ |

SubscriptsMeaning

| | |
|---|------------------|
| c | Continuous phase |
| d | Dispersed phase |